NASA CONTRACTOR REPORT

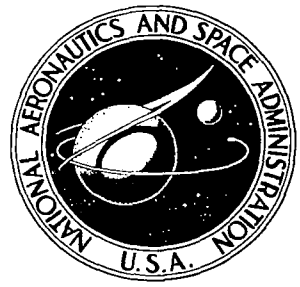

NASA CR-2014

DEVELOPMENT OF A SOLID ELECTROLYTE CARBON DIOXIDE AND WATER REDUCTION SYSTEM FOR OXYGEN RECOVERY

by L. Elikan, J. P. Morris, and C. K. Wu

Prepared by
WESTINGHOUSE ELECTRIC CORPORATION
Pittsburgh, Pa. 15235
for Langley Research Center

NATIONAL AERONAUTICS AND SPACE ADMINISTRATION • WASHINGTON, D. C. • MAY 1972

1. Report No.	2. Government Accession No.	3. Recipient's Catalog No.
NASA CR-2014		

4. Title and Subtitle	5. Report Date
DEVELOPMENT OF A SOLID ELECTROLYTE CARBON DIOXIDE AND WATER REDUCTION SYSTEM FOR OXYGEN RECOVERY	May 1972
	6. Performing Organization Code

7. Author(s)	8. Performing Organization Report No.
L. Elikan, J. P. Morris, and C. K. Wu	
	10. Work Unit No. 127-53-41-05

9. Performing Organization Name and Address	11. Contract or Grant No.
Westinghouse Electric Corporation Pittsburgh, Pennsylvania 15235	NAS1-8896
	13. Type of Report and Period Covered
12. Sponsoring Agency Name and Address	Contractor Report
National Aeronautics and Space Administration Washington, D.C. 20546	14. Sponsoring Agency Code

15. Supplementary Notes

16. Abstract

A 1/4-man solid electrolyte oxygen regeneration system, consisting of an electrolyzer, a carbon deposition reactor, and palladium membranes for separating hydrogen, was operated continuously in a 180-day test. Oxygen recovery from the carbon dioxide-water feed was 95%. One percent of the oxygen was lost to vacuum with the hydrogen off-gas. In a space cabin, the remaining 4% would have been recycled to the cabin and recovered.

None of the electrolysis cells used in the 180-day test failed. Electrolysis power rose 20% during the test; the average power was 283.5 watts/man. Crew time was limited to 18 min/day of which 12 min/day was used for removing carbon.

The success achieved in operating the system can be attributed to an extensive component development program, which is described. Stability of operation, ease of control, and flexibility in feed composition were demonstrated by the life test.

17. Key Words (Suggested by Author(s))	18. Distribution Statement
Solid Electrolyte Oxygen Reclamation System 1/4 Man Size 180 Day Test	Unclassified - Unlimited

19. Security Classif. (of this report)	20. Security Classif. (of this page)	21. No. of Pages	22. Price*
Unclassified	Unclassified	181	$3.00

*For sale by the National Technical Information Service, Springfield, Virginia 22151

TABLE OF CONTENTS

ILLUSTRATIONS

TABLES

DEVELOPMENT OF A SOLID ELECTROLYTE CARBON DIOXIDE AND WATER REDUCTION SYSTEM FOR OXYGEN RECOVERY

L. Elikan, J. P. Morris, and C. K. Wu
Westinghouse Research Laboratories
Pittsburgh, Pennsylvania 15235

1. INTRODUCTION AND SUMMARY

Solid electrolyte electrolysis of metabolically formed carbon dioxide and water is one of the more promising processes for reclaiming oxygen in a regenerative life support system. The carbon dioxide and water are broken down into oxygen, hydrogen, and carbon and all of the oxygen is recovered.

Although two other oxygen regeneration processes, the Sabatier with methane dump/water electrolysis and Bosch/water electrolysis, have received more extensive development and testing than the solid electrolyte system, a recent tradeoff study of advanced integrated life support systems, the AILSS (Reference 1) study, selected the solid electrolyte system as the most promising for a non-resupply mission of 500 days duration. The projected date for the mission was 1976 to 1980. Factors leading to the selection of the solid electrolyte system included its flexibility in being able to handle mixtures of CO_2 and water in any ratio, ease of control, absence of need for gas-liquid separation, absence for need of a separate water electrolysis unit, and fewer interfaces.

1.1 Concept Description

The approach to oxygen regeneration being developed by Westinghouse is shown schematically in Fig. 1. The diagram includes all major components except the furnaces for heating the electrolysis unit and carbon deposition reactor and the vacuum pump for hydrogen removal.

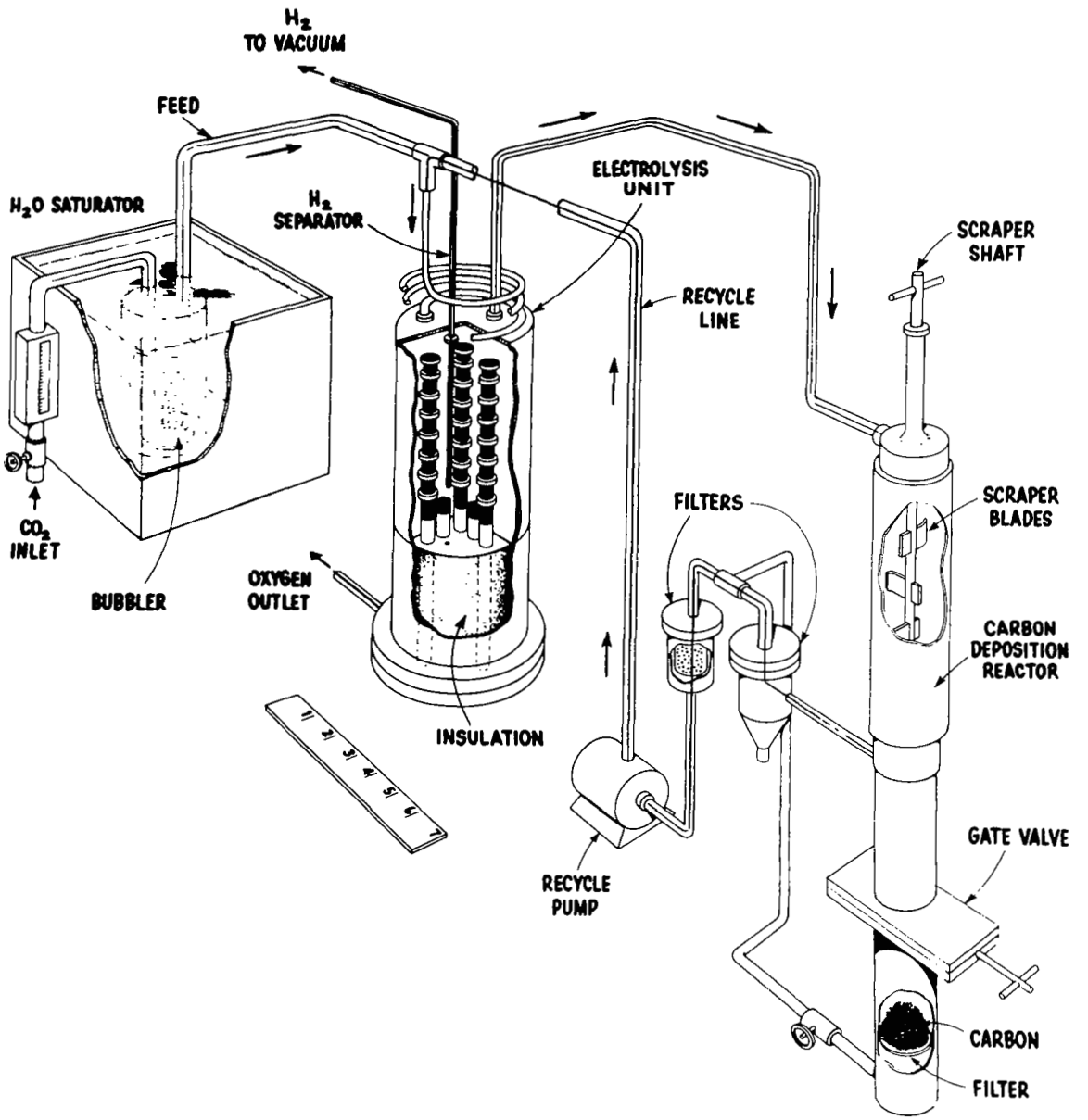

Fig. 1 - Schematic diagram of breadboard regeneration system

Oxygen and hydrogen are generated in the electrolysis step by the following reactions:

$$CO_2 \rightarrow CO + 1/2\ O_2 \qquad (1)$$

$$H_2O \rightarrow H_2 + 1/2\ O_2 \qquad (2)$$

The CO and H_2 form on the cathode side of the ceramic electrolyte and the O_2 forms on the anode side. Transfer of oxygen through the crystal lattice of the $(ZrO_2)_{0.9}\ (Y_2O_3)_{0.1}$ electrolyte occurs by migration of oxygen ions (O=).

Carbon is produced in a catalytic reactor from the CO formed in reaction (1):

$$2\ CO \rightarrow CO_2 + C\ (solid) \qquad (3)$$

The carbon dioxide produced by Equation (3) is recycled to the electrolyzer where it is also converted to CO and oxygen. Thus, the only products from the system are oxygen, hydrogen which is discarded to space (unless desired for use on board), and solid carbon. The carbon is collected in the carbon deposition reactor and can be stored in the food storage area as the food supply is consumed.

The operating principles of the solid electrolyte electrolysis unit and system thermodynamics have been reviewed in previously issued reports by Elikan, Archer, and Zahradnik (Reference 2) and by Elikan and Morris (Reference 3).

1.2 Previous Work on Development of Solid Electrolyte Oxygen Regeneration Systems

Chandler and his co-workers (References 4,5,6) began work on developing solid electrolyte systems for aerospace oxygen regeneration in the early 1960's. They succeeded in building and operating a number of small scale systems, including an engineering model which produced 150 cc/min of oxygen. However, short life of the electrolysis unit and loss of catalyst activity after 137 hours of operation made it clear that further development was necessary.

Weissbart and Smart have studied alternate electrolyte materials (Reference 7), and more recently (References 8,9) have pursued the development of an alternate solid electrolyte cell geometry based on the use of flat discs.

Under a prior contract with NASA Langley, Westinghouse demonstrated that the two major components of solid electrolyte system could be designed and built to achieve long life and high performance (Reference 3). Multi-celled stacks of solid electrolyte cells, operating at a current density of 200 mA/cm^2 and a total current of 2 amps, achieved operating lives exceeding 100 days. Also, a continuous carbon deposition reactor, utilizing the reactor wall itself as a catalyst, was operated continuously for 100 days.

Once long life was demonstrated for the major components, the next logical step was the assembly of an integrated bench scale system to assess the problems of component interaction, process control, overall reliability, and maintainability.

1.3 Program Outline

The primary objective of the program described in this report was the design, construction, and operation of a closed-loop breadboard system that would produce 125 cc/minute (approximately 1/4-man) of oxygen from a mixed feed containing approximately 2/3 carbon dioxide and 1/3 water. The original goal of 100 days of continuous operation was readily achieved and was extended to 180 days.

1.3.1 Component Development

Prior to the actual design and construction of the breadboard, further development of the individual system components was carried out. This work began in March, 1969, and was completed (except for some life tests which refused to quit) in March, 1970.

Deterioration at the oxygen electrode-joint interface was the principal cause of failure of the electrolysis stacks tested under the previous contract (Reference 3). A program to improve fabrication procedures for

multi-celled stacks resulted in the development of a new electrode fabrication technique and a method for maintaining closer tolerances on dimensions of ceramic parts which reduced joint resistance. As a result, anode deterioration was eliminated as a cuase of failure. The procedures for fabricating the electrodes and assembling the stacks are described in Appendixes A and B.

Operating a closed-loop process requires that the electrolyzer be capable of accepting a feed which contains recycle from the carbon deposition reactor. This feed will contain an appreciable percentage of carbon monoxide, since equilibrium considerations prevent the complete conversion of CO to CO_2 by Equation (3). Also, it is desired to produce a product stream from the electrolyzer as rich in CO as possible, since this will minimize the size of the carbon deposition reactor and/or the amount of recycle required. Extensive testing was, therefore, carried out to determine the extent to which the degree of decomposition[(a)] of CO_2 and H_2O to CO and H_2 affected the life of the electrolysis stacks. This study defined the practical range over which the operating variables (degree of decomposition and current density) could be varied without reducing cell life. The tests are described in Appendix C.

Other developmental efforts were concentrated on:

1. Improving the performance of the carbon deposition reactor by increasing reactivity and decreasing iron consumption. (See Appendix D.)
2. Characterizing the performance and devising a control method for palladium membranes. (See Appendix E.)
3. Testing materials of construction for resistance to oxidation and carbon deposition.

(a) The degree of decomposition (DD) is a measure of the conversion of CO_2 and H_2O to CO and H_2 at the electrolyzer exit. Corrections are made for the hydrogen diffused through the palladium membranes and for contamination of the stream by nitrogen. The DD is calculated from the volumetric flow rate (cc/min) as follows:

$$DD = \frac{\text{exit CO} + \text{exit } H_2 + H_2 \text{ diffused}}{\text{total exit gas} + H_2 \text{ diffused} - \text{exit } N_2}$$

1.3.2 Breadboard Design, Construction, and Operation

Breadboard design was initiated late in the second half of 1969 and completed early in 1970. Emphasis was placed on flexibility and built-in redundancy to insure long life, as well as sufficient control to allow unattended operation for long periods of time. An example of built-in redundancy was the inclusion of spare electrolysis stacks within the electrolysis module. These spares could be used when desired without shutting down and opening the system. The electrolysis unit design also permitted the isolation of broken or leaky stacks without system shutdown.

Construction of the breadboard was completed in May. Initial testing of the unit was carried out without recycling the gas discharge of the carbon deposition reactor (open loop mode). During these tests, the electrolyzer and carbon deposition reactor were characterized, recycle rate requirements were estimated, startup and shutdown procedures were established, and control system modifications were suggested. This work is described in Appendix F.

A two-day test in which the carbon deposition reactor product stream was recycled to the electrolyzer (closed loop mode) was run prior to starting the 180-day life test on July 9, 1970. After the life test was completed on January 8, 1971, the system was disassembled to determine the condition of the system components.

1.3.3 Oxygen Regeneration System With Various CO_2 Concentrators

A preliminary paper study was performed to determine the effects on system design and equivalent weight of integrating the solid electrolyte oxygen regenerator with various CO_2 concentrators. Four different concentration systems -- molecular sieve, steam desorbed resin, carbonation cells, and hydrogen-depolarized electrochemical cells -- were considered.

1.4 Report Organization

The breadboard description and life test results, as well as the results of the regenerator-concentrator interface study, are contained

in the body of the report. Data and computations, as well as discussion, related to the pre-breadboard development are generally contained in the appendixes. Also in the appendixes are the system operating instructions (Appendix G) and the 180-day test log (Appendix H).

Every effort has been made to include all relevant data, both favorable and unfavorable, so that the engineer or scientist reading this report can understand fully the results obtained.

2. CONCLUSIONS

2.1 Conclusions Based Upon Operation of Breadboard System

Development of the solid electrolyte oxygen regeneration system has reached the stage where the feasibility of constructing a multi-man system for manned testing has been demonstrated. This overall conclusion is based on the successful operation for 180 days of an integrated, closed-loop breadboard system which produced 125 cc/min of oxygen from a mixed feed of carbon dioxide and water. The following specific results were achieved in constructing and operating the breadboard.

1. The closed-loop concept -- in which the product stream from the carbon deposition reactor is recylced to the electrolyzer and the only products are oxygen, carbon and hydrogen -- has been demonstrated by an operating system of long life and high performance. Ninety-five and one-tenth percent of the oxygen in the carbon dioxide-water feed during the 180-day test was recovered as O_2. Of the 4.9% unrecovered, 1.2% was lost to vacuum with the hydrogen off-gas. In a space cabin, the remaining 3.7% would be recycled to the cabin with the oxygen and would not be lost.

2. The breadboard was operated on feeds containing 15% to 35% water with the balance being carbon dioxide (except for trace quantities of nitrogen), thus illustrating that the feed to the regeneration system can contain CO_2 and H_2O in essentially any ratio.

3. The breadboard was operated with N_2 levels between 6% and 12% in the recycle stream without apparent decrease in system performance.

4. The electrolysis power requirement on the first day of the 180-day test was 242 watts/man (0.49 watts/cc of O_2/min); the

average power required was 283.5 watts/man and the total increase in power over 180 days amounted to less than 20% of the initial value.

5. The reliability of the electrolysis unit was greater than anticipated, based on test results with three-cell stacks: none of the electrolysis cells used in the 180-day test failed.

6. Crew time was limited to 18 minutes/day. The total crew time required during the life test was 54.3 hours. Of this, 398 minutes were spent on routine maintenance, 700 minutes on fault identification and correction, and the remaining 2160 minutes on carbon tending.

7. Maintainability of the system was demonstrated.

   a. Electrolysis unit design permitted the isolation of broken or leaky electrolysis stacks without system shutdown.

   b. Spare electrolysis cells were built into the operating module. Maintaining these spares at operating temperature and in the operating gas atmosphere for the entire 180 days did not affect their measured performance; their V-I characteristics at the conclusion of the life test were identical to their performance at the outset.

   c. Wiring from the cells to an external panel allowed spare electrolysis cells to be used when desired without opening the system.

   d. No buildup of carbon in the transfer lines, pumps, or electrolyzer was observed.

8. Stable operation of the system was easily accomplished; the system was left unattended (no one in same building) for 15-20 hours every day.

9. A carbon deposition reactor which utilizes the wall of the reactor as a catalyst was effective in removing carbon from the

system. The potential advantages of this approach in comparison with the use of expendable cartridges include reduced weight and volume of spare parts, a constant rate of conversion of CO to CO_2 and carbon, and, probably, reduced crew time. A more complete comparison, however, of the cartridge approach with the continuous reactor approach is needed before one is selected for a manned test.

10. Suitability of palladium membranes for separating hydrogen from the process stream was demonstrated by successful operation of the system. Changes in the membrane thickness and brazing techniques employed are recommended in order to increase the average membrane life.

11. The ability to cool and reheat the process stream in copper lined tubing and vessels without blockage due to carbon deposition was demonstrated.

2.2 Component Development

The success achieved in the operation of the breadboard system was built on the component development accomplished during the developmental phase of this program. The electrolysis battery fabrication technique, the system operating conditions, and the design of the carbon deposition reactor and hydrogen diffuser were based on the results of this phase. Specific conclusions reached in this phase include those listed below.

1. Sintered Pt-ZrO_2 electrodes, containing 70% platinum and 30% ZrO_2 by volume, have a porous structure and are tightly adherent to the electrolyte. They are suitable for use as either the anode or cathode of a solid electrolyte electrolysis cell. Both electrode composition and electrode weight are easily controlled for this type of electrode.

2. A significant decrease in the rate of performance decline for multi-celled stacks of solid electrolyte electrolysis cells was

achieved as a result of the combined effects of (a) using sintered Pt-ZrO_2 electrodes, (b) maintaining close tolerances in the machining of the solid electrolyte components, (c) placing the anode on the interior of the cells (away from the point where the gold wire is placed during brazing) and (d) the use of individual cells of large surface area.

3. The current density utilized and the degree to which CO_2 and H_2O are converted to CO and H_2 in the electrolysis cells exert a strong influence on the life of the cells. Five three-cell stacks tested at current densities of 200 ma/cm^2 or less and at a degree of gas decomposition of 0.7 or less had an average life of 228 days. These units required an average of 198 watts/man initially and this figure increased by only 0.2% per day over their entire life.

4. Operation at a current density of 200 ma/cm^2 or higher and, simultaneously, at a degree of gas decomposition approaching 0.8 cause reduction of the electrolyte and decrease in the effective cell life to 30 days or less.

5. However, degrees of gas decomposition exceeding 0.8 can be achieved by reducing the current density in the cells operating on highly decomposed gases and/or by using electrode materials such as nickel and cobalt for the cathodes on these cells.

6. The ratio of iron to carbon in the carbon removed from the carbon deposition reactor can be reduced to 0.027 or less by leaving a thick layer of carbon (0.5 to 1.0 cm) on the catalyst surface at the time of scraping.

7. Palladium tubes, operated at 850°C in an atmosphere containing CO, CO_2, and water in addition to hydrogen, showed no sign of mechanical or performance deterioration in a 71-day life test. The permeation rate was found to vary with the hydrogen partial pressure to the 0.65 power.

2.3 Integration of Carbon Dioxide Concentrator with Solid Electrolyte Oxygen Regenerator

A study was made of the effects on design and equivalent weight of coupling the solid electrolyte oxygen regenerator to four different CO_2 concentrators. The four CO_2 concentrators were: steam desorbed resin, molecular sieve, hydrogen depolarized cell, and carbonation cell.

The study indicated that all four concentrators can be integrated with the solid electrolyte system. The hydrogen depolarized cell and the carbonation cell concentrators, however, will require modifications to and an increase in size of the solid electrolyte unit. The estimated equivalent weights of the integrated systems (to provide sufficient oxygen for a nine-man, 500-day mission) are:

Steam desorbed resin	3098 lbs
Molecular sieve	3265
Hydrogen depolarized cell	3153
Carbonation cell	3284

3. RECOMMENDATIONS

Based on the successful 180-day life test of the breadboard system, Westinghouse recommends that the development program for solid electrolyte oxygen regeneration be continued so that a unit of multi-man capacity can be utilized in the next manned life support test of long duration.

Work should be started immediately on the conceptual design of a multi-manned system. In the first system to be coupled with a CO_2 concentrator, the interface between the concentrator and the regenerator should be defined to minimize interdependence. This will maximize the probability for successful operation of both systems. Modification of the interface, or of the systems themselves, to take advantage of possible synergistic effects should be postponed until the second generation.

Emphasis should be placed on the following items in the conceptual design study.

1. Thermal control. Each component must be maintained at the desired operating temperature, despite changes in the oxygen generation rate, conductivity of the insulation, or electrical properties of the electrolysis cells. To minimize system power requirements, the resistive and chemical reaction heats generated in the electrolysis and carbon deposition processes should be utilized.
2. Conceptual design of equipment to accomplish automatic or semi-automatic scraping and handling of carbon.
3. Selection of carbon deposition approach. A choice should be made between the use of disposable catalyst cartridges and the use of a continuous carbon deposition reactor in which the catalyst

is self-contained but carbon must be removed periodically. The decision should be based upon:

a. feasibility of automatic scraping and handling procedure above.

b. probability of trouble-free system operation with the catalyst cartridge approach.

c. a comparison of the total system equivalent weights using the two approaches.

d. crew time projected for each approach.

4. Design of the electrolyzer to insure good flow distribution and sufficient ruggedness to withstand handling by the crew.

5. Design of all components to facilitate trouble-shooting and maintenance, including the ability to shut down one component of the system while the remainder of the system remains in operation.

A modest experimental effort, to be carried out in parallel with the conceptual design study, would aid in obtaining an optimum design. This work should include efforts to increase the life of the palladium membranes, to further increase the life of electrolysis stacks operating with degrees of decomposition between 0.6 and 0.7, and to build stacks that can operate at degrees of decomposition of 0.75 or higher.

Completion of a satisfactory conceptual design should be followed by the detailed design and construction of a solid electrolyte oxygen regeneration system of multi-man capacity.

4. DESCRIPTION OF BREADBOARD SYSTEM

4.1 Flow Diagram and Material Balance

A flow diagram of the breadboard system and a material balance for a 1/4-man oxygen rate are presented in Fig. 2. Stream compositions and flow rates are given for all significant locations. The raw feed rate is based on an oxygen requirement per man of 2.0 lb/day of which 1.57 lb comes from carbon dioxide and 0.43 lb comes from water. The recycle stream composition and flow rate approximate the actual operating conditions for most of the life test.

4.2 Design Philosophy

A major consideration in building the breadboard was sufficient built-in redundancy and flexibility to insure long life. The electrolysis unit was designed for easy maintenance. This was done by installing in the unit more electrolysis stacks than were actually needed to provide 125 cc/minute of oxygen, by providing each stack with a shut off valve so that it could be isolated from the system in case it were broken, and by providing leads from each stack to an outside control panel. With these provisions, a defective stack could be identified, isolated, and replaced with a fresh stack without opening the system. Other redundant components included four palladium tubes and an extra recycle pump. Flexibility was provided by using oversized pumps. Sufficient automatic control was provided to allow unattended operation for long periods of time. No attempt to minimize system weight was made. Off-the-shelf sensors, control elements, furnaces, tubing, valves, etc., were used wherever possible.

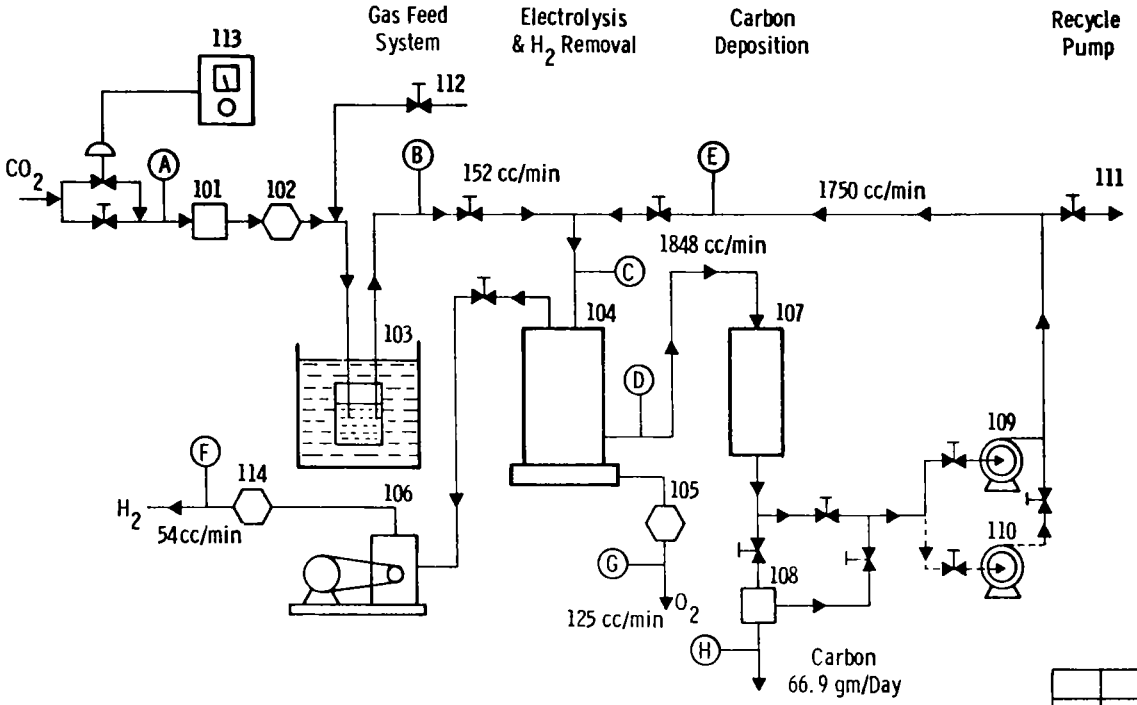

	EQUIPMENT
101	MASS FLOW METER
102	WET TEST METER
103	WATER SATURATOR
104	ELECTROLYSIS UNIT
105	WET TEST METER
106	VACUUM PUMP
107	CARBON DEP REACTOR
108	CARBON COLLECTOR
109	RECYCLE PUMP
110	AUX PUMP
111	OPEN LOOP DISCHARGE
112	OPEN LOOP FEED
113	CO_2 FEED CONTROLLER
114	WET TEST METER

Stream Composition And Flow Rate

	A		B		C		D		E		F		G		H	
	M/D	%	M/D	%	M/D	%	M/D	%	M/D	%	M/D	%	M/D	%	M/D	%
CO	0	0	0	0	42.9	39.6	54.6	51.9	42.8	43.0	0	0	0	0	0	0
CO_2	5.57	100	5.57	64.5	55.9	51.6	44.1	41.9	50.3	50.5	0	0	0	0	0	0
H_2	0	0	0	0	4.9	4.6	4.31	4.1	4.98	4.98	3.07	100	0	0	0	0
H_2O	0	0	3.07	35.5	4.5	4.2	2.10	2.0	1.49	1.49	0	0	0	0	0	0
O_2	0	0	0	0	0	0	0	0	0	0	0	0	7.11	100	0	0
C	0	0	0	0	0	0	0	0	0	0	0	0	0	0	5.57	100

M/D = Gram Moles/Day

Fig. 2—Flow diagram and projected material balance for 1/4-man oxygen regeneration system

4.3 Component Description

4.3.1 Electrolysis Unit

The electrolysis unit comprised twenty oxygen production stacks, six palladium tubes for removing hydrogen, a base plate, and a housing. Each oxygen production stack consisted of seven bell and spigot electrolysis cells, plus an end cap and a base tube, connected together in series. Both inner and outer electrodes were sintered composites of Pt and $(ZrO_2)_{0.9}(Y_2O_3)_{0.1}$. The coating weight was 12-15 mg/cm^2. The bell and spigot concept and electrode arrangement are illustrated in Fig. 3. The electroding technique utilized is described in Appendix A, and the overall fabrication technique for the electrolysis stacks is described in Section B.3 of Appendix B. In the breadboard system the inside electrode was the anode and produced the oxygen. The advantage of this arrangement was that no metal parts of the electrolyzer came into contact with hot oxygen.

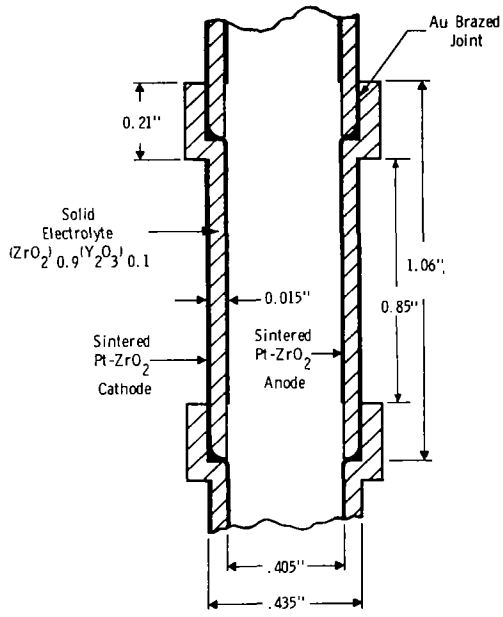

Fig. 3 -- Bell and spigot electrolysis cells and electrode arrangement

Figure 4 shows the design of the base plate. Numbered circles in the top view represent sockets that held the electrolysis stacks. The base plate was provided with four 15-terminal insulated headers for attaching current leads and eight two-terminal headers for thermocouple leads. It also contained a built-in oxygen manifold that connected with all of the stacks. A shutoff valve was installed at each manifold connection to allow those stacks not in use to be isolated from the manifold. The material of construction was Inconel 600.

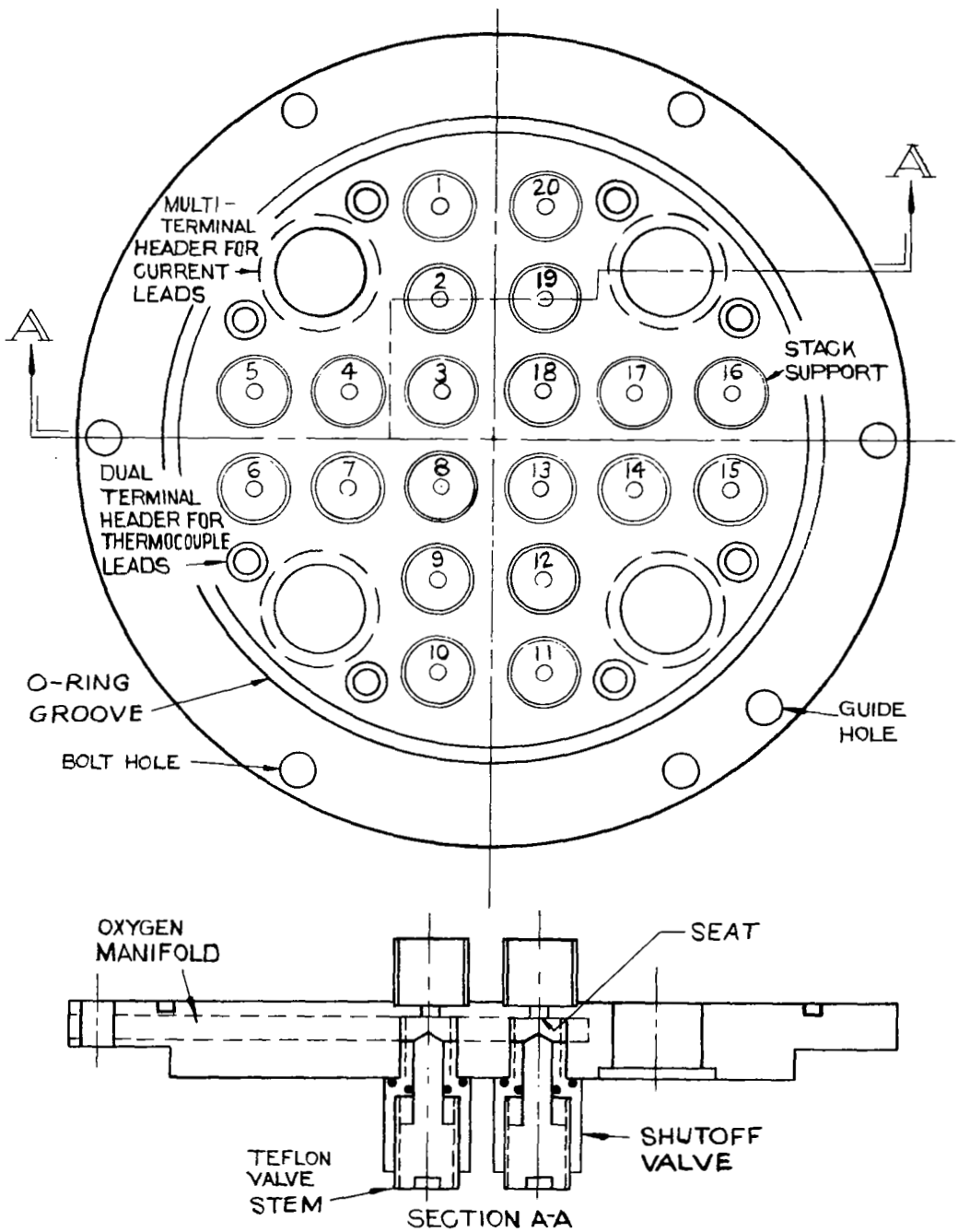

Fig. 4 - Base plate for electrolysis unit

Outside and inside views of the housing are shown in Fig. 5 and 6. The housing was constructed entirely of Inconel 600 and all seams and joints were heliarc welded. Baffle plates divided the electrolysis chamber into four compartments, each housing five electrolysis stacks. The gas feed entered at the top from a preheating coil and flowed alternately downward and upward through the four compartments and out the exit port. Short circuiting of the flow path at the bottom was minimized by embedding the lower ends of the baffles in the insulation around the base tubes.

To prevent carbon deposition on the Inconel parts that extended through the temperature gradient zones at the top and bottom of the furnace, the parts were clad with copper, which is noncatalytic. Deoxidized copper tube linings were fitted inside the gas feed and discharge tubes by swaging before the tubes were coiled or bent. For protection in the lower zone, the bottom 4 inches of the inner wall

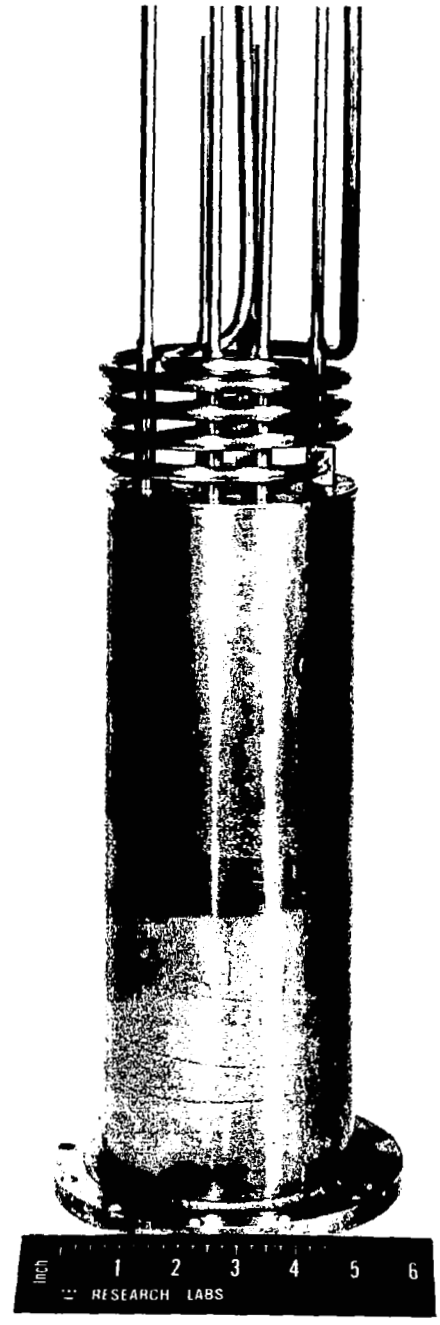

Fig. 5 -- Outside view of housing of electrolysis unit showing gas lines and vacuum manifold connecting tubes at top

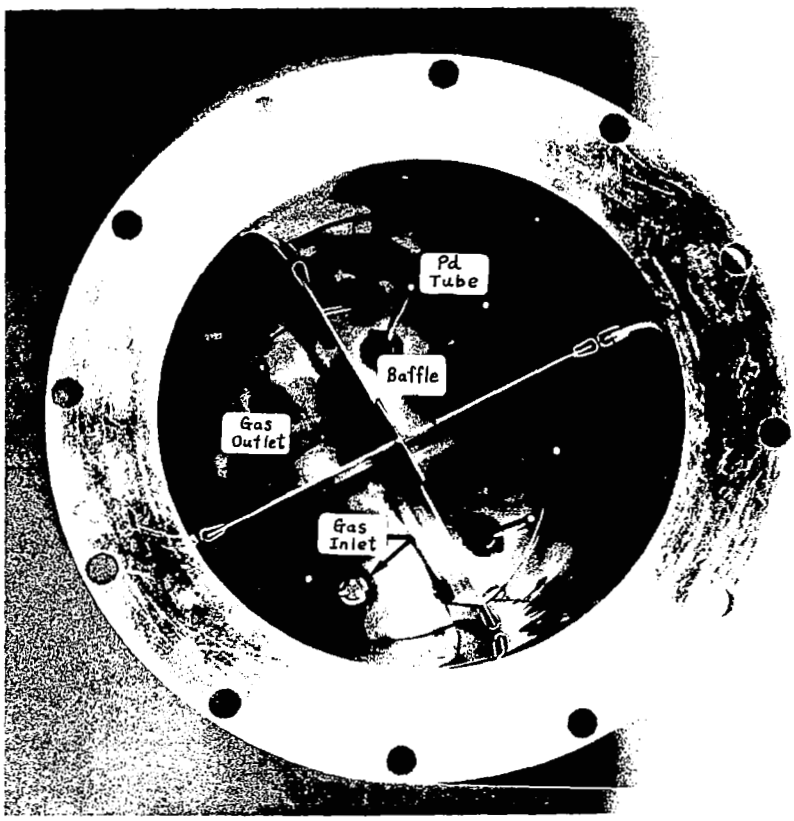

Fig. 6 -- Inside view of housing showing baffles and palladium membranes.

of the housing was heavily electroplated with copper after a thin initial coat of gold.

Figure 7 shows the stacks mounted on the base plate with lead wires and part of the insulation in place. The stacks were cemented into the base plate sockets with a room temperature vulcanizing rubber that withstands temperatures to 260°C. As each stack was mounted, current leads and thermocouple wires were attached and connected to the insulated headers. The final step before attaching the housing was to add 5 inches of Fiberfrax block insulation around the base tubes.

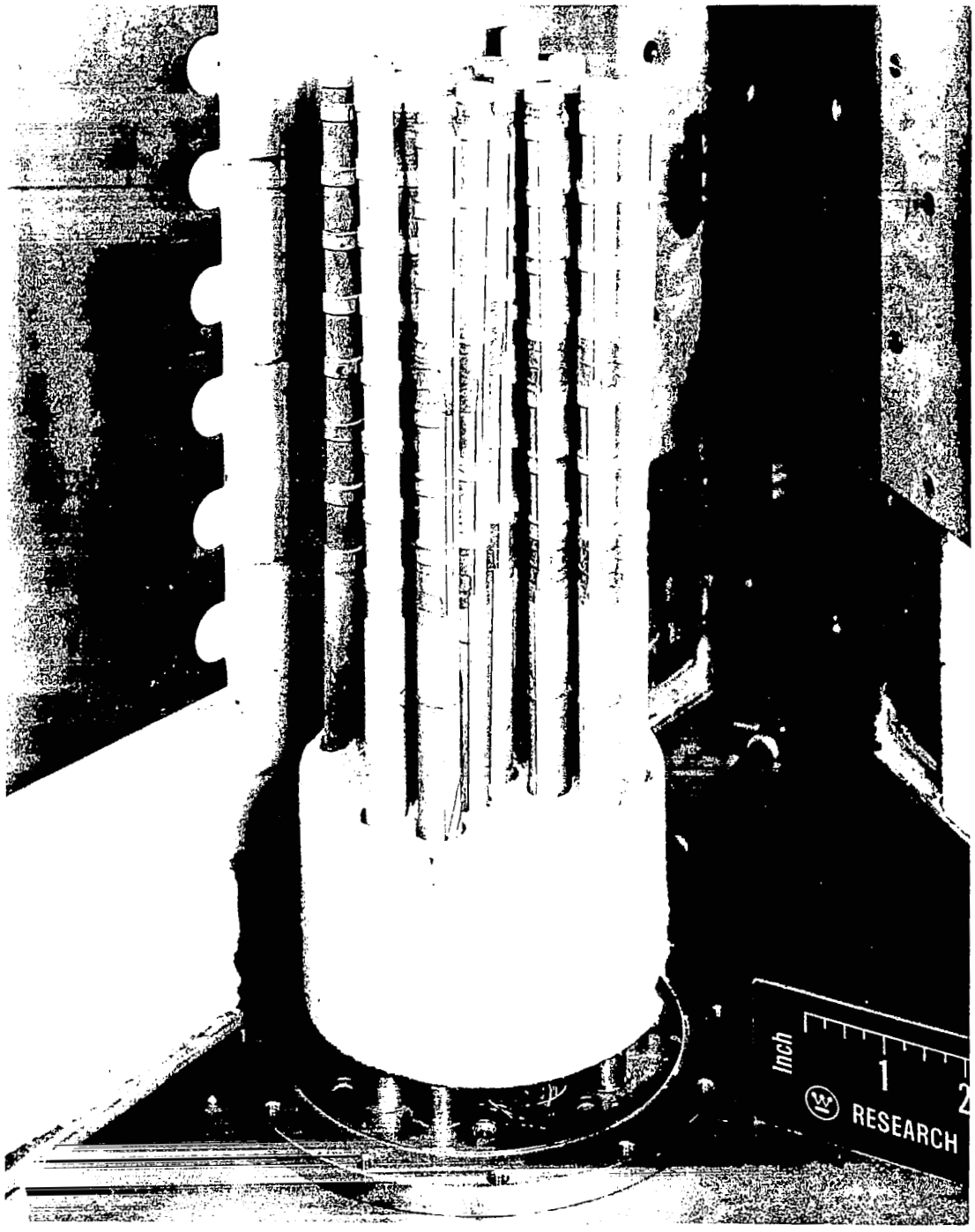

Fig. 7 - Electrolysis stacks mounted on base plate with wiring and part of insulation in place.

4.3.2 Hydrogen Separation

The six palladium-tube membranes used for hydrogen separation were contained in the electrolysis unit as shown in Fig. 6. The gas inlet and outlet compartments (at bottom and left center in Fig. 6) contained one membrane each. Two membranes were placed in each of the other two compartments. The membrane tubes were 1/8-in. o.d. by 0.005 in. wall by 8 in. long, and were closed at the free end. In addition to the six 8-in. long membranes, a 3-in. long membrane was installed in the gas exit port to serve as a hydrogen gauge.

The open ends of the palladium membranes were copper brazed to Inconel tubes which were attached to the housing in the manner shown in Fig. 8. This method was adopted for convenience in welding and to make replacement of membranes possible (although not during operation of the unit).

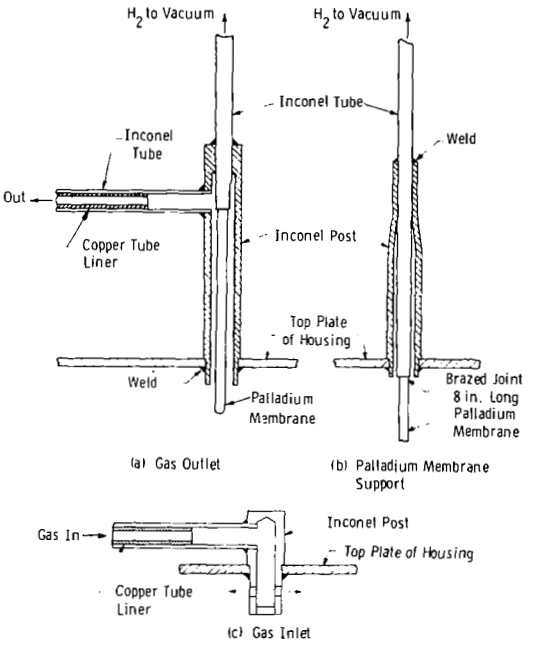

Fig. 8 -- Attachment of palladium membranes and gas lines to housing of electrolysis unit

The vacuum system is illustrated in Fig. 9. It included a vacuum pump, a manifold with a shutoff valve for each palladium membrane, a control valve, and two pressure guages. One valve was used to isolate the 3-in. palladium membrane and the absolute pressure gauge from the manifold so that the partial pressure of hydrogen in the system gas could be read.

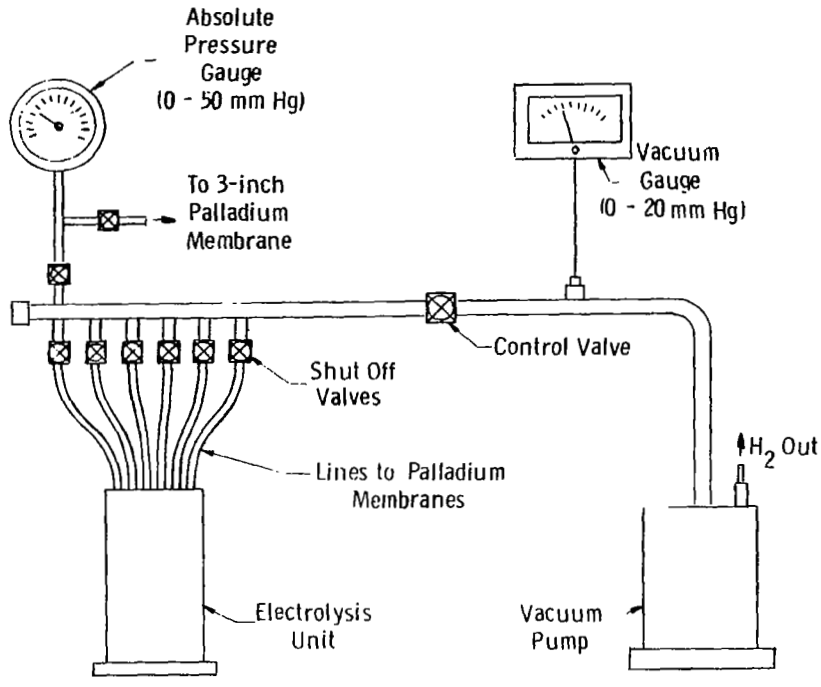

Fig. 9 -- Vacuum system for hydrogen separation

4.3.3 Carbon Deposition Reactor

A schematic drawing of the carbon deposition reactor is shown in Fig. 10. The reactor consisted of a cylindrical reaction vessel, a hand-operated scraper for removing the carbon deposit from the reactor wall, and a removable carbon collection jar. The lining of the reaction chamber was made of 1015 carbon steel and served as the catalyst for the carbon producing reaction. It was 8 in. long and averaged 2 in. i.d. It was made thicker at the top to compensate for the greater rate of iron consumption that was expected at the feed end.

The scraper was made of Inconel 600 and consisted of a rotatable shaft to which five 1/2-in. wide blades were welded. Clearance between the cutting edges of the blades and the reactor wall varied from 3/16-in. at the top to 5/16-in. at the bottom because of the tapered construction of the catalyst tube. The purpose of the large clearance was to leave

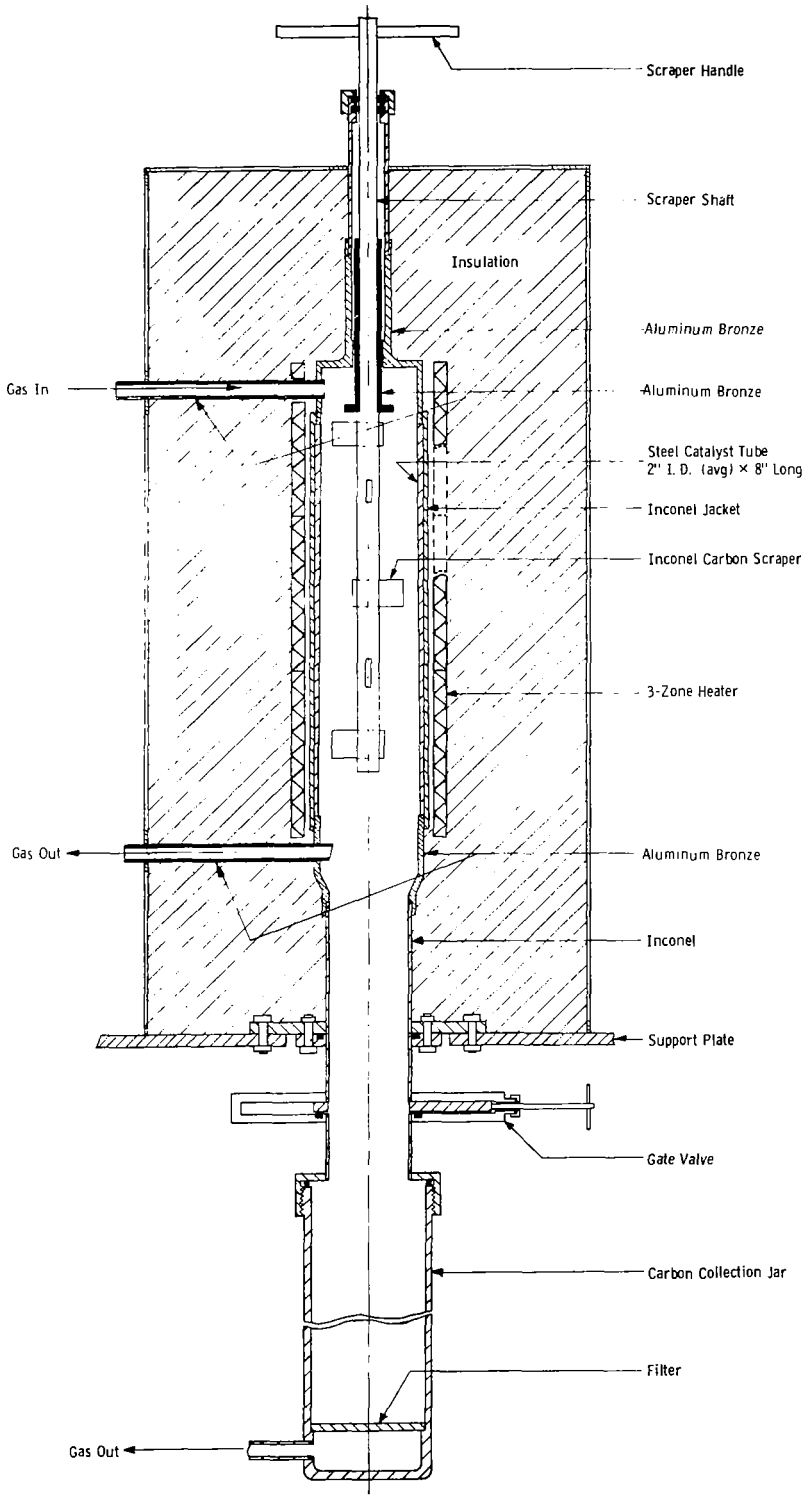

Fig. 10 - Carbon deposition reactor for breadboard system

a thick carbon layer on the wall after scraping. Previous experience had shown that this technique reduced iron consumption by the carbon (see Appendix D). The scraper shaft was hollow and was used as a thermocouple well.

The inlet and outlet vestibules and gas lines of the reactor were constructed of aluminum bronze (Ampco Metal Grade 8). This alloy was thought to be noncatalytic to carbon deposition and was used to prevent clogging of the entrance and exit of the reactor by carbon.

The carbon deposition reactor was sized to hold one day's production of carbon so that the breadboard system could be left unattended on weekends for periods up to 24 hours. The size with respect to the ability to produce carbon at the required rate was deemed to be more than adequate. This judgment was based on the results of a reaction rate study conducted with a differential reactor. The work is described in Appendix D.

4.3.4 Auxiliary Equipment

Gas circulation through the electrolysis unit and around the loop was effected with a diaphragm pump (Neptune Dynapump, Model 2) which was rated at 3600 cc/min at 55 in. of water. An auxiliary pump was installed in parallel. A porous stainless steel filter (Nupro Inline Filter No. 6F) preceded each pump to remove carbon dust. The maximum pumping rate used in the life test was 1800 cc/min and the maximum delivery pressure was 15 in. of water. The pressure drop across the filters gradually increased as they became clogged with carbon and oversized pumps were needed to avoid too frequent cleaning of the filter elements. No attempt was made to maximize pumping efficiency. In addition to the porous steel filters, a coarse filter chamber with clean-out plugs was connected directly to the carbon deposition reactor outlet.

The electrolysis unit was heated by a four-zone split-tube furnace. The furnace chamber measured 5 in. i.d. by 12 in. long and the

insulated vestibules at the ends of the chamber were 4 1/2 in. long. The carbon deposition reactor was heated with a three-zone furnace. The heating elements were wound directly onto the reactor shell.

The water saturator, which was used to introduce the water feed into the CO_2 feed stream, consisted of two bubblers connected in series and held in a constant temperature bath.

The two furnaces, the recycle pumps, and the filters are shown in the photograph of the breadboard system in Fig. 11. Figure 12 shows the control panel.

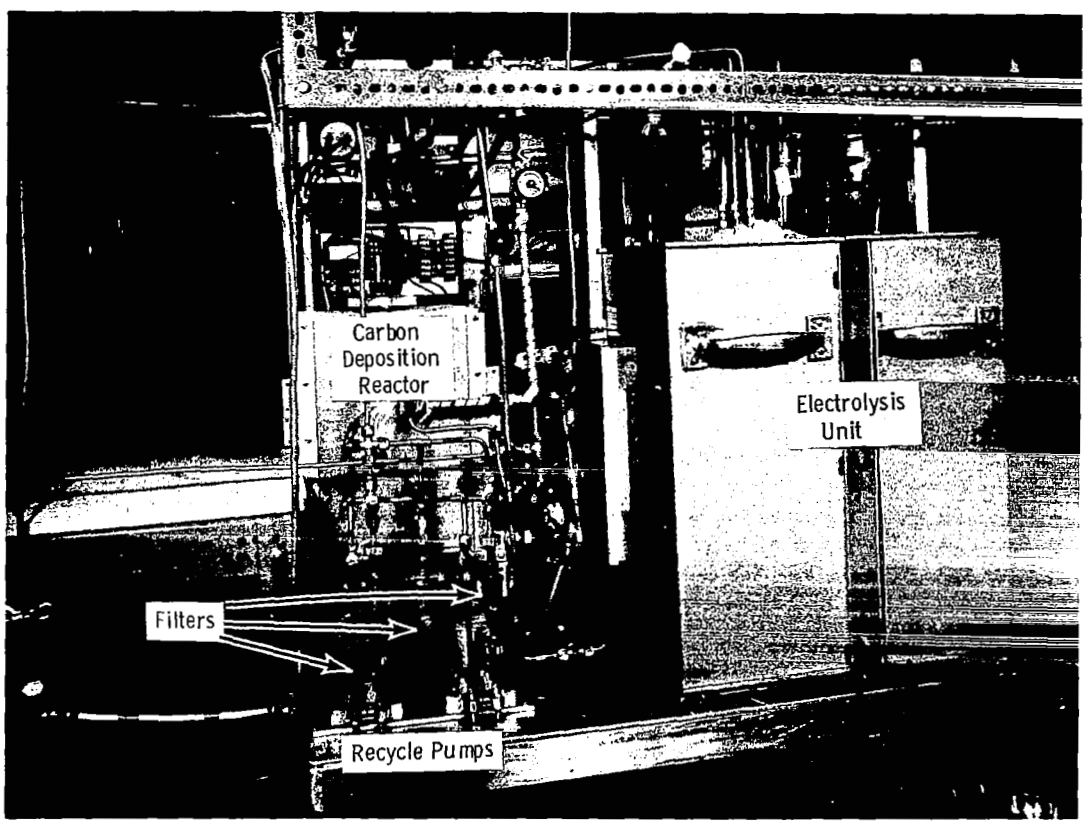

Fig. 11 -- Breadboard oxygen regeneration system

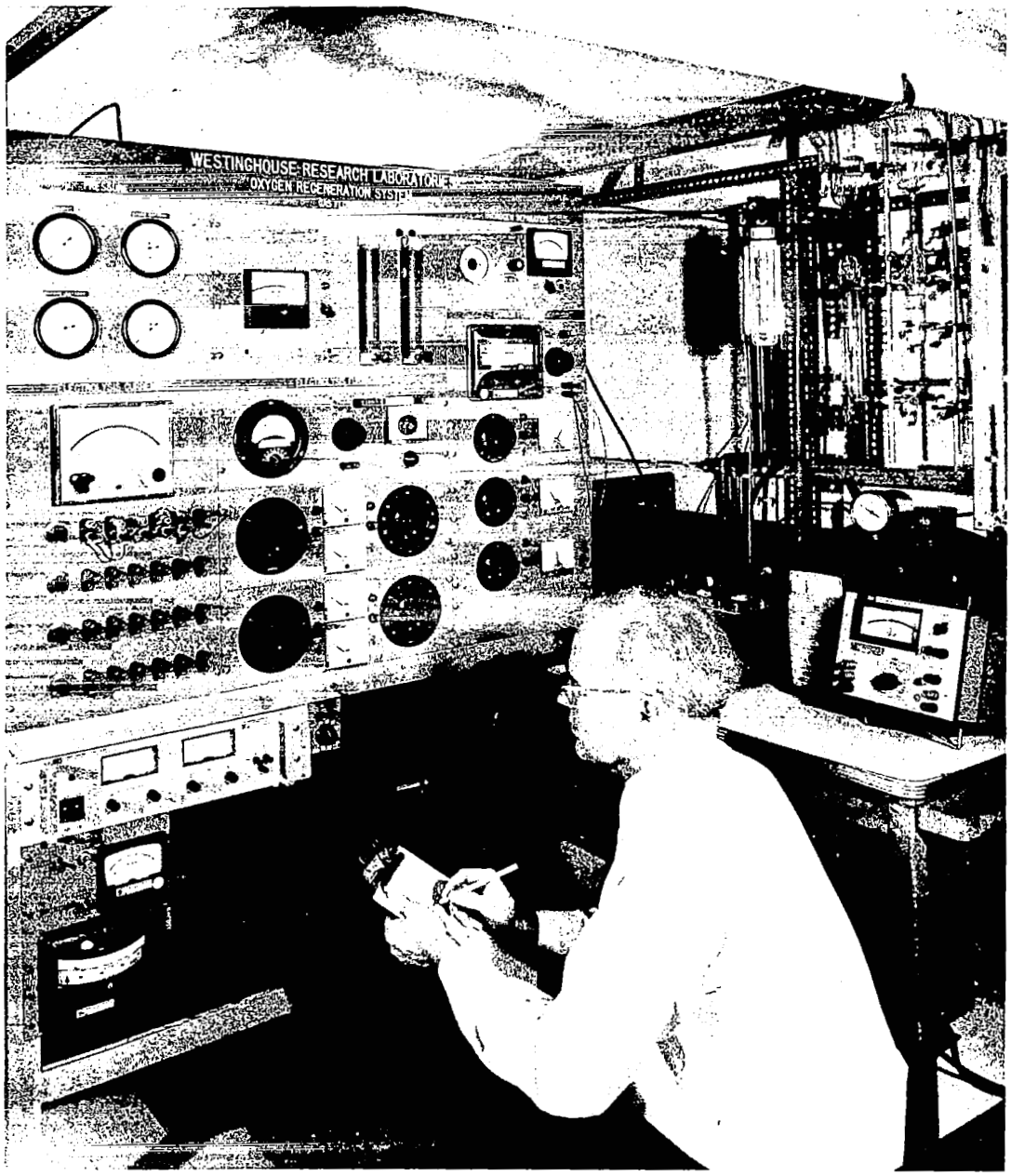

Fig. 12 - Control panel.

4.4 Control of Operation

The control philosophy for operating the system called for maintaining constant oxygen production, constant feed composition, constant system pressure, and constant gas composition at the electrolyzer exit. A constant rate of oxygen production was obtained by controlling the electrolysis current, and constant feed composition was obtained by controlling the temperature of the water saturator. For overall system control, the primary requirement was to match the raw feed rate to the rate of oxygen production to prevent gross changes in system pressure. This was accomplished by providing proportional control of the CO_2 feed, using system pressure as the control signal.

The need for controlling the gas composition leaving the electrolyzer was indicated by prior experience which had shown that 3 to 5% H_2 in the gas was required to promote the carbon deposition reaction (Reference 3, pp 66-69) and that the overall degree of decomposition of CO_2 and H_2O should not exceed about 0.7 to insure long cell life (see Appendix C).

Control of H_2 concentration at the electrolyzer exit was effected by means of a needle valve in the vacuum line between the palladium tube manifold and the vacuum pump (see Fig. 9). This valve was used to control the manifold pressure which, in turn, affected the pressure drop across the palladium membranes. Regardless of the valve setting, the concentration of H_2 in the system adjusted itself automatically until the permeation rate through the membranes equaled the rate of H_2 input as water.

Control of the degree of decomposition was effected by varying the recycle rate. As the recycle rate is increased, the degree of decomposition decreases until limited by equilibrium of the carbon deposition reaction or by the reaction capacity of the reactor. The degree of decomposition can also be influenced by varying the reactor temperature.

4.5 Instrumentation and Measurements

The instruments and measuring techniques used to acquire data on the breadboard system are outlined below:

1. CO_2 feed rate

   a) Mass flowmeter - Hastings-Raydist, Model CLL500

   b) Calibrated wet test meter for integrating flow - American Meter Company, Model AL-17-1

   c) Proportional controller in auxillary feed stream with electronic sensing element mounted on one leg of water manometer - Matheson Gas Products, Lab-Stat Model 8220.

2. H_2O feed rate

   a) Water saturator temperature controller - Cole-Parmer Model TE1

   b) Weighed make-up water added each day

3. Oxygen output

   a) Float type flowmeter - Matheson Gas Products, Model 620

   b) Calibrated wet test meter for integrating flow - American Meter Company, Model AL-17-1

4. Carbon output

   a) Emptied carbon jar every other day and weighed deposit

5. Hydrogen output

   a) Thermocouple vacuum gauge calibrated to indicate hydrogen flow - Hastings-Raydist, Model VT-4

   b) Calibrated wet test meter to integrate flow - American Meter Company, Model AL-17-1

6. Recycle flow rate

   a) Float type flowmeter - Matheson Gas Products, Model 620

7. Electrolysis current

   a) Constant current power supply - Hewlett-Packard Model 6428B

   b) Calibrated ammeter

8. Driving voltage

   a) Calibrated voltmeter

   b) Voltmeter on power supply

9. Electrolysis furnace power

   a) Variable transformer and ammeter for each furnace zone

   b) Line voltage regulator

10. Carbon deposition furnace power

   a) Variable transformer and ammeter for each furnace zone

   b) Line voltage regulator

11. Temperature measurements

   a) Thermocouple through furnace wall in each furnace zone

   b) Eight thermocouples attached to stacks inside electrolysis unit

   c) Thermocouple probe inside scraper shaft of carbon deposition reactor

   d) Thermocouple in base plate of electrolysis unit

12. Pressure measurement

   a) Oxygen manifold - diaphragm gauge, 0 to 10" water, Marshalltown Mfg.

   b) Electrolyzer exit - same

   c) Carbon deposition reactor exit - same

   d) Between filter and recycle pump - same

   e) Palladium tube manifold - Wallace & Tiernan, No. FA-16030

   f) Between hydrogen control valve and vacuum pump - Hastings-Raydist, Model VT-4

13. Chemical analysis (See Appendix I)

a) Oxygen product - gravimetric analysis for CO_2 and H_2O twice per week. Occasional mass spectrometer analysis.

b) Carbon product - gravimetric analysis for iron every fourth day. Occasional analysis for carbon and hydrogen.

c) Hydrogen product - gravimetric analysis for CO_2 and H_2O once each week. Occasional mass spectrometer analysis.

d) Electrolyzer exit gas - mass spectrometer analysis once each week.

e) Carbon deposition reactor exit gas - mass spectrometer analysis once each week.

f) CO_2 feed - occasional mass spectrometer analysis.

5. RESULTS OF LIFE TEST

5.1 Overall Performance

The 180-day life test was started on July 9, 1970 and was completed successfully on January 8, 1971. Total oxygen production was 1,159 cu ft. The production rate, which was constant within a few percent, averaged 0.254 man. The power required varied from 242 watts/man to 313 watts/man with an average requirement of 283.5 watts/man (i.e., to produce 2.0 lbs/day of O_2.

The reliability of the electrolysis unit exceeded all expectations. Even though six of the electrolysis stacks (Nos. 1, 2, 3, 4, 5, and 11) were run throughout the life test and produced more than 95% of the total oxygen, not a single cell failed. The total operating time of these stacks, including open loop testing prior to the life test, was more than 200 days.

Carbon production was 26.45 lb and the weight of iron catalyst consumed by the carbon was 0.72 lb. The weight ratio of carbon to iron was 36.7 to 1, a substantial improvement over the ratio of 27 to 1 achieved in the previous investigation (Reference 3, p. 78).

A data log of the life test is given in Appendix H.

5.1.1 Operation and Maintenance Time

Operation of the system was stable and little operator time was needed for control. After the first 10 days of the life test, the apparatus was completely unattended for 15 hours each day on week days and for 20 hours each day on weekends.

Both hydrogen removal and carbon deposition were self-regulating. An upset of either from the steady state condition caused an immediate

change in the recycle gas composition which tended to return the hydrogen removal rate or the carbon deposition rate to its original level.

Operator time, other than that needed for taking data, averaged about 18 min. per day of which 12 min. per day was used for the scraping and removal of carbon. The carbon deposit was scraped twice each day and the collection jar was emptied once every two days.

Total maintenance time was 1098 min. This time was used, for the most part, for cleaning the filters ahead of the recycle pumps, for locating and repairing gas leaks, and for identifying leaking palladium membranes.

Leaking palladium membranes constituted the only major equipment failure. Of six membranes that were installed, only one survived the life test. Three membranes cracked during preliminary testing of the system and two developed slow leaks during the life test itself.

The separate maintenance tasks and time consumed for each are listed in Table I.

5.1.2 Operating Adjustments

Several adjustments in the operation of the system were necessary during the life test. All were accomplished, however, without reducing the rate of oxygen production. This is shown by Table II and Fig. 13, summarizing the operating conditions and results of the test.

The first significant adjustment was to change the temperature profile of the carbon deposition reactor to improve reactor performance. This change, which was made on the 41st day, is discussed in Section 5.4.1.

On the 75th day one of three operating palladium membranes was closed off because of excessive leakage. The two remaining membranes had ample capacity to maintain the rate of hydrogen removal at the original level and no change in operating conditions was required. However, on the 142nd day, after a second palladium membrane was removed from service, the hydrogen separation capacity was no longer adequate and it was necessary to decrease the hydrogen production rate by lowering the water feed

TABLE I

MAINTENANCE ON BREADBOARD SYSTEM
DURING LIFE TEST

Test Day	Maintenance Task	Time Required, Min.
	Routine Tasks:	
5	Leak check	90
28	Clean stainless steel inline filter	15
33	Repair gas leak	15
33	Clean oxygen flowmeter	10
34	Clean carbon deposition reactor gas outlet	23
46	Clean stainless steel and coarse filters	6
48	Clean stainless steel and coarse filters	6
48	Clean pressure gauge line	10
51	Clean stainless steel and coarse filters	13
53	Clean stainless steel and coarse filters	6
56	Clean stainless steel and coarse filters	6
60	Clean filters and install new pump	24
63	Replace toggle valve	6
64	Clean coarse filter	6
65	Clean stainless steel and coarse filters	11
67	Clean coarse filter	3
68	Clean CDR inlet and outlet lines	27
71	Clean coarse filter	3
74	Clean coarse filter	10
78	Clean recycle flowmeter	15
79	Clean oxygen flowmeter	5

TABLE I (Concluded)

Test Day	Maintenance Task	Time Required, Min.
	Routine Tasks:	
86	Clean stainless steel and coarse filters	6
89	Clean oxygen flowmeter	5
99	Clean stainless steel and coarse filters	6
104	Clean stainless steel filter	6
109	Clean stainless steel and coarse filters	12
125	Replace stainless steel filter elements	20
140	Clean stainless steel and coarse filters	6
153	Clean stainless steel and coarse filters	6
154	Replace copper tube fitting	10
162	Replace furnace thermocouple	5
173	Clean stainless steel and coarse filters	6
	Total	398
	Nonroutine Tasks:	
20	Break up carbon bridge in CDR	30
32	Replace water bath temperature controller	10
56	Palladium tube leak check	120
75	Palladium tube leak check	210
77	Electrical check of electrolysis stacks	120
142	Palladium tube leak check	120
153	Replace water bath temperature controller	10
153	Remove water from pressure lines and recycle pump	50
165	Base plate cooling water replaced with air	30
	Total	700
	Overall Total	1098

TABLE II

RESULTS OF 180 DAY LIFE TEST

	1	2	3	4	5	6	7	8	9	10	11	12	13	14	15
Test Days	CO_2 Feed,[a] cc/min	H_2O Feed,[a] cc/min	Recycle Flow,[a] cc/min	Oxygen Produced,[a] cc/min	Hydrogen Removed,[a] cc/min	Carbon Produced, g/day	Elect. Temp., °C	Avg. CDR[b] Temp., °C	Elect. Current, amps	Stacks in Oper.	Current Density, ma/cm^2	Driving Voltage, volts	Current Eff., %	Oxygen Purity, %	Power Per Man, watts
0-10	96.5	58.1	1373	126.0	52.3	51.5	900	530	5.26	7	125.2	12.2	87.2	97.0	253.6
11-20	96.7	55.3	1353	126.5	48.7	63.2	900	530	5.31	7	126.4	12.6	84.8	96.0	263.4
21-30	100.2	57.2	1565	125.1	46.9	65.9	900	542	5.59	7	133.1	12.7	82.4	96.6	282.6
31-40	100.8	61.5	1780	127.8	53.0	70.5	900	542	5.64	6	156.6	12.6	82.5	96.5	276.9
41-50	102.8	54.4	1780	129.9	53.4	69.6	900	552	5.69	6	158.0	12.7	83.8	96.5	277.0
51-60	102.8	55.8	1780	129.6	53.3	71.8	900	552	5.70	6	158.3	12.8	83.0	96.5	280.3
61-70	103.8	50.4	1780	128.4	54.2	69.9	900	549	5.70	6	158.3	12.8	82.7	96.0	282.9
71-80	106.9	51.5	1780	127.8	52.5	69.7	900	547	5.71	6[c]	146.0	12.5	81.8	96.5	278.1
81-90	104.3	52.3	1780	127.8	56.3	67.1	900	548	5.70	6	158.3	12.8	81.9	96.0	284.3
91-100	103.7	52.0	1780	125.7	54.9	65.4	900	546	5.70	6	158.3	12.6	80.8	96.0	284.5
101-110	105.8	50.9	1780	126.0	54.0	65.8	900	548	5.70	6	158.3	12.7	80.9	95.5	286.1
111-120	105.6	56.6	1780	126.0	53.1	69.2	900	546	5.70	6	158.3	12.7	80.9	94.5	286.1
121-130	106.2	56.1	1780	124.7	52.1	62.4	900	552	5.72	6	158.8	12.8	79.8	95.0	292.4
131-140	121.8	52.2	1780	126.7	44.4	65.1	900	554	5.80	6	161.1	12.9	80.0	94.0	294.1
141-150	124.8	23.9	1780	123.7	26.9	64.6	900	557	5.80	6	161.1	12.7	78.1	95.0	296.5
151-160	125.8	28.1	1780	123.9	29.4	69.1	900	558	5.80	6	161.1	12.8	78.1	93.8	298.4
161-170	123.1	30.2	1780	124.4	29.5	68.7	900	558	5.82	6	161.6	12.9	78.2	94.5	300.6
171-180	122.7	29.5	1780	127.7	28.6	70.7	900	559	6.11	6	169.7	12.9	76.6	94.5	307.4

a Flow at ambient conditions (25°C and 735 mm Hg)

b CDR = Carbon Deposition Reactor

c Ten stacks were used for 32 hours and 8 stacks were used for 16 hours on days 77 and 78

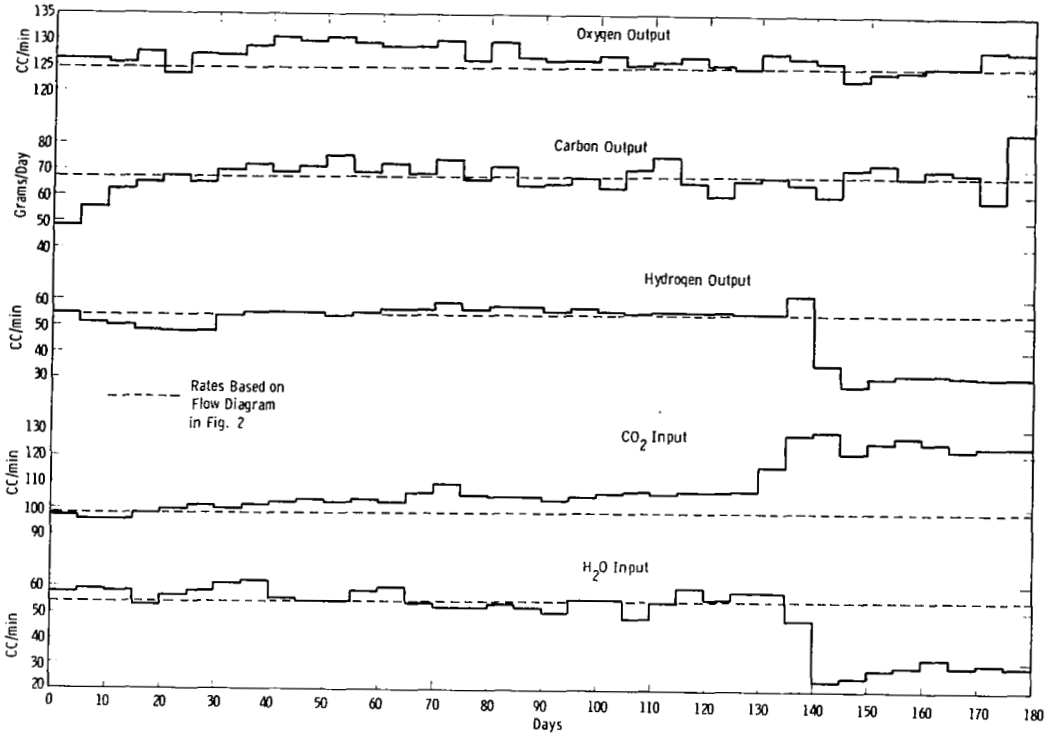

Fig. 13 -- Average inputs and outputs of materials for consecutive 5 day periods in life test.

rate. The CO_2 feed rate was increased at the same time so that the rate of oxygen production would remain constant. These changes are reflected in columns 1, 2, and 5 of Table II.

The ability of the system to operate safely, even when unattended, was demonstrated on the 77th day. During the night, a janitor unplugged the power leads to two zones of the electrolysis furnace. When the furnace started to cool, a safety switch shut off the electrolysis current to protect the cells. On discovery of the mishap seven hours later, the system was placed on open loop and the furnace was heated slowly back to the operating temperature. Closed loop operation was then resumed. The total down time was 15 hours. For the next few days the system was run at a low current density (by operating 10 stacks) while the condition

of the stacks was checked. No damage was detected. The lower current density during this period was responsible for the drop in power requirement per man that is shown in column 15 of Table II for test days 71-80. (The "down" period overlapped two test days. Since complete data were not available for these two days, both were omitted from the life test and the test was extended two days.)

No operating adjustment was needed to counteract nitrogen accumulation in the system. Nitrogen was introduced as an impurity in the CO_2 feed which was a commercial grade of gas containing 0.05 to 0.10% N_2. The concentration of N_2 in the recycle stream increased until the rate of input was offset by small leaks and by losses occurring during carbon removal. The average concentration was about 6% but concentrations up to 12% were observed. The presence of nitrogen at these levels seemed to have no adverse effects on the performance of the system.

Although a trace of methane was generated in the carbon deposition reactor, it was subsequently decomposed in the electrolysis unit (without carbon deposition) and, in contrast to the behavior of nitrogen, no buildup occurred. The average concentration of CH_4 in the carbon deposition reactor exit gas was 0.10%. The maximum concentration observed was 0.23%.

5.2 Overall Material Balances

Table III presents overall material balances for days 0-100, 0-140, 0-180. (A sample calculation for a 5-day period is given in Appendix J.) Closure of the material balances is extremely good. The major deviation is for carbon during the final 40 days of the test. The good material balance closure lends confidence to the data reported. It can be attributed to the use of calibrated wet test meters to integrate gas flows and to frequent analysis of the oxygen, hydrogen, and carbon products.

The most important information obtained from the overall material balance calculation is the net conversion to O_2 of the oxygen

TABLE III

OVERALL MATERIAL BALANCES

		0-100 Days	0-140 Days	0-180 Days
Carbon		cu ft	cu ft	cu ft
Input:	as CO_2	518.02	741.53	994.08
Output:	Solid carbon (CO_2 equiv.)	491.20	685.24	882.13
	as CO_2 in Oxygen	19.07	31.24	41.87
	as CO_2 in Hydrogen	2.72	4.84	8.23
	as CO in Hydrogen	3.32	5.92	10.05
	Total	516.31	727.24	942.38
Deviation		-0.33%	-1.90%	-5.34%
Hydrogen				
Input:	as H_2O	282.00	391.75	448.52
Output:	as H_2	267.36	375.67	429.07
	as H_2O in Hydrogen	0.67	1.19	2.03
	as H_2O in Oxygen	6.36	10.41	13.96
	Total	274.39	387.27	445.06
Deviation		-2.73%	-1.15%	-0.77%
Oxygen				
Input:	as CO_2	518.02	741.53	994.08
	as H_2O	141.00	195.88	224.27
	Total	659.02	937.41	1218.35
Output:	as O_2	648.34	904.40	1158.56
	as CO_2 in Oxygen	19.07	31.24	41.87
	as H_2O in Oxygen	3.18	5.21	6.98
	as CO_2 in Hydrogen	2.72	4.84	8.23
	as CO in Hydrogen	1.66	2.96	5.03
	as H_2O in Hydrogen	0.34	0.60	1.02
	Total	675.31	949.25	1221.69
Deviation		+2.44%	+1.25%	+0.27%
Net conversion of CO_2 and H_2O to O_2		98.4%	96.5%	95.1%

input in CO_2 and H_2O. Table III shows that 95.1% was converted during the entire 180 days. Of the 4.9% lost, 1.1% was lost to the H_2 off-gas and, in a space cabin, would be lost to the space vacuum. The remaining 3.8% would be recycled to the cabin with the breathable oxygen.

5.3 Electrolysis Unit Performance

5.3.1 Operating Characteristics

The electrolysis unit easily survived the life test with only occasional use of any of the redundant stacks. Performance of the stacks used was outstanding. The variations with time in driving voltage, current efficiency, power consumption and oxygen purity are shown in Fig. 14. The driving voltage per stack (including electrical leads) averaged 12.2

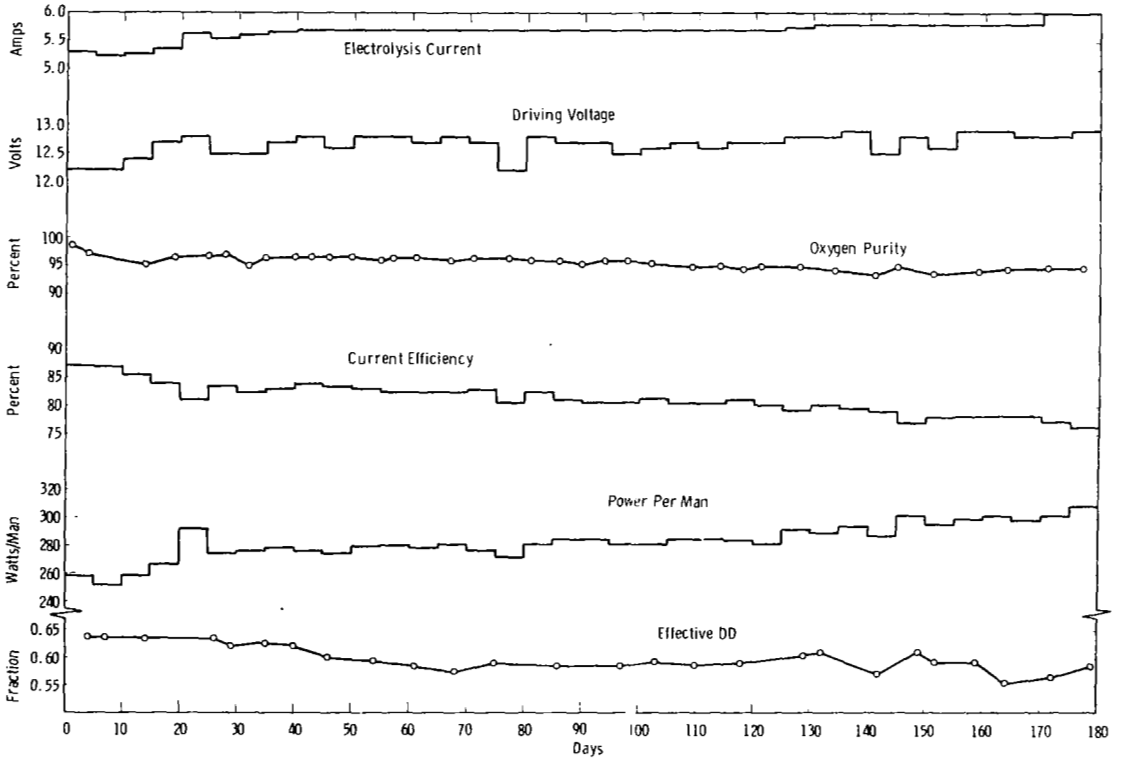

Fig. 14 -- Performance of electrolysis unit versus days of operation

volts in the first ten days and 12.9 volts in the final ten days. The corresponding values for current efficiency were 87.2% and 76.6%.

A comparison of the performance of the 1/4-man electrolysis unit with that of three-cell stacks used in a preliminary study of the effects of operating conditions (see Appendix C) is shown in Table IV. The driving voltage/cell for the 1/4-man unit is higher because no correction for lead resistance was made and because polarization was higher. The higher polarization resulted from poor gas circulation in the larger unit (see Appendix F.3).

TABLE IV

COMPARISON OF PERFORMANCE OF THREE-CELL ELECTROLYSIS STACKS AND 1/4-MAN UNIT

	3-Cell Stacks	1/4-Man Unit
Electrode Composition	Pt-ZrO_2 cermet	Pt-ZrO_2 cermet
Electrolyte Composition	$(ZrO_2)_{0.9}(Y_2O_3)_{0.1}$	$(ZrO_2)_{0.9}(Y_2O_3)_{0.1}$
Active Area/Cell, cm^2	6	6
Current Density, ma/cm^2	166-200	125-170
Average Cell Voltage, volts	$V = 1.44 + 0.0020t$[a]	
Initial	1.44	1.74[b]
Final	1.80	1.84[b]
Degree of Decomposition	0.6-0.7	0.55-0.6
Oxygen Purity, %		
Initial	97.0	99.2
Final	89.0	94.5
Current Efficiency, %		
Initial	91.6	87.6
Final	84.0	77.0
Electrolysis Power, watts/man	$P = 198 + .404t$[a]	
Initial	198	242
Final	271	305
Average	235	283.5
Time in Operation, days	180	180
Degradation Rate, watts/man/day	0.40	0.28

a. Statistical correlation of preliminary test results where t = days of operation.

b. No lead resistance correction.

The lower current efficiency in the 180-day test was due to an electrical leak to ground, which partially shorted stack 12. This stack was internally connected in series with Stack 11 which was one of the operating stacks. The ground was caused by Stack 12 contacting the housing or a broken palladium membrane.

The decline in current efficiency with time was caused mainly by increased ground shunt current which varied from 5.7% initially to 11.9% on the 180th day. Only 30% of the decline can be attributed to increased gas leakage through the cell joints. A breakdown of the difference between the theoretical current efficiency and the measured efficiency is presented in Table V. The calculation of the theoretical current efficiency and an estimation of current losses are given in Appendix F, Sections F4 and F5.

TABLE V

BREAKDOWN OF CURRENT EFFICIENCIES
OF ELECTROLYSIS STACKS VERSUS TIME

Day	Theoretical Current Efficiency, ε, %	$-\Delta\varepsilon$ Due to Gas Leakage, %	Measured Current Efficiency, %	$-\Delta\varepsilon$ Due to Ground Shunt Est. by Diff., %	$-\Delta\varepsilon$ Due to Ground Shunt Est. from Current Measurement, %
Initial	96	-2.7	87.6	5.7	----
27	95	-2.9	82.7	9.4	----
70	95	-3.4	83.4	8.2	11.6
128	95	-3.8	79.9	11.3	----
180	94	-5.5	76.6	11.9	8.8

The power degradation rate for the 1/4-man unit was 0.16%/day. This was lower than experienced with the three-cell stacks which degraded at a rate of 0.20%/day.

The rise in driving voltage during the life test of the 1/4-man unit was due to gradual increases in both cell resistance and polarization.

This was clearly shown by current interrupt tests which are summarized in Table VI. Resistance rose an average of 40% and polarization rose 60% for the six operating stacks. The unused stacks were found to have almost the same resistance at the end of the test as they had at the time of initial break-in.

TABLE VI

AVERAGE CELL RESISTANCE AND POLARIZATION
OF ELECTROLYSIS STACKS VERSUS TIME

Test Day		Stack Number						
		1	2	3	4	5	11	Avg.
Initial[a]	R[b] =	0.25	0.25	0.27	0.28	0.33	0.27	0.28
	V_p[c] =	0.27	0.24	0.30	0.24	0.33	0.33	0.29
27	R =	0.26	0.28	0.32	0.29	0.37	0.30	0.30
	V_p =	0.36	0.37	0.36	0.31	0.40	0.34	0.36
70	R =	0.34	0.31	0.35	0.33	0.40	0.33	0.34
	V_p =	0.38	0.42	0.47	0.38	0.42	0.35	0.40
128	R =	0.36	0.34	0.38	0.38	0.43	0.34	0.37
	V_p =	0.41	0.46	0.47	0.44	0.42	0.37	0.43
180	R =	0.35	0.36	0.40	0.45	0.43	0.35	0.39
	V_p =	0.44	0.50	0.49	0.51	0.42	0.39	0.46

a. At start of open loop runs, 33 days before start of life test

b. R = cell resistance, ohms

c. V_p = polarization voltage, volts

The electrolysis current to each operating stack was measured occasionally to determine the uniformity of current distribution and to detect changes that would indicate a decline in performance of a stack. The results, given in Table VII, show that current distribution was almost constant with time; the stacks aged uniformly.

TABLE VII

PERCENTAGE OF TOTAL CURRENT CARRIED
BY INDIVIDUAL STACKS
DURING 180 DAY LIFE TEST

Day	Stack Number					
	1	2	3	4	5	11
51	16.4	18.3	14.5	13.5	13.4	23.9
70	16.2	15.1	13.0	15.6	13.5	26.6
86	16.7	15.5	13.9	14.6	15.4	23.9
93	16.6	14.5	14.6	15.4	14.6	24.3
142	15.7	17.4	15.7	14.5	15.7	21.0
172	15.6	18.2	13.9	14.8	16.5	21.0
180	15.0	15.9	15.3	14.8	15.0	24.0
Average	16.1	16.4	14.4	14.7	14.9	23.5

Stacks 1, 2, 3, 4, and 5 carried approximately the same electrolysis current. Stack 11 appeared to carry a much higher current, due mainly to the ground shunt through Stack 12. The true current density of Stack 11 was probably higher than that of the other operating stacks, however, because it was located upstream and operated in gas of lower decomposition voltage.

The major impurity in the oxygen was CO_2. Lesser amounts of H_2O, N_2, and CO were also present. The CO concentration, determined by infrared spectroscopy, was 175 $\pm$ 25 ppm. (In a space cabin, this CO would be eliminated completely by passing the exit O_2 through a catalytic recombiner.) It is believed that the CO leakage occurred primarily at the shutoff valves of non-operating stacks, especially at the stack broken during battery assembly.

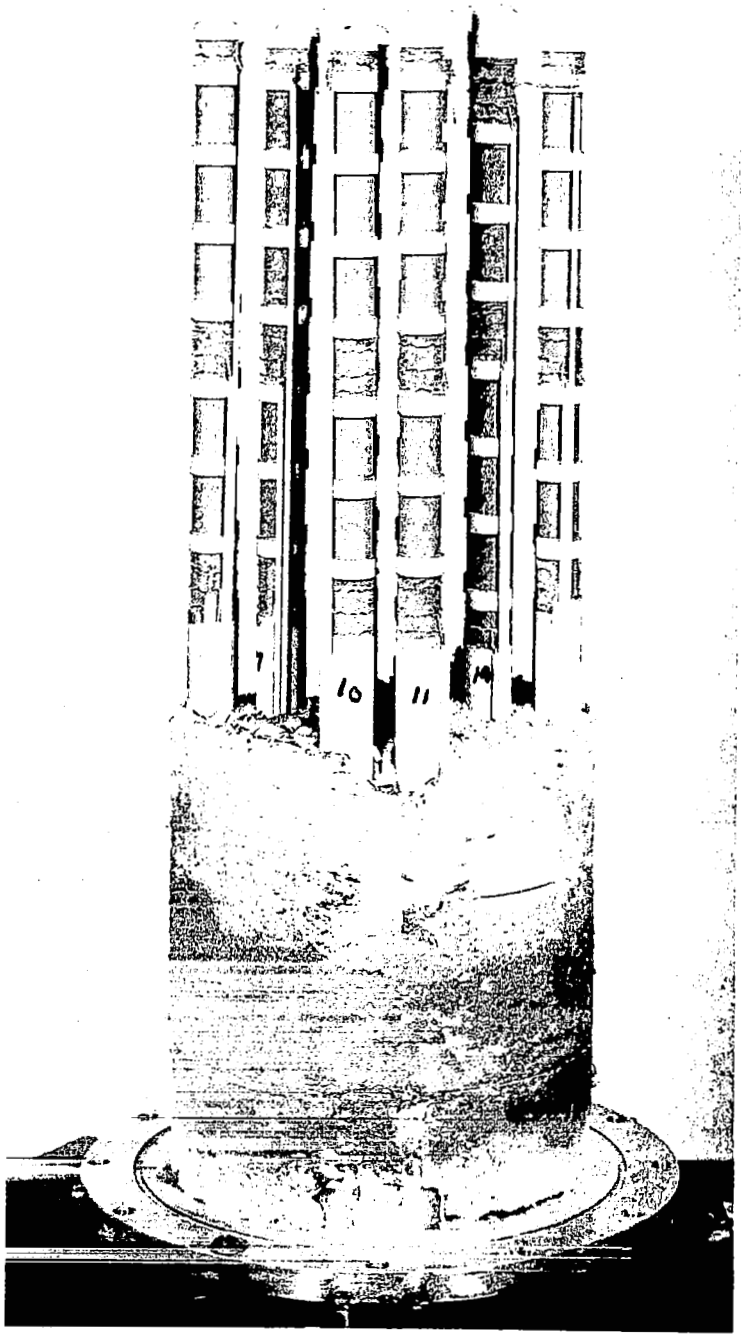

Fig. 15 - Electrolysis unit with housing removed at end of 180-day life test.

5.3.2 Condition of Electrolysis Unit After Test

After the life test the electrolysis unit was cooled slowly to room temperature and disassembled for visual inspection. Except for two broken stacks, one of which was broken during construction of the unit, the stack assembly looked almost like new. No electrode evaporation or peeling was noted and no carbon had formed anywhere inside the chamber. The insulation around the base tubes of the stacks was sound, although discolored where it had touched the copper plating on the housing wall. A photograph of the interior of the unit is shown in Fig. 15.

The inlet and outlet tubes were completely free of carbon deposits. The copper linings were clean and bright and appeared to be unaffected by the test. The Inconel exit tube, however, had become embrittled and broke near the attachment to the housing while the tube was being disconnected from the system piping. Metallographic examination revealed that the tube had been embrittled by extensive internal oxidation along the grain boundaries, as shown in Fig. 16.

Similar embrittlement of the Inconel shell of the electrolyzer did not occur. Samples cut from the wall of the inlet and outlet compartments were only lightly oxidized on the inside and outside surfaces and showed little oxidation along grain boundaries. The difference in behavior of the shell and the gas exit tube may have been due to contamination of the tube by copper from the liner, thereby reducing the oxidation resistance of the Inconel.

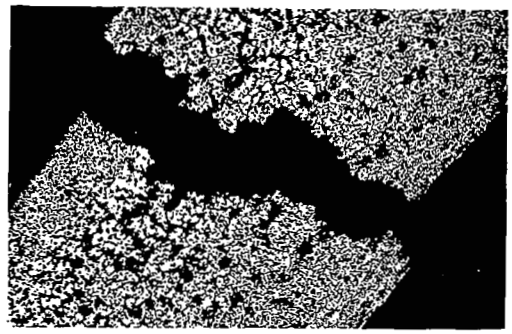

Fig. 16 -- Inconel exit tube at fracture. 100X

Although oxidation of the gas exit tube caused no difficulty in the 180-day life test, a change in the material of construction of the two gas lines should be considered to insure adequate life. A metal

alloy is needed that is resistant to oxidation at the operating temperature of of the electrolyzer and is also noncatalytic to carbon deposition at lower temperatures.

5.4 Carbon Deposition Reactor Performance

5.4.1 Operating Characteristics

The performance of the carbon deposition reactor can be evaluated on the basis of its ability to maintain the degree of decomposition (DD) of the gas at the electrolyzer exit at the design value of 0.60 or less. The plot of DD in Fig. 14 shows that the performance was inadequate during the first 40 test days of the life test but was satisfactory thereafter. Poor performance at the start was found to be due to an incorrect temperature profile. The reactor was coldest at the entrance and the temperature increased toward the exit. When the inlet temperature was raised 30°C to about 540°C and the outlet temperature was lowered 30°C to 510°C, immediate improvement resulted. The new profile apparently promoted a higher reaction rate at the entrance where kinetics was controlling and also at the exit where equilibrium was controlling.

A more exact index of performance than degree of decomposition is the ratio of CO_2 to CO in the exit gas -- the higher this ratio, the better the performance. (At ratios above 1.15, the degree of decomposition value was usually at 0.6 or below, which was the desired condition.) A plot of the CO_2 to CO ratio versus test day is presented in Fig. 17 together with plots showing the H_2 concentration of the exit gas and the iron content of the carbon deposit. These three plots show a definite correlation with each other that is particularly evident for days 110 through 145, a period in which the H_2 concentration rose to over 8%. (The rise in H_2 concentration was caused by the decline in performance of the fifth palladium membrane.) Hydrogen is known to promote the carbon deposition reaction (Reference 3, pp. 66-69). Figure 17 indicates that it also promotes attack on the iron by carbon. The curves suggest

that the H_2 concentration should be kept below 4 or 5 percent to prevent excessive loss of iron.

Power consumption by the carbon deposition reactor was 132 watts. An overall heat balance for the reactor is presented in Appendix K.

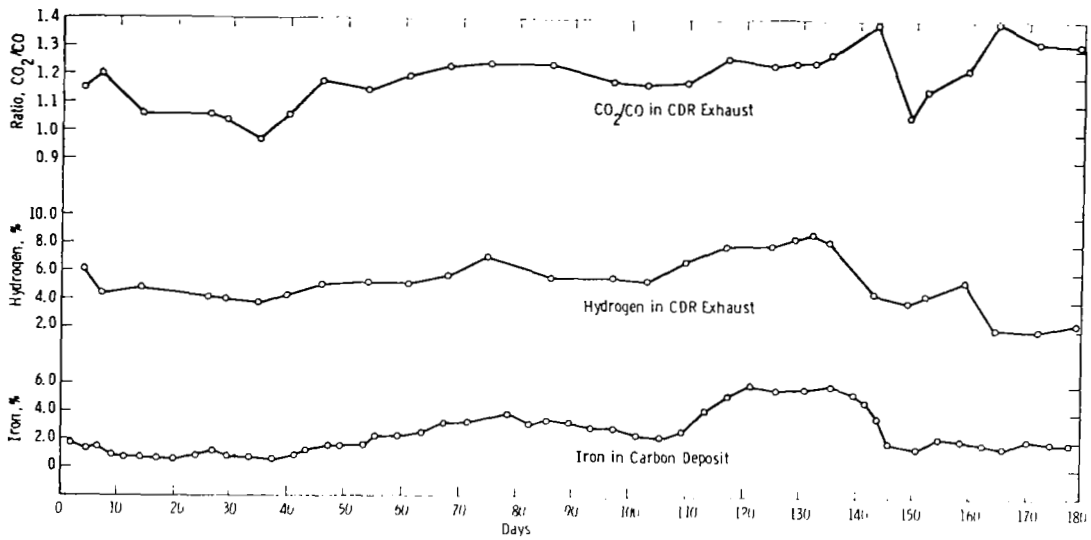

Fig. 17 -- Performance of carbon deposition reactor versus days of operation

5.4.2 Post Test Characterization

After completion of the life test the carbon deposition reactor was operated as a single component at conditions similar to those used for the final open loop test (see Appendix F, Table F-2, Test 6). The purpose of the run was to determine whether catalyst activity had increased or declined during the life test. In the open loop test, the rate of CO conversion was 204 cc/min. In the repeat run after the life test, the rate was 246 cc/min, indicating that enhancement of catalyst activity had occurred, probably as a result of the modified temperature profile.

5.4.3 Condition of Reactor After Test

On cooling the reactor to room temperature, the brazed joint between the aluminum bronze inlet vestibule and the Inconel jacket failed and the sections came apart. The bronze was badly scaled on the outside and oxidation had undermined the fillet of the braze (72% silver - 28% copper) and had penetrated into the joint itself. The bronze gas inlet tube also broke where it was brazed to the vestibule, also because of oxidation.

Stains on the ceramic insulators of the heater coil near these joints indicated that both joints had been leaking prior to shutdown. The leaks were small, however, because the total leak rate for the system was found to be only 2 cc/min on the last day of operation.

The leak rate was determined in the following way: The electrolysis current and the CO_2 feed were shut off and the teflon valves in the baseplate were closed. With the recycle pump running to maintain normal flow conditions, CO_2 was introduced through a bubble counter and the rate was adjusted until the pressure in the system was constant at the normal operating level. The CO_2 feed rate then equaled the leak rate.

A third failure involved the aluminum bronze bushing on the scraper shaft. The bushing was ruptured by carbon depositing underneath, despite a silver-copper solder seal at each end of the bushing. Pieces of the bushing broke off and were seen in the carbon as early as the 39th day. Bulging of the top section of the bushing because of carbon growth underneath made turning of the scraper very difficult during the final month of operation.

The failures of aluminum bronze parts show that aluminum bronze is not a suitable material of construction for the reactor. A suitable replacement material is Inconel 600 that has been heavily copper plated to prevent carbon deposition.

Inspection of conditions inside the reactor revealed the following:

1. Except for failure of the bronze bushing, the scraper was in excellent condition. The blades and shaft had not been attacked by the carbon and they showed no evidence of wear. A picture of the scraper, taken after the life test, is shown in Fig. 18.

2. Thick carbon deposits had formed on the walls of both bronze vestibules, suggesting that this alloy may not be entirely noncatalytic.

3. Carbon had deposited behind the catalyst tube at the top, causing distortion, even though the tube had been copper brazed to the Inconel jacket. The joint probably had not been filled completely with braze metal. Braze metal completely filled the lower joint and it remained sound.

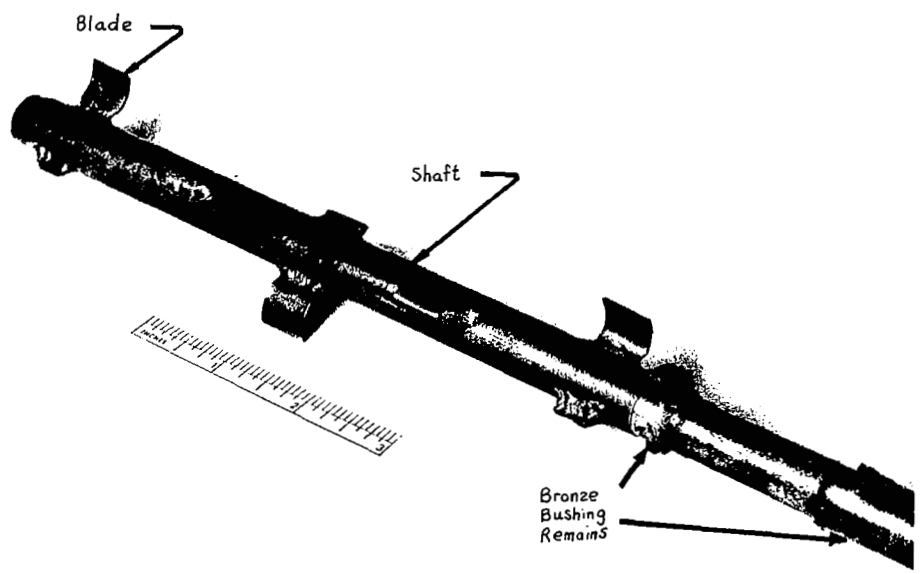

Fig. 18 -- Carbon scraper after life test.

The extent of carbon attack on the catalyst tube was determined by splitting the reactor lengthwise and measuring the wall thickness at intervals along the length. The initial and final contours of the inner face are compared in Fig. 19, which also shows typical temperature profiles within the reactor.

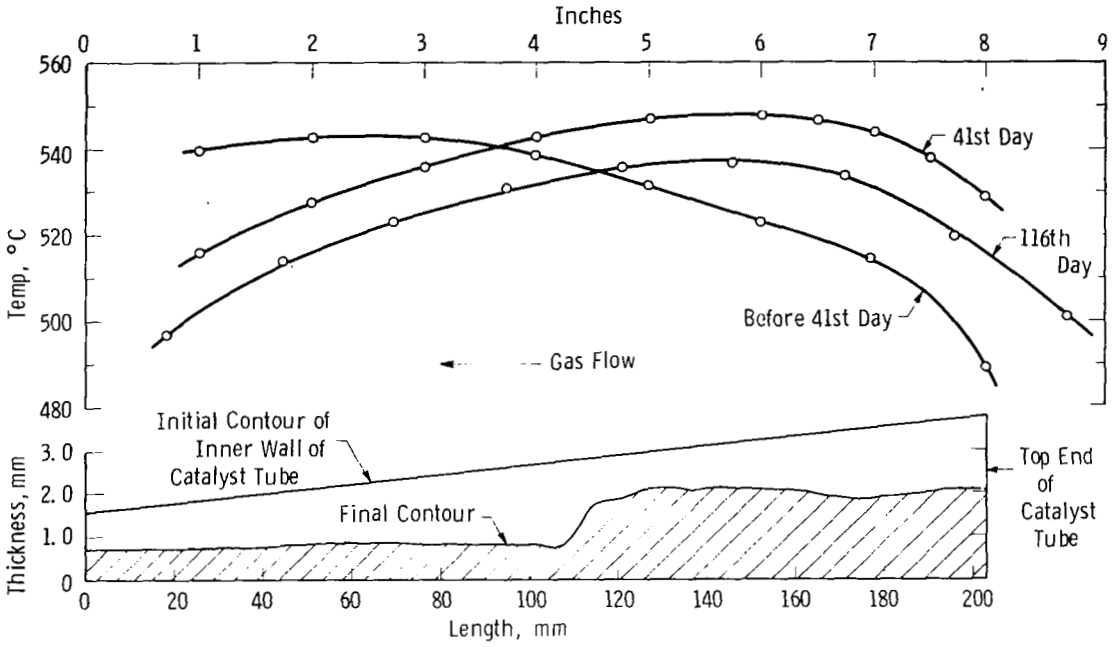

Fig. 19 -- Typical temperature profiles in reactor and variation in wall thickness of catalyst tube at end of life test.

The most significant finding was that the catalyst tube had not been penetrated at any point. However, catalyst consumption was not as uniform as had been anticipated. More iron was consumed from the lower half of the tube than from the upper half and the greatest attack occurred at the center. In contrast, the catalyst tube used in the 100-day test of the previous contract was attacked most near the top and penetration of tube occurred (Reference 3, pp. 82-85). The more even attack in the present life test was due to a higher gas flow rate and a lower CO concentration in the feed, which caused the reaction to spread out over a greater length.

The abrupt change in wall thickness of the catalyst tube near the midpoint has not been explained. It is not known whether more carbon was produced in the lower half of the reactor or whether carbon production was uniform and only the iron content varied. Some clarification may come from studying the carbon deposit remaining in the reactor after the life test. Time limitations prevented checking the iron content of this carbon prior to the writing of this report.

5.5 Hydrogen Separation

5.5.1 Performance of System

Except for the deterioration of palladium membranes with time, previously noted in Section 5.1.2, the hydrogen separation system worked extremely well. The rate of hydrogen removal was completely self-regulating and only the concentration of hydrogen in the recycle stream required occasional control. The thermocouple vacuum gauge, which measured the pressure in the line between the control valve and the vacuum pump, was a very reliable indicator of the rate of hydrogen removal. The calibration curve is shown in Fig. 20.

A permeation rate study conducted with a 2.5 in. long palladium membrane prior to construction of the bread-board system (see Appendix E) gave results that conformed to the following relation:

$$Q = k \ell \left(p_1^{0.65} - p_2^{0.65}\right)$$

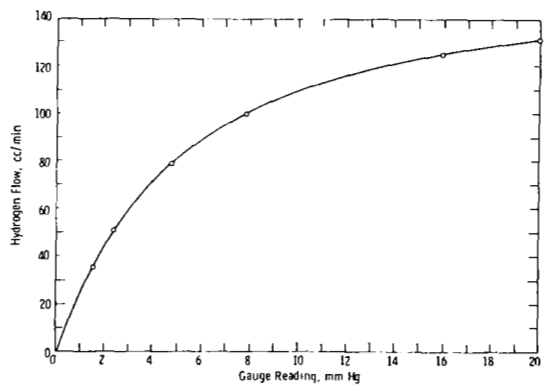

Fig. 20 -- Relationship between thermocouple vacuum gauge reading and hydrogen discharge rate

where

Q = rate of hydrogen permeation, cc/min

ℓ = length of palladium membrane, cm

p_1 = average partial pressure of hydrogen in gas stream, mm Hg

p_2 = partial pressure of hydrogen on vacuum side of membrane, mm Hg

k = permeation rate constant, $\frac{cc}{(min)\ (cm)(mm\ Hg)^{0.65}}$

In experiments run at 850°C, the value of k was found to be 0.166.

The outside diameter of the palladium membrane tubes was 0.318 cm and the outside surface area per cm of length was 1.00 cm^2.

Values of k calculated from data obtained in the 180-day test, using the above relationship, are presented in Table VIII, together with the days on which palladium membranes were closed because of high leakage. The results show an apparent decline of k during the 30 to 40-day periods preceding the closing of membranes 4 and 5. The decline in each case was apparently due to a gradual collapse of the membrane (see Fig. 21). The collapsed section impeded the flow of hydrogen to the vacuum system, causing the pressure within the membrane to be higher than in the manifold. The net effect was to reduce the rate constant which was based on the measured pressure of the manifold. In each case after closing the faulty membrane, the k value increased.

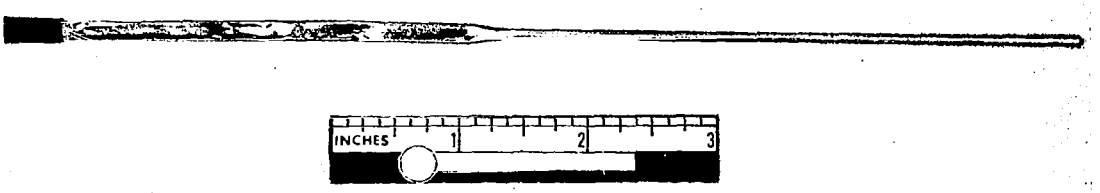

Fig. 21 -- Partially collapsed palladium membrane from compartment 3 of electrolyzer

TABLE VIII

HYDROGEN PERMEATION THROUGH PALLADIUM MEMBRANES
DURING 180-DAY TEST

Test Day	Palladium Membrane Length, in.	Hydrogen Removal Rate, cc/min	p_1 [a], mm Hg	p_2 [b], mm Hg	Apparent Rate Constant k
14	27	51.6	31.1	13.6	0.194
29	27	45.8	27.5	10.5	.167
35	27	52.3	25.7	8.3	.178
46	27	52.7	32.7	10.0	.149
56	3-in. long Pd membrane closed				
68	24	52.6	38.6	8.6	.129
75	Pd membrane 4 closed				
86	16	51.7	37.1	5.2	.168
97	16	51.9	37.4	5.2	.168
110	16	54.3	45.7	5.2	.134
125	16	51.8	54.9	5.2	.120
129	16	50.7	58.8	5.2	.112
142	Pd membrane 5 closed				
149	8	26.9	27.3	4.5	.224
152	8	30.0	30.0	4.7	.232
159	8	32.1	37.2	5.0	.206

a. p_1 = average partial pressure of hydrogen in electrolyzer atmosphere.

b. p_2 = absolute pressure of hydrogen on vacuum side of palladium membrane.

Extrapolation of the k value obtained at 850°C in the rate study to 910°C, the temperature during the life test, gives a k value of 0.200. This is close to the value obtained on test day 14 when the membranes were relatively new. The temperature coefficient used in the extrapolation was taken from Waldschmidt (Reference 10).

A leak prevented the 3-in. long palladium membrane that was tested as a hydrogen gauge from performing satisfactorily. Although the leak rate was small at first, useful measurements could be obtained only by extrapolating the readings back to zero time (time of isolating gauge from vacuum manifold) to correct for a steady increase in gauge reading with time because of the leak. On the 56th day, the membrane was closed permanently because the leak rate began to increase.

5.5.2 Condition of Palladium Membranes After Test

Palladium membranes 1, 2, and 3[(a)] broke during preliminary operation of the breadboard system and were closed off before the start of the life test. The breaks occurred at the joints with the Inconel support tubes. The most probable cause of failure was an accident that occurred during assembly of the electrolyzer housing. The palladium membrane-Inconel tube assemblies were inadvertently pushed from a storage shelf and fell several feet to the floor. Helium leak checks showed that none of the joints leaked; however, the fall may have caused incipient cracking which led to failure on heating.

Membranes 1 and 2 had broken off completely at the joints and had fallen so that the lower ends rested on the insulation around the base tubes of the stacks. The top two inches of membrane 1 and the bottom inch of membranes 1 and 2 were severely eroded, although there was practically no loss of weight. Photographs of eroded areas are shown in Fig. 22.

(a) Referring to Fig. 6, membrane 1 was located in the feed compartment (compartment 1) at bottom left. The other membranes and compartments are numbered sequentially in the counterclockwise direction.

Membrane 3, which had cracked but had not fallen, was less eroded at the bottom than membrane 2 even though both were contained in the same compartment. Membranes 4, 5, and 6, which were located farther downstream in compartments 3 and 4, suffered almost no erosion.

Metallographic examination of eroded membranes revealed a single phase structure and extensive grain growth, as shown in Fig. 23. On some parts of the surface an unidentified film was present. Spark mass spectrographic analysis showed that the palladium in the eroded areas was highly contaminated with copper and that traces of other metals were also present. The major source of copper was undoubtedly the preheating coil for the feed gas, which was copper lined. The copper coating on the electrolyzer shell was at a lower temperature and was located outside the flow path of the gas.

The errosion phenomenon was most intense near the gas inlet port in compartment 1 and had almost disappeared by the time the gas reached compartments 3 and 4. This suggests that the impurities in the gas were responsible for the erosion and that the impurity concentration decreased as the gas flowed through the electrolyzer because of scavenging by the metal walls.

Membranes 4 and 5 operated 74 days and 141 days, respectively, before excessive leakage necessitated their removal from service. Both membranes looked almost new after the test except that the top half of each had collapsed, as shown for one membrane in Fig. 21. On testing the membranes after the life test, the leakage was found to have been due to porosity in the vicinity of the brazed joint. The start of leakage probably coincided with collapse of the membrane in the joint region. Collapsing apparently started near the center of the membrane,

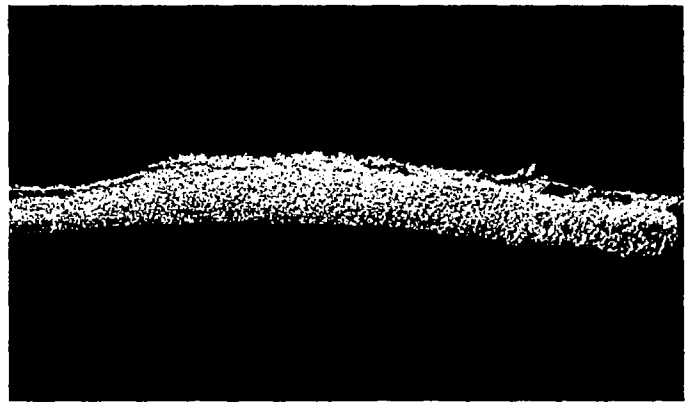

(a) At open end. 5X

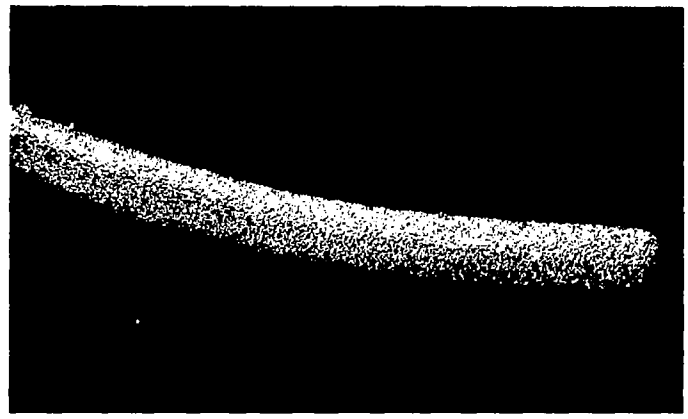

(b) At closed end. 5X

(c) Near closed end. 24X

Fig. 22 -- Enlarged views of eroded areas of palladium membrane in feed compartment of electrolyzer.

New

Used

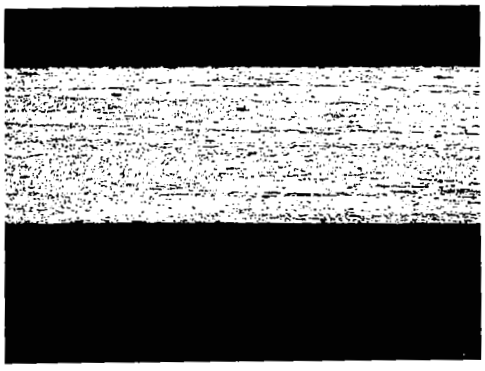

Longitudinal Section

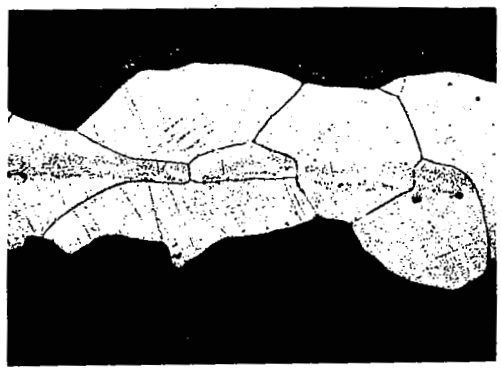

Longitudinal Section

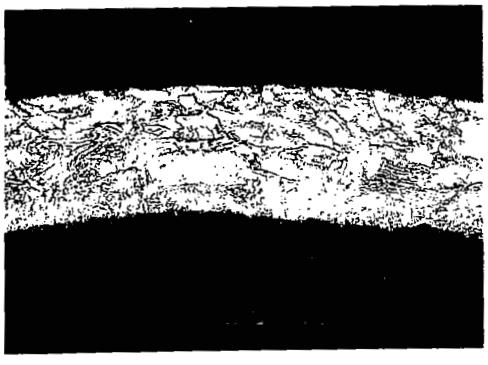

Transverse Section

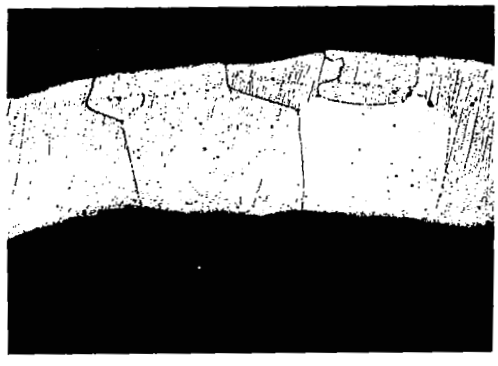

Transverse Section

Fig. 23 -- Longitudinal and transverse sections of new and eroded palladium membranes. 250X

where the electrolyzer temperature was highest, and progressed slowly up the membrane to the joint.

Membrane 6, which operated throughout the life test with practically no leakage, also appeared like new except for a 1.5 in. long collapsed section near the top. It also was beginning to become porous at the joint and at the closed end, however.

It is believed that the difficulties encountered with the palladium membranes can be reduced or eliminated by taking the following corrective measures:

1. Use thicker palladium membranes for greater strength.
2. Use a more stable brazing alloy, such as gold-nickel, in place of copper to prevent porosity at the joints.
3. Locate all membranes downstream from the feed compartment to reduce contamination.
4. Lower the operating temperature by 50°C.

No difficulties were experienced in using palladium membranes in earlier preliminary tests, and one test lasted 71 days (see Appendix E). The major differences were that the preliminary tests were run at a lower temperature than the 180-day test (50 to 60°C lower in the case of the 71-day test) and that there were no sources of impurities other than the feed gas itself.

6. INTEGRATION WITH CARBON DIOXIDE CONCENTRATORS

The carbon dioxide and water fed to the solid electrolyte oxygen regeneration system will be removed from the cabin atmosphere and concentrated by a carbon dioxide concentrator system. Numerous approaches for concentration have been considered including molecular sieves, steam desorbed solid amines, electrodialysis, carbonation cells, hydrogen depolarized electrochemical cells, membrane diffusion, liquid absorption, and direct freezout (Reference 1).

The current study was undertaken to determine the effect that using different concentration methods would have upon the system configuration, equipment design and size, and power requirements for the solid electrolyte oxygen regeneration system. This was done by first defining the interface requirements and then estimating the total weight and power requirements for the combined concentrator-regenerator system.

The mission chosen for study was the 9-man, 500-day, non-resupply mission which was the subject of the Advanced Integrated Life Support Systems (AILSS) Study by the Hamilton Standard Division of United Aircraft (Reference 1). Weight and power data from the AILSS study were utilized because they were the most complete and up-to-date information available. Redesign of the solid electrolyte system in order to arrive at an independent estimate of weight and power was beyond the scope of this contract, but should be included among the tasks in the conceptual design study discussed previously in Section 3.

Four systems were chosen as the most promising based on the AILSS report and discussions with NASA personnel: molecular sieve, steam desorbed resin, hydrogen depolarized electrochemical cells, and carbonation cells. Descriptions of these systems, taken from the AILSS report, are presented in Appendix L.

6.1 Coupling with Steam Desorbed Resin Concentrator

The steam desorbed resin concentrator utilizes an organic amine polymer to absorb CO_2 from the process air. Steam is used to liberate the CO_2 and regenerate the amine. The process has been described by Tepper and co-workers (Reference 11) and by Martin and Brose (Reference 12).

Because the concentrator generates CO_2 in a highly cyclic manner, some type of accumulator between it and a solid electrolyte system will be necessary. In the AILSS report, the equipment provided to allow a feed to the solid electrolyte system of constant flow and composition included:

1) a condenser separator to reduce the moisture in the gas leaving the concentrator to approximately 3%,

2) a room temperature accumulator,

3) a humidifier in which sufficient water is added to the CO_2 to achieve the desired total oxygen rate (approximately 25 mole percent of the CO_2 stream in the AILSS study).

For the initial coupling of a steam desorbed resin concentrator and a solid electrolyte oxygen regenerator, the interface suggested in the AILSS report seems highly desirable, because it will permit the two systems to operate essentially independent of each other. For some future stage of development, however, it may be desirable to eliminate the condenser separator and provide an accumulator of minimum size (with a holdup time equivalent to one desorption cycle, for example). The accumulator would be embedded in the insulation of the electrolyzer to maintain the temperature of the wet CO_2 above the condensation point of the water. The accumulator would then serve to maintain the humidity of the electrolyzer feed. In this case, the electrolysis unit must be able to adjust automatically to changes in incoming gas composition and flow rate. (See Table IX). The solid electrolyte oxygen regeneration system developed in this program has such a capability.

Table IX

INTERFACE CHARACTERIZATION OF STEAM DESORBED RESIN
CO_2 CONCENTRATOR/SOLID ELECTROLYTE SYSTEM

	Anticipated Range	
	With AILSS Interface	With Modified Interface
Gas Feed to Electrolyzer		
CO_2	80%	60-90%
H_2O	10%	10-40%
N_2	0-2%	0-2%
O_2	0-2%	0-2%
Others (amine)	trace	trace
Gas Flow	20.4 lbs/day	15-25 lbs/day
Electrical Heat for Humidification of Electrolyzer Feed	0.04 kW	0

A second modification, which was carefully considered, is to place steam boiler tubes in the insulation surrounding the electrolysis unit of the oxygen regenerator to utilize waste heat to produce part or all of the steam required by the CO_2 concentrator. Calculations indicated, however, that based on breadboard system performance this modification would not be feasible because of the heat losses associated with gas recycle in the solid electrolyte system. Only actual tests of a multi-man system can tell if the recycle rate can be lowered and waste heat made available for this purpose.

The interface between the two units is shown schematically in Fig. 24. For control, a pressure signal from the acumulator would be used to regulate the total current being passed through the electrolyser; an increase in accumulator pressure would cause an increase in electrolysis current. The increased current would cause a decrease in the pressure of the solid electrolyte system which, in turn, would call for a higher rate of feed from the accumulator. To allow for

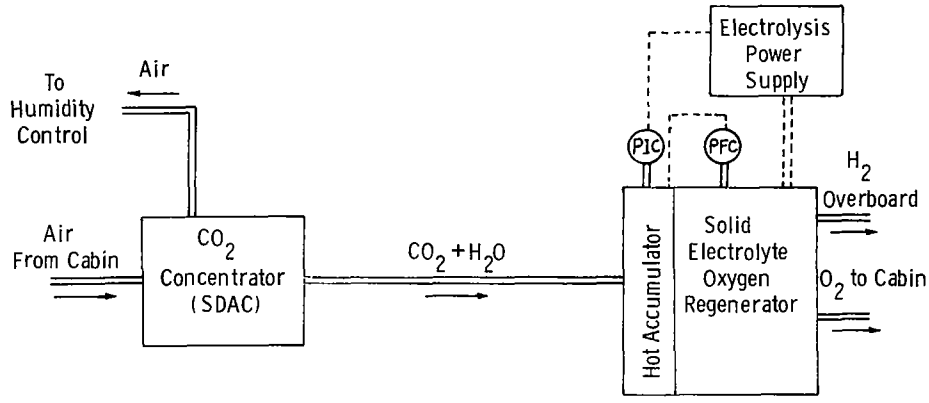

Fig. 24 -- Interface between steam desorbed CO_2 concentrator and solid electrolyte oxygen regenerator

for variations in the water vapor partial pressure during the cycle, the area for hydrogen diffusion would have to be increased by a factor of two (in comparison with the AILSS design).

Table X shows that the equivalent weight of the solar cell powered system would be 3098 lbs.

6.2 Coupling with Molecular Sieve Concentrator

The molecular sieve concentrator is a four-bed system employing two canisters containing silica gel to remove water vapor from the process air and two canisters containing artificial zeolite to adsorb CO_2. Desorption of the CO_2 is accomplished by reducing the pressure and applying heat. The process is described in the AILSS report.

Because the concentrator is cyclic in operation, an accumulator between the concentrator and the solid electrolyte oxygen regenerator is necessary. In coupling the concentrator to the solid electrolyte oxygen regenerator, no modification of the system described in the AILSS report is envisioned.

The total equivalent weight for the molecular sieve concentrator-solid electrolyte system is 3265 lb.

6.3 Coupling with Hydrogen Depolarized Concentrator

The hydrogen depolarized concentrator (Reference 13) has the lowest equivalent weight of the CO_2 concentration processes considered in the AILSS report and has the additional advantage of being continuous. It employs an electrochemical cell which transfers CO_2 from the process air to a hydrogen atmosphere. Oxygen is also removed from the air and reacts with the hydrogen to produce electrical power. Since oxygen that is consumed must be regenerated, the capacity of the solid electrolyte oxygen generator must be increased.

TABLE X

EQUIVALENT WEIGHT OF SOLID ELECTROLYTE/STEAM DESORBED RESIN CO_2 CONCENTRATOR SYSTEM FOR A 9-MAN 500-DAY MISSION

Steam Desorbed Resin CO_2 Concentrator	
Overall equivalent weight of concentrator	1148[a] lbs
Eliminate one condenser and spares	-20[b]
Eliminate humidifier and spares	-39
Reduce size of accumulator; add insulation	No Change
Eliminate portion of radiator load due to condenser preceding accumulator	-44[a]
Eliminate power for rehumidification of electrolyzer feed.	-27
Solid Electrolyte Oxygen Regenerator	
Overall equivalent weight of oxygen regenerator	2072[a]
Increase area for palladium hydrogen diffuser and spares	11[b]
Eliminate radiator load saved by transfer of some electrolyzer heat to hot accumulator	-3
Total Equivalent Weight	3098 lbs

a. From AILSS report, see Appendix L.

b. Based on estimates by Eric Auerbach, Hamilton Standard Division of United Aircraft Corporation

Because the delivered CO_2 contains a high proportion of hydrogen, the interface with the solid electrolyte system must provide a means for hydrogen removal. An alternative approach is to modify the operation of the concentrator so that the CO_2 product contains little or no hydrogen, in which case the concentrator no longer operates as a fuel cell but consumes electrical power. The latter approach was not considered because data were not available.

The interface between the fully depolarized concentrator and the solid electrolyte oxygen regenerator is characterized in Table XI. For removing the hydrogen in the Concentrator product, a palladium membrane hydrogen diffuser is installed at the interface, as illustrated in Fig. 25. If this hydrogen is fed to the oxygen regenerator, it becomes highly diluted by the recycle stream and more palladium is required for its removal.

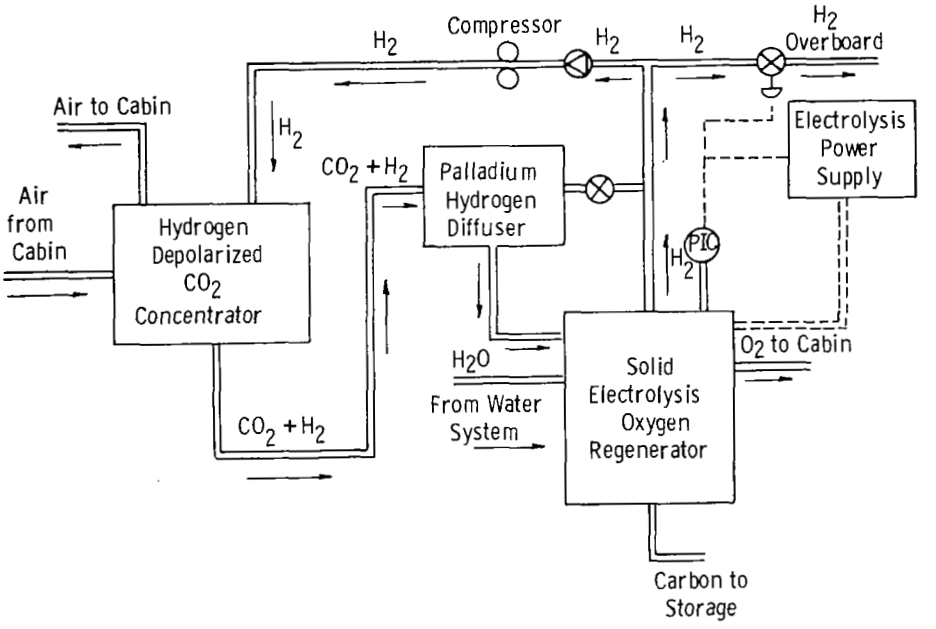

Fig. 25 -- Interface between hydrogen depolarized CO_2 concentrator and solid electrolyte oxygen regenerator with separate palladium hydrogen separator

Table XI

INTERFACE CHARACTERIZATION OF HYDROGEN DEPOLARIZED CO_2 CONCENTRATOR/SOLID ELECTROLYTE SYSTEM

	Anticipated Range
Gas Delivered by Concentrator	
CO_2	22-27%
H_2O	7-21%
H_2	55-65%
N_2	<1%
Others	--
Gas Flow	15-25 lbs/day

One hundred and fifty 1/8-in. diameter palladium membranes, each 10 in. long, would be required for the diffuser. The diffuser would consist of ten 1-in. diameter Inconel cells containing 15 membranes each. These cells would be embedded in the insulation of the electrolysis unit where they would be heated to 750 to 800°C. The cells would be connected in parallel and each would have a single vacuum connection. Two shut-off valves would be required with each cell to isolate the cell in case of leakage.

Control of the oxygen generation rate would be obtained by regulating the electrolysis current to maintain a constant pressure within the solid electrolyte unit. The hydrogen separator would require no automatic controls. However, the hydrogen feed to the concentrator, which is taken from the hydrogen discharge line, would be controlled. This would be achieved by regulating the overboard hydrogen dump valve, utilizing the same pressure signal from the electrolyzer that controls the electrolysis current.

The equivalent weights of the basic components and the changes resulting from integration for a solar cell powered system are itemized

in Table XII. The total equivalent weight is 3153 lbs. The estimated weight of the palladium membrane hydrogen diffuser is based on the results of the 180-day and 71-day life tests.

6.4 Coupling with Carbonation Cell Concentrator

The carbonation cell concentrator (Reference 14) utilizes two or three electrochemical cells connected in series. The first cell removes CO_2 and some oxygen from the process air. The second and third stages separate the CO_2 and oxygen. No hydrogen is used in the process and the cell consumes electrical energy.

Because the carbonation cell delivers CO_2 continuously, it can be coupled directly to the solid electrolyte oxygen regenerator, eliminating the need for an accumulator. The condenser separator can also be eliminated because the solid electrolyte system uses a wet feed.

Only the first electrochemical stage of the concentrator would be needed. The second and third stages would be replaced with a solid electrolyte oxygen separator, operating at high current density to remove the free oxygen that is delivered with the CO_2. The power requirement for separating free oxygen from a gas mixture is much lower than that needed to produce oxygen from CO_2 and H_2O because no decomposition is involved.

The interface between the concentrator and the oxygen regenerator is characterized in Table XIII and a schematic diagram of the integrated systems is shown in Fig. 26. Although shown as a separate unit in the diagram, the oxygen separator would be part of the same insulated package as the oxygen regenerator.

Control of the oxygen generation rate would be straight forward. A pressure signal from the solid electrolyte oxygen regenerator would regulate the electrolysis current to match the feed rate of CO_2 and H_2O and maintain a constant pressure. The electrolysis current to

Table XII

EQUIVALENT WEIGHT OF SOLID ELECTROLYTE/HYDROGEN DEPOLARIZED CO_2 CONCENTRATOR SYSTEM FOR A 9-MAN 500-DAY MISSION

Concentrator	
Weight of basic unit	255[a] lbs
Spares and redundant units	193[a]
Eliminate accumulator	-29[b]
Eliminate condenser separator and spares	-36[b]
Eliminate radiator load of condenser separator	-2[a]
Net power, including that for pump and compressor and allowing 1400 lbs credit for power generated	24
Palladium Hydrogen Diffuser	
Weight of basic unit	34
Weight of spare unit	34
Weight of recycle compressor and spare	22
Electric power for recycle compressor (75 watts)	34
Heat hydrogen in CO_2 feed to 800°C including additional radiator load	35
Solid Electrolyte Oxygen Regenerator	
Overall equivalent weight of regenerator	2072[a]
Weight correction for increased oxygen production including spare unit and redundancy	+144
Power correction for increased oxygen production (720 watts)	+324
Increase in radiator load	49[a]
Total Equivalent Weight	3153 lbs

a. From AILSS report; see Appendix L.

b. Based on estimates by Eric Auerbach, Hamilton Standard Division of United Aircraft Corporation.

Table XIII

INTERFACE CHARACTERIZATION OF CARBONATION CELL CO_2 CONCENTRATOR WITH SOLID ELECTROLYTE SYSTEM

	Anticipated Range
Gas Feed to Electrolyser	
CO_2	40-60%
H_2O	10-15%
N_2	<1%
O_2	20-30%
Others	--
Gas Flow	25-35 lbs/day

the solid electrolyte oxygen separator would be supplied by a controlled voltage source. By fixing the voltage at 0.5 volt, all free oxygen would be separated and no CO_2 or H_2O would be decomposed. No other control of the oxygen separator would be required.

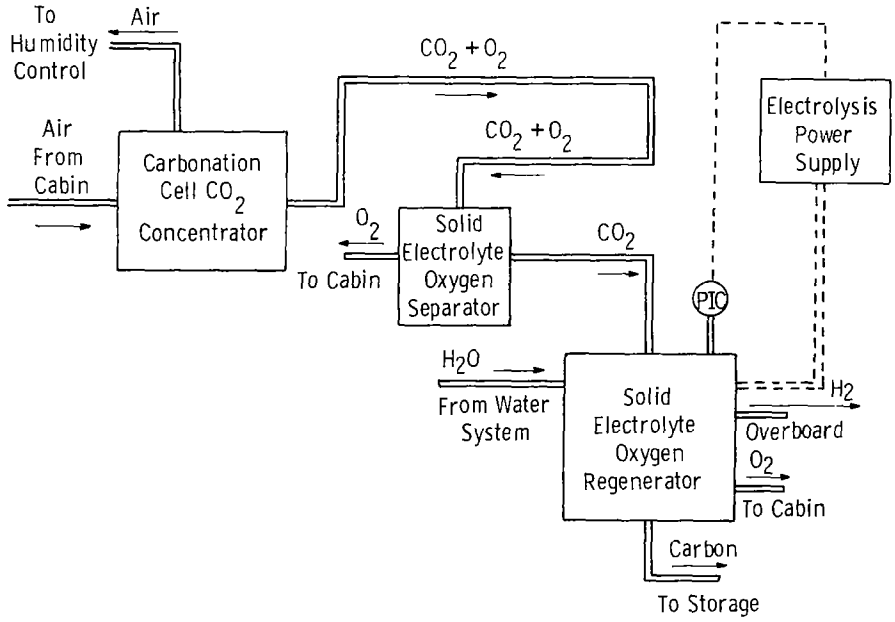

Fig. 26 -- Interface between carbonation cell CO_2 concentrator and solid electrolyte oxygen regenerator

The combined equivalent weight of an electrochemical carbon dioxide removal and concentration system, solid electrolyte oxygen separator, and solid electrolyte oxygen regeneration system is estimated as 3284 lbs, as shown in Table XIV. The estimated weight and power of the solid electrolyte oxygen separator is based on the use of cells operating at 400 ma/cm^2.

TABLE XIV

EQUIVALENT WEIGHT OF SOLID ELECTROLYTE/CARBONATION CELL CO_2 CONCENTRATOR SYSTEM FOR A 9-MAN 500-DAY MISSION

Concentrator	
Weight through first stage	156[a] lbs
Spares/Redundant units	156[a]
Electrical power (965 watts)	433[a]
Radiator load	131[b]
Solid Electrolyte Oxygen Separator	
Weight of basic unit	49
Weight of spare unit	49
Electrical power (440 watts)	198
Radiator load	30
Solid Electrolyte Oxygen Regenerator	
Overall equivalent weight of basic unit	2072[b]
Total Equivalent Weight	3284 lbs

a. Based on estimates by Eric Auerbach, Hamilton Standard Division of United Aircraft Corporation.

b. From AILSS report; see Appendix L.

6.5 Summary of Integration Study

This study indicated that all four CO_2 concentrators considered can be integrated with the solid electrolyte oxygen regenerator. The two electrochemical processes, however, will require modifications to and an increase in size of the solid electrolyte unit.

Table XV summarizes the estimated weights and power requirements. Two systems, the steam desorbed resin and the hydrogen depolarized cell, have somewhat lower equivalent weights than the AILSS estimate of 3220 lbs.

TABLE XV

ESTIMATED PHYSICAL WEIGHT, ELECTRICAL POWER, AND EQUIVALENT WEIGHT OF FOUR CO_2 CONCENTRATOR/SOLID ELECTROLYTE SYSTEMS FOR A 9-MAN 500-DAY MISSION[a]

	Physical Weight, lbs	Electrical Power, kW	Equivalent Weight, lbs
Steam desorbed resin	1490	2.94	3098
Molecular sieve	1741	2.83	3265
Hydrogen depolarized cell	1655	2.85	3153
Carbonation cell	1448	3.40	3284

a. For solar cell battery powered system.

APPENDIX A

FABRICATION METHOD FOR SINTERED PLATINUM-ZIRCONIA ELECTRODES

A.1 Platinum-Zirconia Slurry Preparation

100 g of ultrafine platinum powder and 11.5 g of stabilized zirconia powder [$(ZrO_2)_{0.9}(Y_2O_3)_{0.1}$, W. R. Grace; particle size < 200Å] were mixed in 150 ml of n-butyl acetate for 30 minutes. The slurry was then homogenized and the excess solvent was removed by sedimentation until the total volume was reduced to 75 ml.

A.2 Electrode Application and Air Sintering

Before applying the electrodes, the electrolyte surface was cleaned by boiling in aqua regia for 30 minutes. After boiling in water to remove the aqua regia, the specimen was allowed to dry in air at 200°C. It was then air fired to 1000°C to remove any traces of organic material. The following steps were then carried out to apply an outside electrode.

1. The electrolyte was optically masked.
2. A thin layer (2-3 mg/cm^2) of slurry was applied on the substrates with a spray gun from a distance of 6 inches, using an air pressure of 14 psi. To achieve a uniform thickness, the substrate was rotated while the gun was moved back and forth along the length of the specimen.
3. The sprayed surfaces were dried at 100°C to remove the organic solvent and thus prevent blistering during sintering.
4. The coating was sintered in air at 1400°C. The sintering cycle is outlined in Table A-I.
5. Steps 1-4 were repeated until the final coating weight was reached. Electrodes were applied to the inside of the tube by

spraying from both ends with an inclined angle of about 30°. The coating weights were 1-3 mg/cm^2 per application. Drying and sintering were carried out as described in steps 3, 4, and 5.

TABLE A-I

AIR SINTERING CYCLE FOR THE PRODUCTION OF PLATINUM-ZIRCONIA CERMET ELECTRODES

Step	Purpose	Temperature-Time or Heating Rate
1	Remove slurry agent	Room temperature to 700°C; 10°C per minute
2	Heat to sintering temperature	700°- 1400°C; 20°C/min (fast heating rate to minimize stepwise sintering)
3	Sinter zirconia skeleton	Hold at 1400°C for one hour
4	Cool to room temperature	1400° to 700°C, cool at 20°C per minute or slower; 700°C to room temperature, 10° per minute or slower.

APPENDIX B

SELECTION OF BEST FABRICATION TECHNIQUES FOR ELECTROLYSIS CELLS AND STACKS

B.1 Preliminary Screening of Electrode Application Techniques

The structure of a high performance, long-life electrode must be highly porous to enable reactant gases (CO_2 and H_2O) to diffuse to the electrode interface and electrolysis products (CO and H_2) to diffuse away. The structure must be tightly bonded to the substrate so that no disattachment will occur in prolonged operation. The electrode material must have high electronic conductivity and not interact with other components at high temperature. Two different fabrication techniques were investigated under this contract to produce such an electrode: sputtering and sintering of mixtures containing platinum and zirconia.

B.1.1 Sputtered Pt-ZrO_2 Electrodes

A direct current (dc) reactive sputtering technique was employed to prepare sputtered Pt-ZrO_2 films. A cathode was made of platinum and zirconium. The ratio of the respective surface areas was three. Short segments of half-inch zirconia tubes were used as the target. The deposition parameters were as follows:

Chamber pressure	0.01 Torr
Sputtering atmosphere	Argon, 3% H_2O
Argon flow rate	35 cc/min
Cathode voltage	4.8 kV
Plasma current	200 mA

Microscopic examination of sputtered Pt-ZrO_2 films containing 10 to 20% ZrO_2 showed them to be tightly bonded to the substrate but

lacking porosity. Figure B1a shows a very light coating of 2 mg/cm^2. This discontinuous deposit has a resistance of about 10 ohms, as measured with a multimeter between two points 1 cm apart. When the coating density was increased to 5 mg/cm^2 (Fig. B1b) the electrolyte surface was covered with a continuous film and the resistance was 1 ohm; at 10 mg/cm^2 (Fig. B1c), the resistance of the electrode decreased to 0.2 ohm.

The dense continuous Pt-ZrO_2 films produced by reactive sputtering do not appear promising for electrodes because the lack of porosity would cause substantial resistance to the diffusion of gases through the electrode.

B.1.2 Sintered Pt-ZrO_2 Electrodes

The sintered Pt-ZrO_2 electrode has a porous structure consisting 70% by volume of platinum phase and 30% by volume of stabilized zirconia ceramic phase (see Appendix A for description of the application technique employed). The ratio was selected so that both metal and ceramic phases are continuous. The continuous ceramic phase gives the electrode the proper strength by bonding the electrode structure to the substrate via direct zirconia sintering. It also prevents agglomeration of the metal phase. The continuous metal phase maintains high electrical conductivity.

Both tight adherence and uniform distribution of Pt in the sintered ZrO_2 phase are seen in the cross section shown in Fig. B2. The high porosity of the coating was readily demonstrated by applying a drop of ink to the surface and observing the spreading of the ink by capillary action. The continuous metallic phase provides a high conductivity, a medium thick coat 10 mg/cm^2 gives a resistance of 0.1 to 0.15 ohm when measured with a multimeter between two points 1 cm apart. Based on the above observations, the sintered Pt-ZrO_2 cermet films were selected for use in the tests which determined the effect of other

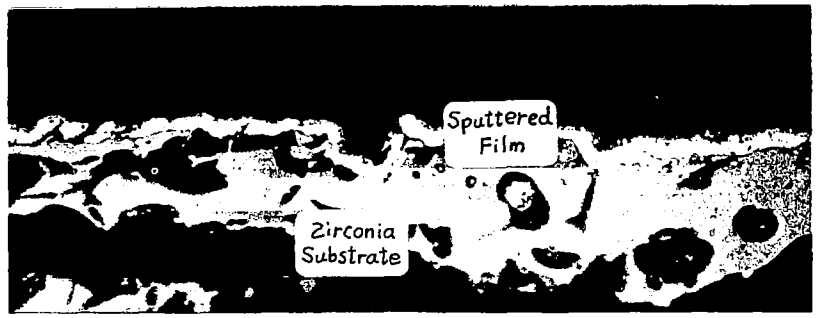

a. Film Density 2mg/cm^2

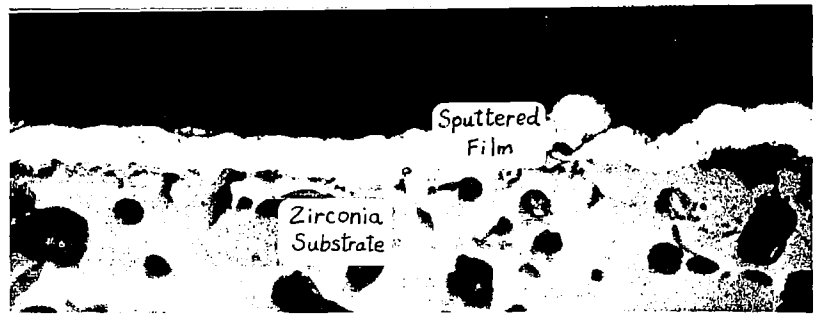

b. Film Density 5mg/cm^2

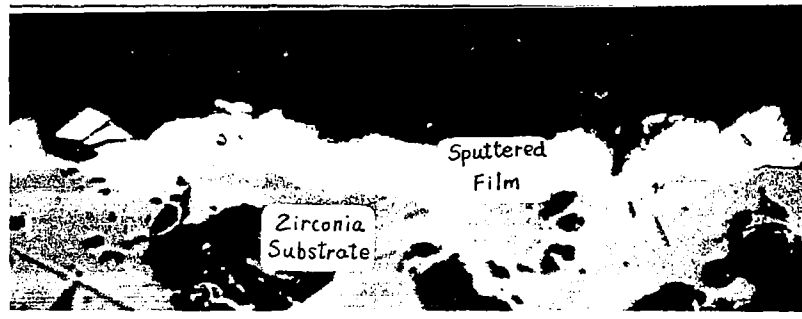

c. Film Density 10mg/cm^2

Fig. B1 Cross sections of electrode films produced by reactive sputtering (1000X)

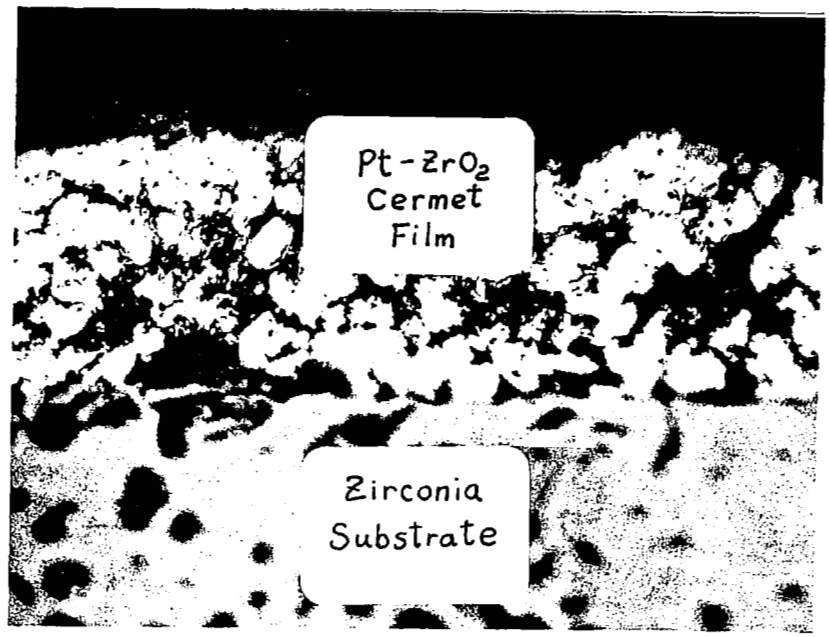

Fig. B2 -- Sintered Pt-ZrO_2 electrode. Cross section view at 1000X

fabrication variables and of operating conditions on the life of solid electrolyte electrolysis units.

B.2 Construction of Electrolysis Stacks

Six solid electrolyte electrolysis stacks (OBS #13, 15, 16, 17, 18 and 19) were constructed for the fabrication variable life tests. The bell and spigot cells were produced from 1/2 inch tubes of stabilized zirconia-yttria, machined to the dimensions shown in Fig. 3 (see Section 4 of the body of the report). The fabrication sequence to make these stacks is illustrated in Fig. B3. All of the electrodes were fabricated with sintered Pt-ZrO_2 cermet, except the inside electrodes of the first two stacks (OBS #13 and OBS #15) which were conventional sintered Pt. Two different noble metal alloys were used as sealants for brazing of cell joints. Platinum-gold alloy was used in OBS #13, 16, 18 and 19, and Pt-Ag-Pd alloy was used in OBS #15 and 17.

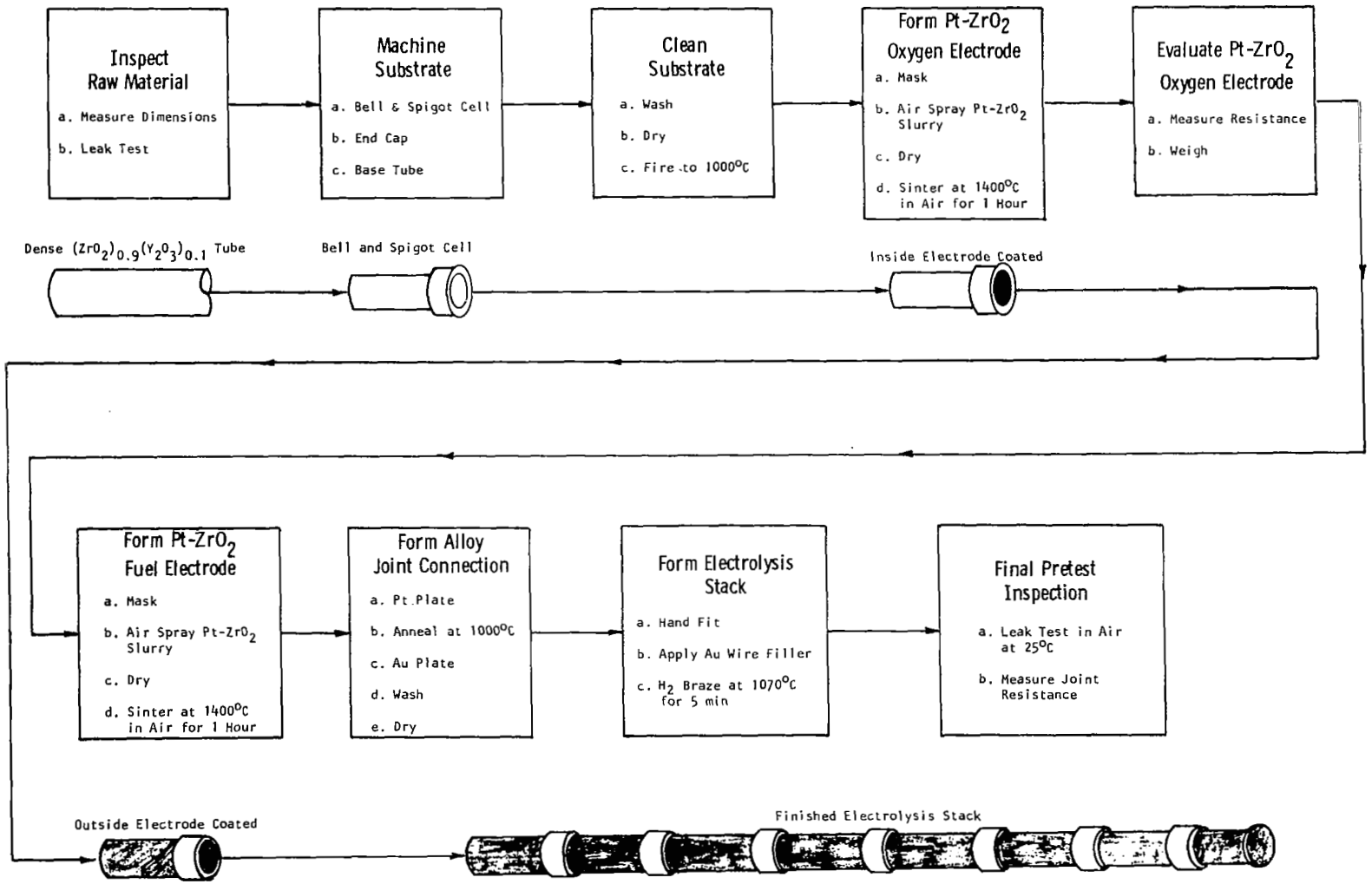

Fig. B3 —Flowsheet of oxygen regeneration electrolysis stack production

B.3 Effect of Fabrication Variables on Performance

The objective of this phase of the program was to select the best techniques for electroding the cells and for joining cells together into series-connected stacks. Selection of the best techniques was based upon reproducibility, initial performance and degradation of performance with time.

The fabrication variables investigated included:

1. Electrode application technique -- sintered Pt-ZrO_2 electrodes were compared with the best composite electrodes (OBS #8).
2. Cell geometry -- cells with 1.7 cm active length were compared with those of 0.58 cm active length; a prime concern was to determine if uniform inside coverage could be achieved with the longer cells.
3. Joining technique -- Pt-Au brazing techniques used previously were compared with a new Pt-Au brazing technique employing tighter tolerances as well as with one employing a Pt-Pd-Ag brazing alloy.
4. Anode location -- O_2 generation at the inside electrode rather than outside electrode was tested.
5. Electrode weight -- 10 mg/cm^2 vs 20 mg/cm^2 was considered for selected electroding technique, cell geometry, brazing alloys and anode location.

In the remainder of Sec. B.3, the effects of these variables are first discussed in terms of the initial performance and then in terms of the long term performance.

B.3.1 Initial Performance

Each electrolysis stack was first operated at 100 ma/cm^2 for several days until a stable voltage was obtained. Initial cell resistance and polarization were then determined by the current-interrupt method (Reference 15). Oxygen production rate was measured, gas samples were

analyzed by gas mass spectrometer, and Faradaic current efficiency was calculated. In Table B-I the initial performances of OBS #13 and OBS #15 through 19 are compared with the initial performance of OBS #8, the best electrolysis stack constructed during the previous contract (Reference 3, pp. 30-33).

TABLE B-I

Comparison of Initial Performance of Bell and Spigot Cell Stacks

		OBS #8	OBS #13	OBS #15	OBS #16	OBS #17	OBS #18	OBS #19
Electrode material								
Anode		Composite[a]	$Pt-ZrO_2$	$Pt-ZrO_2$	$Pt-ZrO_2$	$Pt-ZrO_2$	$Pt-ZrO_2$	$Pt-ZrO_2$
Cathode		Pt	Pt	Pt	$Pt-ZrO_2$	$Pt-ZrO_2$	$Pt-ZrO_2$	$Pt-ZrO_2$
Electrode weight								
Anode	mg/cm^2	10.3	12.0	10.1	12.3	10.2	10.1	19.7
Cathode	mg/cm^2	8.7	12.5	11.5	10.7	9.5	10.5	18.3
Joint sealant alloy		Pt-Au	Pt-Au	Pt-Pd-Ag	Pt-Au	Pt-Pd-Ag	Pt-Au	Pt-Au
Current	amps	0.4	1.2	1.2	1.2	1.2	1.2	1.2
Active area/cell	cm^2	2	6	6	6	2	6	6
Temperature	°C	900	900	900	900	900	900	900
Gas flow rate	cc/min	170	100	100	85	85	85	85
Cell resistance								
Cell # 1	ohms	0.51	0.24	0.27	0.34	1.2	0.41	0.29
2		0.55	0.30	0.24	0.34	0.85	0.38	0.25
3		0.47	0.26	0.22	0.36	1.35	0.36	0.25
4		0.51	----	----	----	2.0	----	----
5		0.55	----	----	----	0.8	----	----
Average		0.52	0.27	0.24	0.35	1.24	0.38	0.27
Cell polarization								
Cell # 1	volts	0.24	0.39	0.25	0.23	0.49	0.22	0.25
2		0.34	0.24	0.28	0.26	0.50	0.23	0.19
3		0.18	0.24	0.30	0.22	0.49	0.26	0.20
4		0.18	----	----	----	0.43	----	----
5		0.25	----	----	----	0.43	----	----
Average		0.24	0.29	0.28	0.23	0.46	0.24	0.21
Cell driving voltage								
Cell #1	volts	1.25	1.39	1.31	1.40	1.54	1.50	1.40
2		1.35	1.36	1.35	1.35	1.47	1.50	1.35
3		1.10	1.31	1.39	1.45	1.70	1.52	1.37
4		1.10	----	----	----	1.95	----	----
5		1.12	----	----	----	1.50	----	----
Average		1.18	1.35	1.35	1.40	1.63	1.51	1.37
Oxygen purity	%	86	92	93	92	92	95	95

a. Sputtered $Pt-ZrO_2$ and sintered Pt.

The effects of the fabrication variables on initial cell resistance, polarization, and tightness, which can be noted from the results in the table, were:

1. Both initial resistance and polarization for OBS #17 were considerably higher than for any of the other cells tested. This poor performance resulted from a malfunction of the thermocouple used during brazing. As a result the stack was taken to too high a temperature so that most of the brazing alloy migrated over the electrode surface (closing pores and causing higher polarization) and very little flowed into the joint (causing higher resistance).
2. The resistance for the longer (6 cm^2 active area) cells are generally lower than for the shorter cells. (This observation is discussed in some detail below.)
3. The polarization at 200 mA/cm^2 does not appear to be a strong function of electrode material, electrode weight, joining technique, anode location, or cell geometry.
4. Stacks fabricated with the new joining techniques (using tighter tolerances) all had lower leakage rates (as indicated by initial oxygen purity) than did OBS #8. This was true for both brazing alloys employed.
5. The total driving voltage per cell is higher for large area cells than for short cells (see discussion below).

The differences in cell resistance and total voltage per cell between the long cells and the short cells is a direct result of the change in geometry, and do not in themselves indicate a superiority of one electroding or joining technique in comparison to the others.

The longer geometry was tried on the basis of previous optimization studies (Reference 3, pp. 102-113) which indicated that active areas between 4 and 8 cm^2/cell would result in a lower total weight penalty than smaller cells. The basic advantage is that fewer cells and, therefore,

fewer joints are required. Since stack failure usually is associated with the joint area, fewer joints implies lower probability of failure. Therefore, fewer spares are required to achieve a given reliability for a specific mission. The penalty that one pays for such a design is higher total voltage per cell (i.e., lower power efficiency). The optimization studies showed that the anticipated increase in reliability would outweigh the anticipated decrease in power efficiency.

The components of the cell resistance for large area cells (based on OBS #16 and 18) are compared with those for OBS #8 in Table B-II. Since the electrolyte resistance is inversely proportional to the cell active area, the large cell electrolyte resistance was reduced to one third of the small one (0.12 Ω vs. 0.36 Ω). The computation of electrode resistance, joint resistance and interface resistance for OBS #8 were discussed previously by Elikan and Morris (Reference 3, pp. 30-33). The estimation of these resistance components for the large cells was based upon measurements on OBS #16, 18, and 19 and is shown in Table B-III. Assuming that the ratio of film thicknesses was equal to the ratio of electrode coating weights, the average electrode resistance, R_e, for OBS #16 and 18 was 0.221 Ω, corresponding to a ρ/δ = 0.45 ohms. This is approximately the same as the values (0.4 to 0.6 ohms) measured for sintered Pt electrodes of the same weight density.

TABLE B-II

Comparison of Resistances of Short and Long Bell and Spigot Cells

Description	Short Bell and Spigot Cell	Long Bell and Spigot Cell
Active cell length	L = 0.583 cm	L = 1.70 cm
Outside diameter	D = 1.1 cm	D = 1.1 cm
Active cell area	$\pi DL = 0.583 \times 1.1 \times 3.14 = 2\ cm^2$	$\pi DL = 1.7 \times 1.1 \times 3.14 = 5.9\ cm^2$
Electrolyte resistivity at 900°C	$\rho_b = 18\Omega$ - cm	$\rho_b = 18\Omega$ - cm
Electrolyte thickness	$\delta_b = 0.04$ cm	$\delta_b = 0.04$ cm
Electrolyte resistance	$R_b = \frac{\rho_b \delta_b}{\pi LD} = \frac{18 \times 0.04}{3.14 \times 0.583 \times 1.1} = 0.358\Omega$ 1	$R_b = \frac{\rho_b \delta_b}{\pi LD} = \frac{18 \times 0.04}{3.14 \times 1.7 \times 1.1} = 0.123\Omega$ 1
Resistivity thickness quotient		
Anode	$(\frac{\rho}{\delta}) = 0.6$ (composite electrode)	$(\frac{\rho}{\delta})_a = (\frac{\rho}{\delta})_c = 0.45$ (calculated based on experimental values - See Table B-III)
Cathode	$(\frac{\rho}{\delta}) = 0.4$ (Pt electrode)	
Electrode resistance	$R_e = \frac{L}{2\pi D}[\frac{\rho_c}{\delta_c} + \frac{\rho_a}{\delta_a}] = \frac{0.583}{2 \times \pi \times 1.1}[0.6 + 0.4]$ $= 0.08\Omega$ 2	$R_e = \frac{L}{2\pi D}[\frac{\rho_c}{\delta_c} + \frac{\rho_a}{\delta_a}]$ $= \frac{1.7}{2 \times \pi \times 1.1}[0.45 + 0.45] = 0.221\Omega$ 2
Interface resistance	$R_i = 0.03\Omega$ (estimated) 3	$R_i + R_j = 0.021$ ohm (experimental) 3 4
Joint resistance	$R_j = 0.05\Omega$ (computed by the difference of total resistance) 4	
Experimental cell resistance	1 + 2 + 3 + 4 = 0.52 ohms (OBS #8)	1 + 2 + 3 + 4 = 0.365 ohms (Avg of OBS #16 and #18)

TABLE B-III

Calculation of $(\frac{\rho}{\delta})$ and Joint Resistance of Sintered $Pt-ZrO_2$ Electrode Based on the Resistances of Cells with Different Electrode Thicknesses

	Thin Electrodes			Thick Electrode
	OBS #16	OBS #18	Average	OBS #19
W_c, Cathode weight, mg/cm^2	12.3	10.1	11.2	19.7
W_a, Anode weight, mg/cm^2	10.7	10.5	10.6	18.3
R_c, Average cell resistance, ohms	0.35	0.38	0.365	0.27
R_b, Electrolyte resistance, ohms	0.123	0.123	0.123	0.123
$R_i + R_j + R_e$ Sum of resistances of interface, joint, and electrodes	0.227	0.257	0.242	0.147

The thickness ratio of the two electrodes $(\frac{\delta_n}{\delta_k})$ can be calculated by the weight ratio $(\frac{W_n}{W_k})$

where subscripts n and k refer to "thin" and "thick" electrodes, respectively.

For Cathode

$$(\frac{\delta_n}{\delta_k}) = \frac{11.2}{19.7}, \text{ and } \delta_k = 1.75\ \delta_n$$

For Anode

$$(\frac{\delta_n}{\delta_k}) = \frac{10.6}{18.3}, \text{ and } \delta_k = 1.73\ \delta_n$$

Assume the joint and interface resistances are independent of electrode resistance

For thin electrode:

$$(R_e)_n + R_j + R_i = \frac{L\rho}{2\pi D}\left[\frac{1}{\delta_c} + \frac{1}{\delta_a}\right]_n + R_j + R_i = 0.242 \qquad \text{(B-1)}$$

For thick electrode:

$$(R_e)_k + R_j + R_i = \frac{L\rho}{2\pi D}\left[\frac{1}{\delta_c} + \frac{1}{\delta_a}\right]_k + R_j + R_i = 0.147 \qquad \text{(B-2)}$$

Since $(\delta_c)_n \approx (\delta_a)_n = \delta$, $\therefore (\delta_c)_k = 1.75\delta$, $(\delta_a)_k = 1.73\delta$

where L = 1.7 cm, D = 1.1 cm.

Substituting these into (B-1) and (B-2) we have

$$(0.495)\ (\frac{\rho}{\delta}) + R_j + R_i + .242 \qquad \text{(B-3)}$$

$$(0.285)\ (\frac{\rho}{\delta}) + R_j + R_i = .147 \qquad \text{(B-4)}$$

Solving (B-3) and (B-4) simultaneously, we have

$$0.21\ (\frac{\rho}{\delta}) = 0.095,\ (\frac{\rho}{\delta}) = 0.45 \text{ ohms}$$

and $R_i + R_j = 0.021$ ohms

The major improvement in initial performance for the stacks constructed under this contract is improved joint performance. In addition to the higher oxygen purity cited previously, the sum of joint resistance plus contact resistance has been decreased from an estimated .08 ohms for OBS #8 to .021 ohms.

One feature of Table B-I is not clearly understood. The initial resistances of OBS #13 and OBS #15 are significantly lower than those for OBS #16 and OBS #18. The electrode weights for all of these stacks were comparable, $\sim$10 mg/cm^2. The cells with lower apparent resistance pumped oxygen from the inside to the outside of the cells and employed sintered Pt rather than sintered Pt-ZrO_2 as the cathode. Whether cathode location or cathode material caused the reduction in electrode resistance--or some outside influence such as a subtle change in firing procedure--was not established.

B.3.2 Life Test Results

With the exception of OBS #17, all of the stacks tested in this phase of work achieved an operating life of 80 days or longer. Both cell driving voltage and current efficiency showed a high degree of stability during the life test. Cell voltages vs. time are plotted in Figs. B4 and B5. The results are summarized in Table B-IV.

The primary measure of cell performance at a given time is the power required per unit weight (or volume) of oxygen generated. The figure most often cited is the power required to produce enough oxygen to support one man (watts/man). This is an unfortunate choice, since the oxygen required by a man varies with activity level and from person to person. No industry standard "man" has been established. For example, Popma and Collins (Reference 16) selected 1.92 lbs of O_2 per day per man while the AILSS study was based on 1.72 lbs per day.

The power requirements computed in this report are based upon 2.0 lbs of O_2 per man per day, primarily as a result of a man's requirements having been thus defined in the original contract work statement

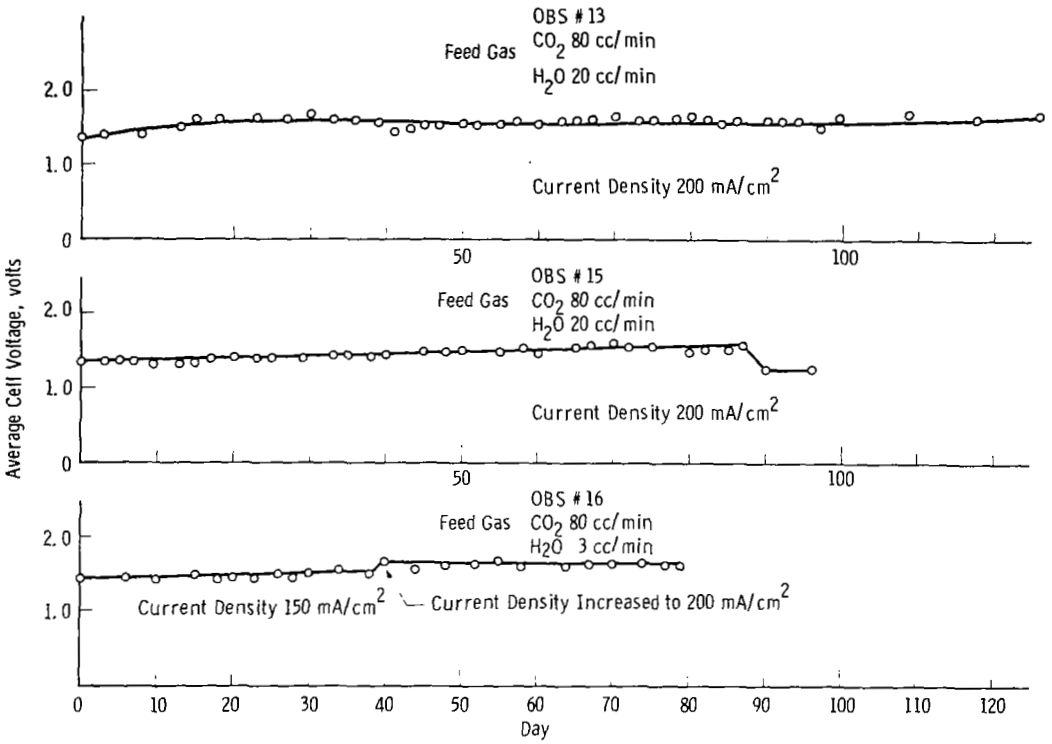

Fig. B4 -- Life test performance of OBS #13, 15, and 16

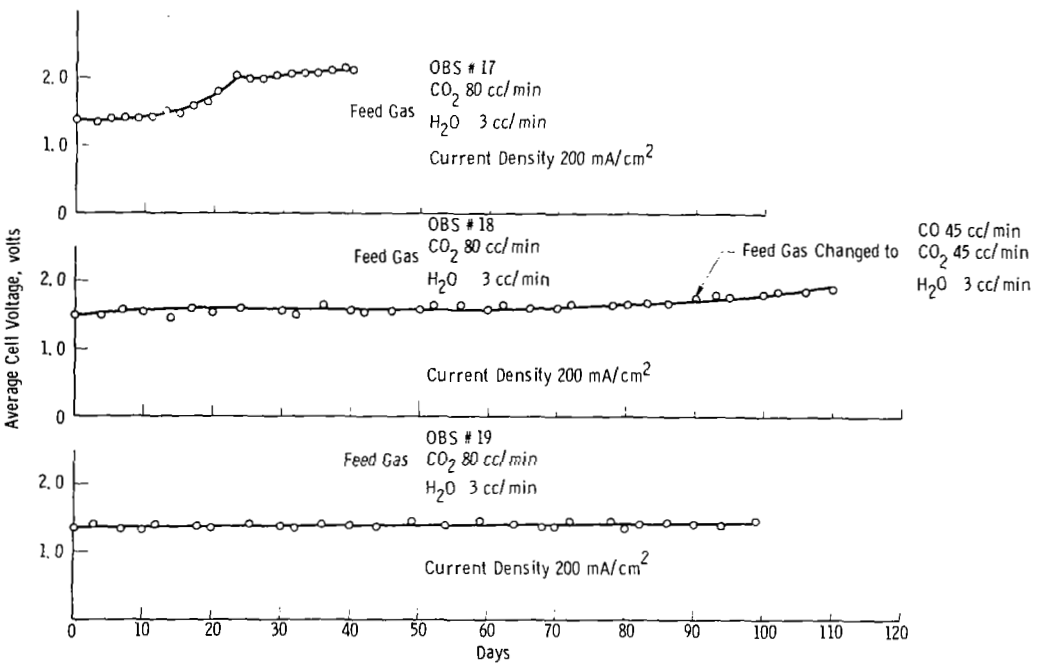

Fig. B5 -- Life test performance of OBS #17, 18 and 19

TABLE B-IV

Summary of Fabrication Variable Life Tests

Current density 200 ma/cm^2, temperature 900°C

Description	OBS #8	OBS #13	OBS #15	OBS #16	OBS #17	OBS #18	OBS #19
Electrode weight (average) mg/cm^2	95	12.3	10.6	11.5	9.9	10.3	19.0
Joint sealant alloy	Pt - Au	Pt - Au	Pt - Pd - Ag	Pt - Au	Pt - Pd - Ag	Pt - Au	Pt - Au
CO_2 flowrate cc/min	170	100	100	80	80	80	80
Water vapor %	20	20	20	3	3	3	3
Number of cells operated	5	3	2	3	3	2	3
Anode position	Outside	Outside	Outside	Inside	Inside	Inside	Inside
Average cell voltage (V.)							
Initial volts	1.18	1.35	1.35	1.40	1.63	1.51	1.35
30th day	1.25	1.57	1.42	1.50	2.1	1.55	1.35
60th day	1.52	1.56	1.50	1.57	----	1.60	1.36
90th day	1.80	1.57	1.50	----	----	1.67	1.40
Final	2.1	1.70	----	1.62	2.1	1.90	1.45
Oxygen purity							
Initial %	86	92	93	92	92	95	95
Final	85	91	88	89	88	93	90
Current efficiency (100E)							
Initial %	89	91	94	92	92	90	94
Final	53	90	89	89	89	89	89
Electrolysis power (P)							
Initial watt/man	167	188	182	193	197	213	181
After 90 days	309	221	214	232	---	244	200
Power degradation rate watt/man/day	1.67	0.37	0.36	0.43	2.9	0.34	0.21
Time in operation days	152	126	96	80	40	Switched to high DD* after 60	Switched to high DD* after 99

* High DD: High degree of decomposition of CO_2 and water

(Contract NAS1-7306). Adoption of a more definitive performance criteria for electrolysis, such as watt hours/lb of oxygen produced is recommended.

Power per man is defined in this work as

$$P = \frac{V \times I \times N_s \times 498}{F_{O_2}} \qquad \text{(B-5)}$$

where

V = average cell driving voltage, volts

I = cell current, amps

N_s = number of cells

498 = cc/min of O_2 at RTP equivalent to 2.0 lbs/day

F_{O_2} = flow rate of pure O_2 produced, cc/min

= oxygen stream flow x oxygen purity

Alternately the electrolysis power/man can be defined in terms of the driving voltage and the current efficiency.

Let E = current efficiency

$$= \frac{\text{pure oxygen produced at a given current flow}}{\text{theoretical oxygen at a given current flow}}$$

$$= \frac{F_{O_2} \frac{cc}{min} \text{ (RTP)}}{3{\cdot}9 \frac{cc\,(RTP)}{min \cdot amp} \times I(amp) \times N_s} \qquad \text{(B-6)}$$

where RTP = room temperature and pressure

Therefore

$$F_{O_2} = 3{\cdot}9 \times I \times N_S \times E \qquad \text{(B-7)}$$

Substituting Eq. (B-7) into (B-5)

$$P = V\left(\frac{IN_s}{F_{O_2}}\right)498 = \frac{498\ V}{3.9\ E} = 126.8\ V/E \qquad \text{(B-8)}$$

The multiplier of V/E in Eq. (B-8) (126.8) is the current flow (amps) required to produce 2.0 lbs of oxygen/day.

The rate of decline in cell performance is indicated by the power degradation rate, defined as

$$\frac{\Delta P}{\Delta t} = \text{power degradation rate}$$

$$= \frac{\text{(Power at time t) - (Power at time zero)}}{t}$$

$$= \frac{P(t) - P(o)}{t}$$

t = the time on test.

The overall performance during the test can be indicated quantitatively by the average electrolysis power required during the test period, i.e.,

$$P_{Avg}(t) = \sum_{j=1}^{t} P(j)/t \qquad \text{(B-9)}$$

For a linear degradation rate

$$P_{Avg}(t) = [P(o) + P(t)]/2$$

$$= P(o) + 1/2 \left(\frac{\Delta P}{\Delta t}\right) t$$

$$= P\ (1/2t) \qquad \text{(B-10)}$$

Thus, if the degradation rate is linear, the average power/man for 60 days is equal to the power/man required on the 30th day, etc.

In the subsections which follow, the effect of various fabrication variables on $P_{Avg}(180)$ is discussed.

B.3.2.1 Overall Effect of New Electroding and Joining Technique

The most dramatic effect to be noted in Table B-IV is reduction in power degradation rate and electrolysis power at the end of 90 days. The average power required at the end of 90 days for OBS #13, 15, 16, 18, and 19, all made using sintered Pt-ZrO_2 anodes and employing closer tolerances for the joint fit, was 222.2 watts/man compared to 309 watts/man for OBS #8, the best of the stacks made with composite anodes and less stringent joint tolerances.

Microscopic examination showed that the two principal causes of failure observed previously (Reference 3, pp. 40-44), electrode peeling and discontinuity at the electrode joint interface, had been essentially eliminated. The comparison shown in Fig. B6 is typical. Except for OBS #17, none of the new cells tested in the fabrication variable tests failed; the life tests were terminated in order to use the test facilities for the study of the effect of operating variables.

It is believed that most of the improvement in life noted above can be attributed to the use of sintered Pt-ZrO_2 electrodes rather than composite electrodes. The lower joint leakage and resistance discussed under initial performance (Sec. B.3.1) were the principal benefits achieved by closer joint tolerances.

It is of particular significance to note that the better joint performance was achieved despite the use of the longer cell geometry which tripled the current density through the joint. This is, perhaps, the strongest evidence available for the dramatic improvement achieved by the new techniques for electroding and joining.

B.3.2.2 Effect of Brazing Alloy

The primary difference noted between the two brazing alloys was that the Pt-Au brazing process seemed to be more easily controlled. The Pt-Ag-Pd joints were brazed at 1200°C while the Pt-Au joints were brazed at 1070°C. Less experience was available to guide in the selection of control methods used for the Pt-Pd-Ag and only one of the two

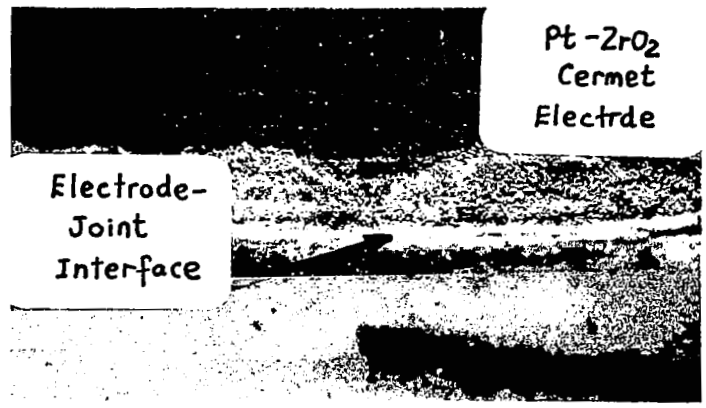

OBS #19
(20X)

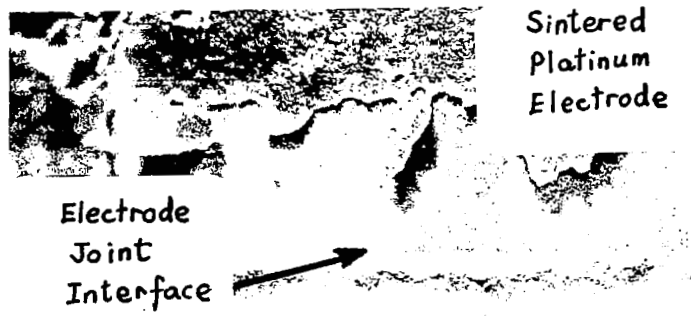

OBS #8
(15X)

Fig. B-6a - Comparison of electrodes and electrode-joint interface of stacks constructed by new fabrication technique (OBS #19) and by old techniques (OBS #8).

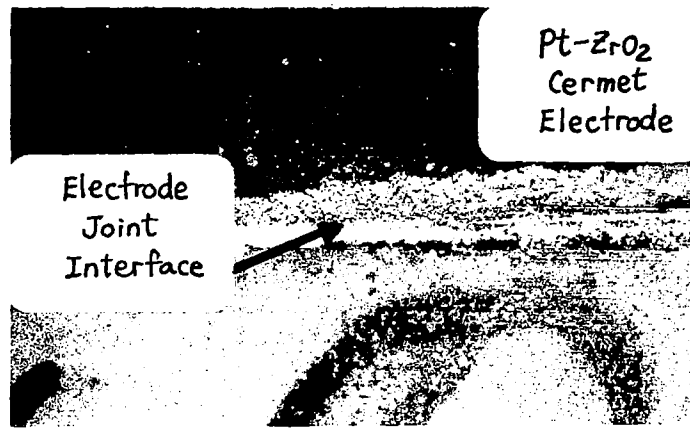

OBS #19
(20X)

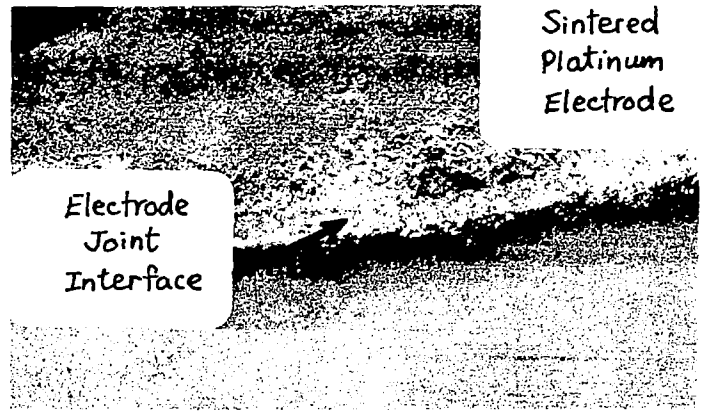

OBS #8
(15X)

Fig. B-6b - Comparison of electrodes and electrode-joint interface of stacks constructed by new fabrication technique (OBS #19) and by old techniques (OBS #8).

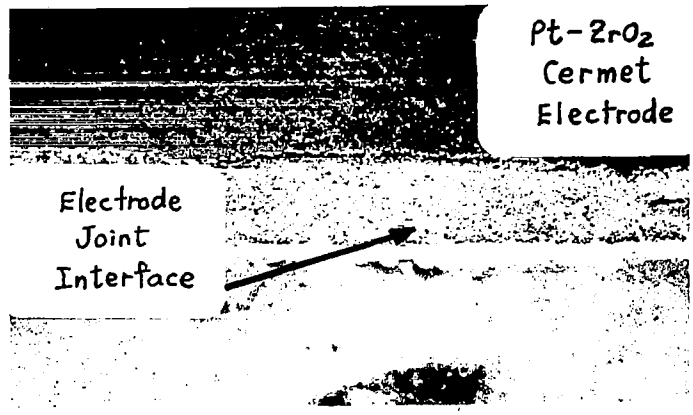

OBS #19
(20X)

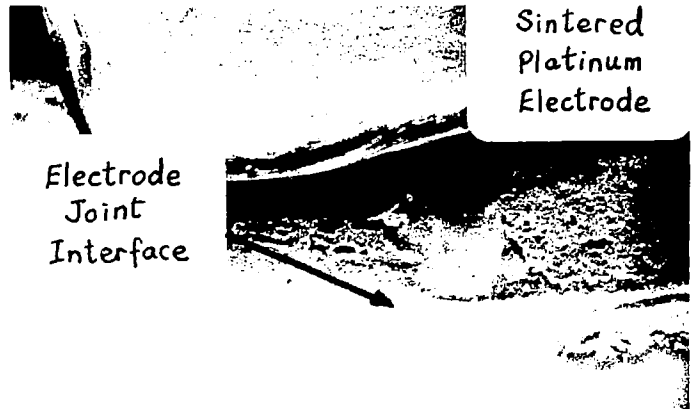

OBS #8
(15X)

Fig. B-6c - Comparison of electrodes and electrode-joint interface of stacks constructed by new fabrication technique (OBS #19) and by old techniques (OBS #8).

stacks constructed and tested was satisfactory. The $P_{Avg}(90)$ for the good stack (OBS #15) was 214 watts/man, which is within the range of the power requirements of the stacks employing Pt-Au joints.

OBS #17 is an example of a Pt-Pd-Ag brazed stack over which full control was not achieved. The stack was overheated. The fact that the Pd alloy did not flow into the joint but migrated above into the cathode of the cells was later confirmed by the cross-section examinations of the cell joint after life test. Initial characterization of OBS #17 showed both cell resistance and cell voltage were abnormally high.

B.3.2.3 Effect of Other Fabrication Variables

In addition to electrode application technique, the cell geometry, and the brazing alloy, other aspects of the fabrication procedure investigated included the placement of the anode (inside vs. outside) and the weight of the electrodes applied.

Increasing the electrode weight from approximately 10 mg/cm^2 to 19 mg/cm^2 caused a significant reduction in $P_{Avg}(90)$. This conclusion is based on a comparison of the performance of OBS #19 against that of OBS #16 and OBS #18, which were identical in all respects except electrode weight.

No significant difference was found utilizing a sintered $Pt\text{-}ZrO_2$ electrode on the outside as the anode rather than a similar electrode on the inside. This conclusion is based on the comparison of OBS #13 and 15 with OBS #'s 16, 18, and 19. The stacks with the anode on the inside showed a $P_{Avg}(90)$ of 217.5 watts/man compared to 224.7 watts/man for stacks with the anode on the outside.

B.4 Selected Fabrication Techniques

The fabrication method chosen for the construction of the electrolysis stacks for the study of operating variable effects and for use in the breadboard employed:

1. Sintered Pt-ZrO_2 anodes and cathodes.

2. Long cell geometry.

3. Pt-Au brazing with close dimensional tolerances.

4. Anode placement on the inside.

5. Electrode densities between 15 and 20 mg/cm^2*

Selection of sintered Pt-ZrO_2 electrodes and close dimensional tolerances was clearly dictated by the significant improvement in long term performance demonstrated in previous sections. The long cell geometry was selected because no detrimental effect on life was noted as a result of tripling the current density through the joint, and previous optimization studies indicated that the small increase in power/man resulting from slightly higher resistance losses would be outweighed by the reduction in the number of spare stacks as a result of reducing the number of joints.

Anode placement on the inside was chosen primarily to allow complete freedom in base plate design for the breadboard.

High weight densities were chosen because of their apparent reduction in electrode resistance without noticeable increase in polarization as well as the statistically significant reduction in P(90).

Pt-Au brazing was selected because of the improved tightness and life characteristics achieved in this study and because longer experience in the use of this alloy allowed better reproducibility than with Pt-Ag-Pd.

---

* All of the cells in Table B-I do not fall in this range since some were constructed prior to completion of the fabrication variable tests.

APPENDIX C

EFFECT OF OPERATING CONDITIONS ON ELECTROLYSIS STACK PERFORMANCE

In order to define the optimum operating conditions for the breadboard electrolysis unit, electrolysis stacks made using the best fabrication procedure defined in Appendix B were life tested under various operating conditions. Feed compositions which might be encountered in a practical operating integrated system were utilized. The effects of the temperature and current density on cell life were also evaluated. The experimental plan for the study is outlined in Table C-I.

TABLE C-I

Experimental Plan for Operating Variable Study

DD	Electrolysis Current, mA/cm^2					
	166	200			300	
0.6	OBS #25 900°C					
0.7	OBS #21 900°C	OBS #23 900°C	OBS #24 900°C	OBS #19 900°C	OBS #26 900°C	OBS #27 1000°C
0.8		OBS #20 900°C	OBS #22 900°C			

Nine three-cell stacks (OBS #19 through OBS #27) were utilized for this study. Fabrication data for these stacks are listed in Table C-II. Note that OBS #19 had been tested for 99 days (See Appendix B) before being used in the operating variable life test and that OBS #20, constructed before the completion of the fabrication variable tests, had platinum-palladium-silver joints.

TABLE C-II

Initial Performance of Individual Cells of Stacks OBS #19 through OBS #27

Feed gas $\frac{CO}{CO_2}$ ratio = 1; water vapor = 3%

		OBS#19	OBS#20	OBS#21	OBS#22	OBS#23	OBS#24	OBS#25	OBS#26	OBS#27
Cathode weight	mg/cm^2	20.0 20.2 18.9	19.2 18.7 18.2	10.1 9.8 9.5	11.7 10.5 9.9	18.7 12.3 15.2	14.2 14.4 15.2	16.4 16.0 12.8	13.0 12.9 12.8	14.4 13.2 11.3
Anode weight	mg/cm^2	16.7 19.3 18.9	18.7 19.7 19.2	11.8 12.3 11.6	9.4 8.9 9.9	15.2 13.7 12.5	13.7 15.3 13.0	15.7 14.3 15.6	14.8 13.9 14.5	14.5 13.5 14.9
Joint sealant		Pt-Au	Pt-Pd-Ag	Pt-Au	Pt-Au	Pt-Au	Pt-Au	Pt-Au	Pt-Au	Pt-Au
Anode arrangement		Inside	Inside	Inside	Inside	Inside	Inside	Inside	Inside	Inside
Operating temperature	°C	900	900	900	900	900	900	900	900	1000
Current density	ma/cm^2	200	200	166	200	200	200	166	300	300
Gas flow rate	cc/min	130	100	100	120	130	130	230	210	210
Initial DD	%	0.7	0.85	0.7	0.8	0.7	0.7	0.6	0.7	0.7
Initial cell resistance	ohms	0.25 0.29 0.25	0.25 0.21 0.25	0.35 0.34 0.35	0.30 0.28 0.25	0.30 0.29 0.21	0.26 0.32 0.27	0.20 0.24 0.21	0.21 0.23 0.29	0.27 0.25 0.30
Initial cell polarization	volts	0.25 0.19 0.11	0.20 0.15 0.24	0.25 0.20 0.20	0.25 0.20 0.20	0.16 0.12 0.17	0.18 0.20 0.15	0.15 0.20 0.20	0.24 0.35 0.30	0.22 0.22 0.33
Initial cell voltage	volts	1.44 1.56 1.48	1.38 1.34 1.32	1.49 1.63 1.53	1.45 1.37 1.38	1.37 1.39 1.45	1.44 1.52 1.48	1.20 1.25 1.28	1.66 1.67 1.75	1.42 1.50 1.50
Initial oxygen purity	%	90	96	92	91	97	99	98	98	99
Initial current efficiency	%	89	91	89	85	93	95	89	95	92
Initial power requirement	watt/man	212	189	222	200	192	196	176	224	202

C.1 Notes Regarding the Operating Conditions

In the closed loop operation of the solid electrolyte oxygen regeneration system, the feed to the electrolysis unit is formed by mixing fresh CO_2 and water with the recycle stream from the outlet of the carbon deposition reactor. For the operating breadboard system, the composition of this mixture was approximately 50% CO_2, 40% CO, and 10% H_2 plus H_2O (see Fig. 2). For this study, the feed gas utilized consisted of equal amounts of CO_2 and CO, saturated with water vapor at room temperature.

The degree of decomposition (DD) has been defined as the volume fraction of CO and H_2 in the gas stream leaving the electrolysis

stack (corrected for hydrogen removed and for nitrogen contamination). For example, if the exit composition is 55% CO, 38% CO_2, 5% H_2, and 2% H_2O and no hydrogen was removed, then the degree of decomposition is 0.60. Since the conversion of CO in the carbon deposition reactor is limited by equilibrium considerations, the gas composition leaving the electrolysis unit will determine the recycle rate and the size of the carbon deposition reactor. Results obtained with the continuous carbon deposition reactor indicated that the CO concentration in the feed must be greater than 35 mole percent, since no reaction occurred at lower concentrations.

In a practical sense, DD's less than 0.6 were considered impractical, because of excessive recycle rate and carbon deposition reactor size. Elikan (Reference 2) reported earlier that DD's greater than 0.9 could not be achieved using CO_2 feed without electrolyte reduction even in tests lasting a few hours. Based on these considerations, we planned to test stacks at DD's between 0.6 and 0.8. To achieve the desired DD's at the desired current densities (indicated in Table C-I) the feed rate was adjusted.

C.2 Effect of Operating Variables on Electrolysis Stack Performance

The pre-test characterization and break-in procedure for each electrolysis stack was the same described in Section B.2.1 of Appendix B. Data obtained during initial cell characterization and the life tests are summarized in Table C-II and C-III. The average cell driving voltage for each stack vs time of operation are plotted in Figs. C1, C2, and C3.

C.2.1 Correlation of Power Required with Severity of Operating Conditions

The five electrolysis stacks operated under moderately severe conditions (OBS #19, 21, 23, 24, and 25) operated 120 days or longer with excellent performance. Those tested at more severe conditions (OBS #20, 22, 26, and 27) declined rapidly and failed within 50 days

TABLE C-III

Summary of Operating Variable Life Tests

		OBS 19	OBS 20	OBS 21	OBS 22	OBS 23	OBS 24	OBS 25	OBS 26	OBS 27
Cell Voltage, volts		1.44	1.38	1.49	1.45	1.37	1.44	1.20	1.66	1.42
	Initial	1.56	1.34	1.63	1.37	1.39	1.52	1.25	1.67	1.50
		1.48	1.32	1.53	1.38	1.45	1.48	1.28	1.75	1.50
		1.45	2.02	1.50	1.49	1.49	1.47	1.24	1.62	1.70
	30th Day	1.58	1.97	1.62	1.43	1.51	1.56	1.38	1.65	Shunted
		1.51	1.94	1.53	1.40	1.58	1.52	1.46	2.95	Shunted
		1.49	2.04	1.56	1.50	1.70	1.42	1.43		
	60th Day	1.62	1.97	1.66	1.44	1.72	1.53	1.65		
		1.53	1.98	1.54	1.42	1.80	1.55	1.54		
		1.50		1.57	1.51	1.67	1.50	1.45		
	90th Day	1.63		1.71	1.46	1.71	1.54	1.70		
		1.53		1.61	1.42	1.86	1.50	1.60		
		1.52		1.91		1.75	1.54	1.52		
	120th Day	1.66		Shunted		1.73	1.65	1.70		
		1.57		1.71		1.73	1.50	1.70		
				1.85		1.79	1.60	1.51		
	150th Day			Shunted		1.91	1.74	1.84		
				1.70		1.82	1.61	1.74		
				2.28			1.60	1.82		
	180th Day			Shunted			2.15	2.22		
				1.87			1.65	2.12		
				2.42			2.06	2.03		
	210th Day			Shunted			Shunted	2.30		
				1.98			2.16	2.44		
		1.51	2.34	2.61	1.50	1.77	2.20	1.90	1.65	1.93
	Final Day	1.67	2.08	Shunted	1.44	1.94	Shunted	2.60	1.68	Shunted
		1.58	2.25	2.14	1.41	1.83	2.30	2.30	Shunted	Shunted
Power/Man, watts										
	Initial	212	189	222	200	192	196	176	224	202
	30th Day	220	415	222	412	210	204	195	363	669
	60th Day	228	719	228	457	238	201	221		
	90th Day	244		236	526	240	202	226		
	120th Day	265		265		244	218	235		
	150th Day			299			239	255		
Current Efficiency, %										
	Initial	89	91	89	89	93	95	89	95	92
	30th Day	88	61	89	44	93	94	89	44	32
	60th Day	86	35	88	40	92	94	88		
	90th Day	81		88	35	92	94	88		
	120th Day	81		87		90	91	88		
	150th Day			75			87	85		
Battery Life, days		135	73	245	100	154	295	215	49	33

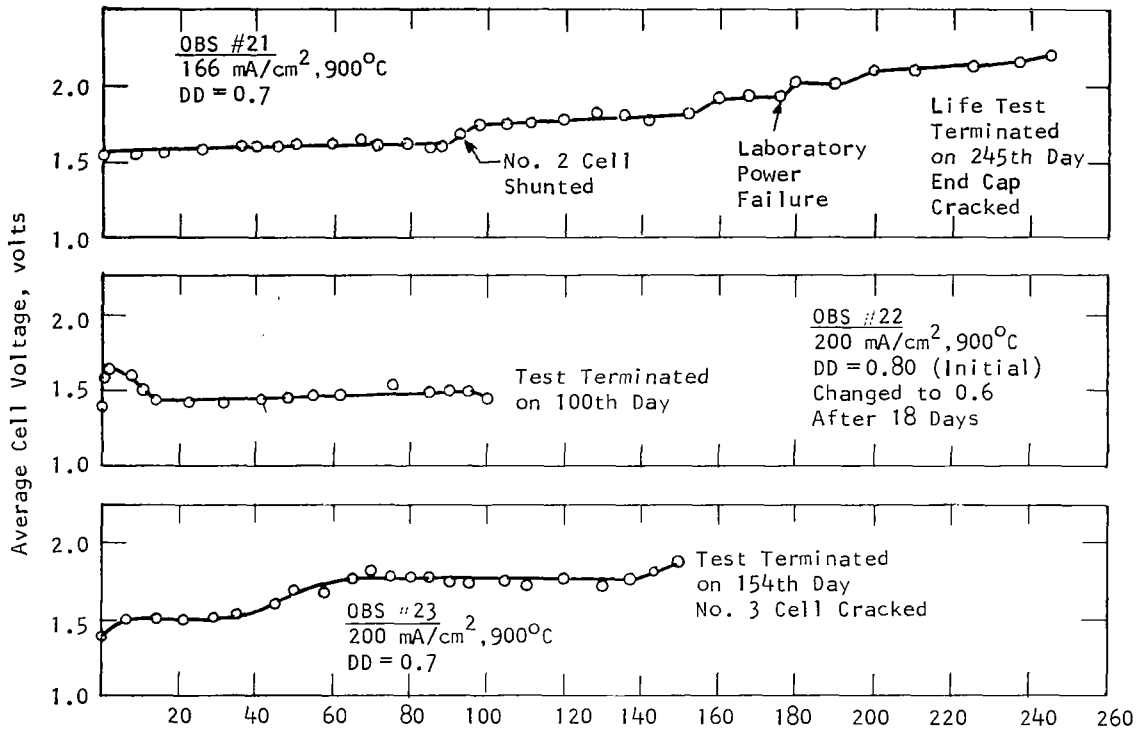

Fig. C1 -- Performance of OBS #21, #22, and #23 During Life Test

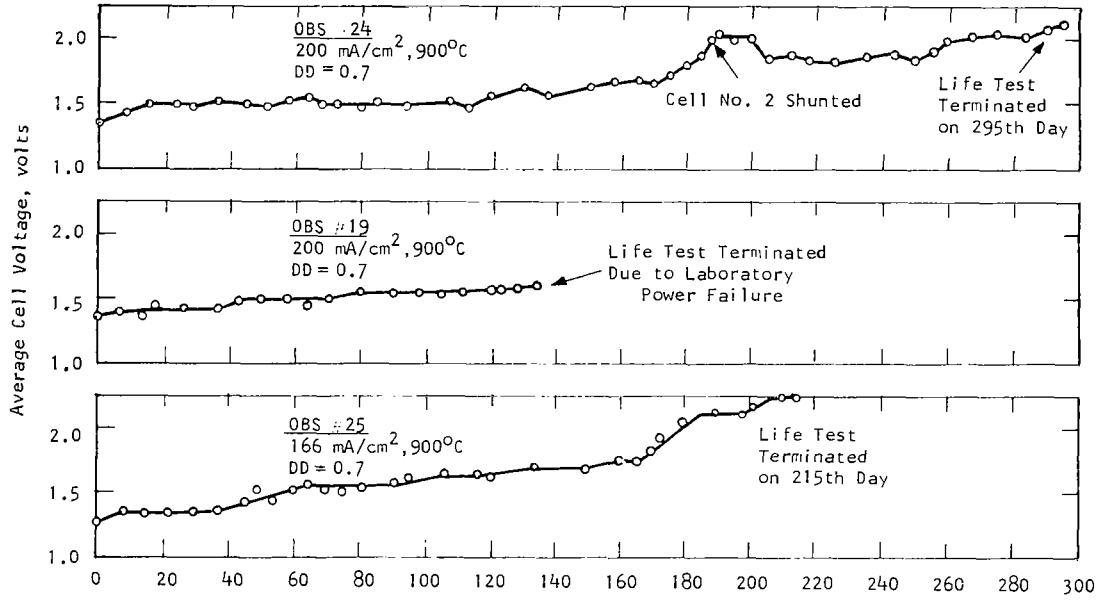

Fig. C2 -- Performance of OBS #24, #25, and #19 During Life Tests

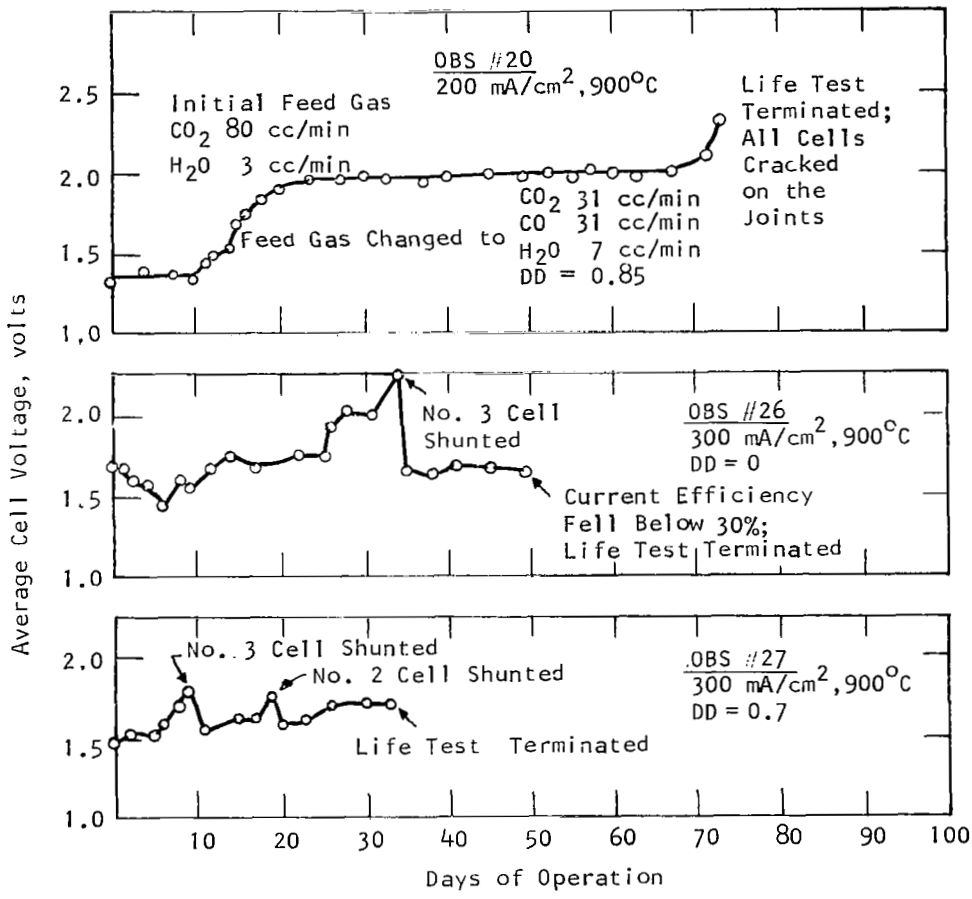

Fig. C3 -- Performance of OBS #20, #26, and #27 during life tests

or less. Comparison of the power requirement per man (see Appendix Section B.3) of electrolysis stacks on the 30th and 90th days are listed in Table C-IV.

C.2.2 Correlation of Power Requirements with Time

Five batteries,OBS #19, 21, 23, 24, and 25, had successfully operated over 120 days with high performance. The operating data of these five batteries were correlated with time of operation. Statistical models were established to correlate the driving voltage/cell and power requirement/man as a function of time. The correlation coefficients of both equations were approximately 0.75. Figure C4 shows both the correlations of these two functions and the experimental results.

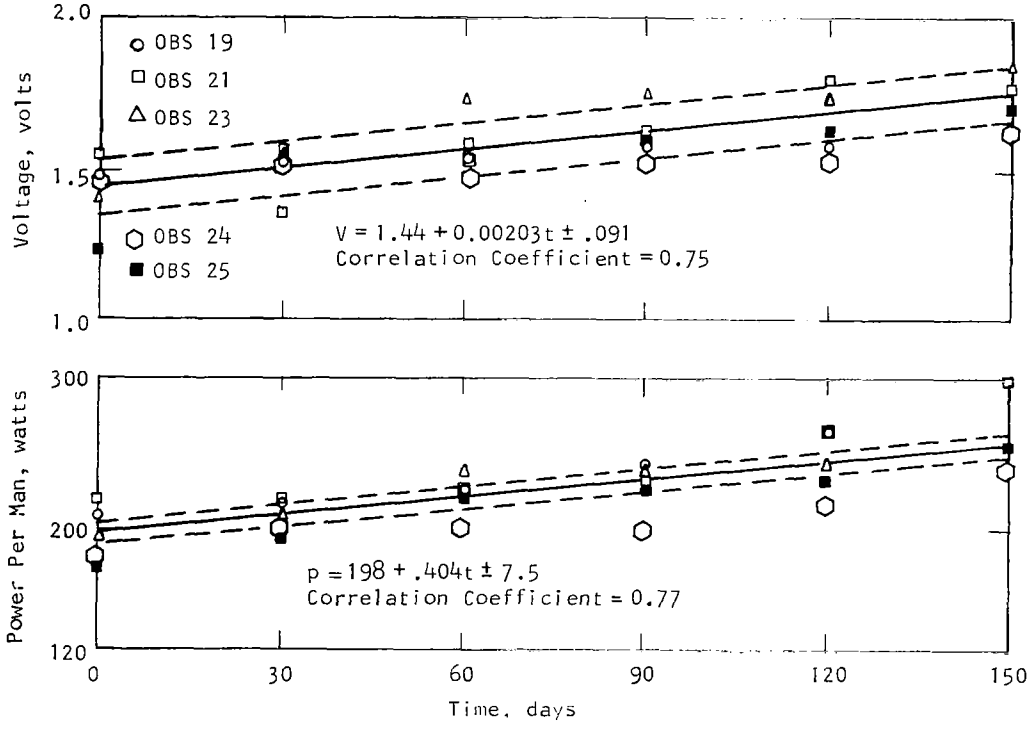

Fig. C4 -- Correlation of Driving Voltage and Power Required with Time

TABLE C-IV

Comparison of Power Requirements
of Electrolysis Stacks on 30th and 90th Days

30th Day

Degree of Decomp.	Current Density, ma/cm^2					
	166	200			300	
0.6	OBS #25[a] 900°C 195 0.63					
0.7	OBS #21 900°C 222 0.0	OBS #19 900°C 220 0.26	OBS #24 900°C 204 0.27	OBS #23 900°C 210 0.60	OBS #26 900°C 363 4.6	OBS #27 1000°C 669 15.5
$\geq$ 0.8		OBS #20 900°C 415 7.5	OBS #22 900°C 412 7.1			

90th Day

0.6	OBS #25 900°C 226 1.6				
0.7	OBS #21 900°C 236 0.46	OBS #19 900°C 244 1.06	OBS #24 900°C 202 0.2	OBS #23 900°C 240 1.6	
$\geq$ 0.8			OBS #22 900°C 526 10.8		

a. OBS#
T
P
R

where T = operating temperature, °C
P = power requirement, watts/man
R = rate of degradation, watts/man/day

The first equation describes the driving voltage as a function of t (day): V = 1.44 + 0.00203 t. The intercept 1.44 volts/cell represents the initial voltage/cell. The slope 0.00203 volts/cell/day is the degradation rate per cell. The power requirement per man is expressed as: P = 198 + .404 t. The average initial electrolysis power is thus 198 watt/man and the degradation rate is 0.404 watts/man/day.

C.2.3 Correlations Between Time to Failure and Initial Cell Properties

Other correlations were carried out in an attempt to define improvements in fabrication technique which might extend the electrolysis cell life. Figure C5 shows the strong correlation between initial joint resistance and the time before the initial cell failure occurred. The cell life can be expressed as an inverse linear function of joint resistance.

A plot of initial polarization vs cell life is shown in Fig. C6. No correlation was obtained for polarizations below 0.20 volt; however, a weak correlation was found for polarizations above 0.25 volt.

Failure frequency is plotted as a function of position in battery in Fig. C7. The probability of failure of the first cell, which operated on fresh feed, was lower than that of the second and third cells.

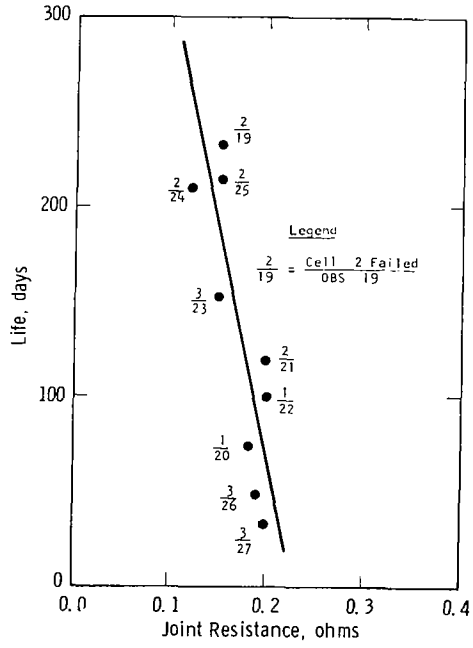

Fig. C5 -- Initial Joint Resistance Vs Time of the Initial Cell Failure

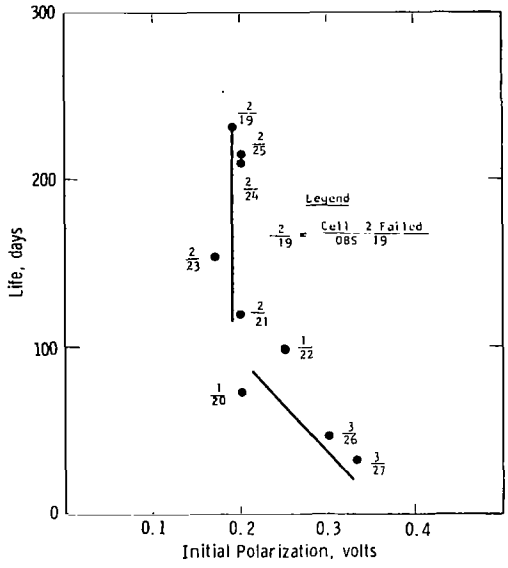

Fig. C6 -- Initial Polarization Vs Time of the Initial Cell Failure

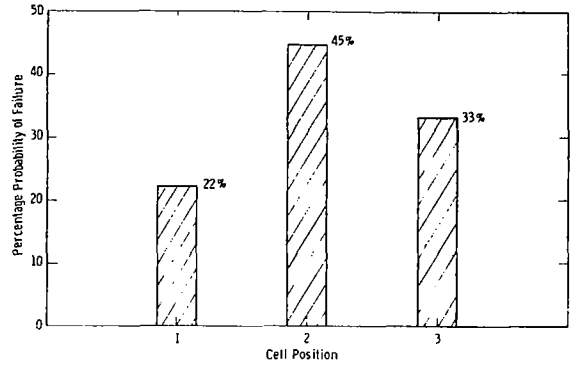

Fig. C7 -- Failure Frequency Vs Position in Battery of 3 Cell Batteries

C.3 Post-test Examination of Electrolysis Stacks

Anodes- The anodes (inside electrodes) of the cells were found to be in good condition (see Table C-V). Loss of platinum through evaporation of the anode was not noticeable even after 295 days of operation. This is in sharp contrast with the composite anodes used previously, on which bare electrolyte was observed after 80-100 days (Reference 3, pp. 40-44). The electrode structure remained porous. Sintering of platinum occurred only in OBS #26 and OBS #27, both of which were operated at high current density. The sintering effect was more severe in OBS #27, probably because of its higher operating temperature.

Cathodes- Although the color of the cathodes darkened, they remained conductive and porous. Adherence was good for those cells

TABLE C-V

Post-Test Examination of Electrolysis Stacks

	OBS#19	OBS#20	OBS#21	OBS#22	OBS#23	OBS#24	OBS#25	OBS#26	OBS#27
Cathode Resistance Before Life Test, ohms*	0.1 0.1 0.1	0.1 0.2 0.2	0.2 0.2 0.2	0.2 0.2 0.2	0.1 0.1 0.1	0.2 0.2 0.2	0.1 0.1 0.2	0.1 0.2 0.2	0.2 0.2 0.2
Joint Resistance Before Life Test, ohms*	0.1 0.2 0.1	0.1 0.2 0.2	0.2 0.2 0.2	0.2 0.2 0.2	0.2 0.1 0.1	0.1 0.1 0.1	0.1 0.1 0.1	0.2 0.2 0.2	0.2 0.2 0.2
Cathode Resistance After Failure, ohms*	0.2 0.2 0.2	0.3 0.2 0.2	0.3 0.2 0.2	0.2 0.3 0.2	0.2 0.2 0.2	0.2 0.3 0.3	0.2 0.2 0.2	0.2 0.2 NM	0.3 0.4 0.2
Joint Resistance After Failure, ohms*	0.1 0.2 0.2	0.2 0.2 0.3	NM NM 0.4	0.2 2.8 0.2	0.2 NM 0.2	0.2 0.3 0.2	0.2 0.6 0.2	0.2 0.8 NM	3.0 1.8 2.5
Cathode Appearance Adherance Porosity	 C G G	 C P G	 C G G	 C P G	 C G G	 C G G	 C G G	 C P G	 C P G
Anode Appearance Adherance Porosity	 U G G	 U G G	 U G G	 U G G	 U G G	 U G G	 U G G	 S P G	 S G G
Electrolyte Appearance Cathode interface Anode interface Joint area	 U U U	 R U R	 U U U	 R U R	 R U R	 R U R	 R U R	 R U R	 R U R

C = color changed G = good U = unchanged P = poor R = reduction

S = sintering of electrode material NM = not measurable

* As measured with ohmeter, a rough measurement.

operated at moderate operating conditions. However, the electrode film peeled badly and black deposits were found beneath the cathodes in those cells operated at degrees of decomposition exceeding 0.79 and in those operated at a current density of 300 ma/cm^2. Mass spectrometric and x-ray analysis indicated that these deposits were platinum particles and that a trace of carbon was presented. The cause of carbon deposition at the cathode-electrolyte interface will be discussed in Section C.4.2.2.

Electrolyte -Half of the electrolysis cells after the life test showed some degree of reduction, indicated by darkening of the electrolyte. This occurred especially on the electrolyte at the outside surface of

the cell joint (see Fig. C8). The reduction in some cases extended into the top part of the cell body. Due to the change in material density caused by the reduction of the electrolyte, cracks occurred in OBS #20, OBS #26, and OBS #27.

Joints -The outside cell joints in most cases appeared to be in good condition. No migration of gold sealant into the outside electrodes was observed. This, too, is in sharp contrast with previous observations (Reference 3, pp. 59-62).

Discontinuities were found by electrical measurements in OBS #21, #23, and #26. Microscopic examination showed that platinum had evaporated from the corner between the inside electrode and the joint. No gold appeared to be present in the area. Therefore, the loss of Pt probably resulted from the initial coating around this corner having been too thin.

C.4 Regarding Further Improvement of Performance

Based on the observations in Section C.3, two causes of cell failure have been postulated, one identified primarily with operation at moderate operating conditions (current density less than 300 ma/cm^2 and degree of decomposition less than 0.8) and the second with operation at high degrees of decomposition and high current densities. A change in fabrication technique to increase life at moderate operating conditions is proposed. High degrees of decomposition are also believed to be achievable without rapid performance decline. The nature of the modifications and reasons for anticipating performance improvement are discussed below.

C.4.1 Obtaining Increased Life at Moderate Operating Conditions

At moderate operating conditions, the principal cause of failure was the evaporation of platinum from the corner between the inside electrode and joint (See Fig. C9). This, in turn, caused voltage differences

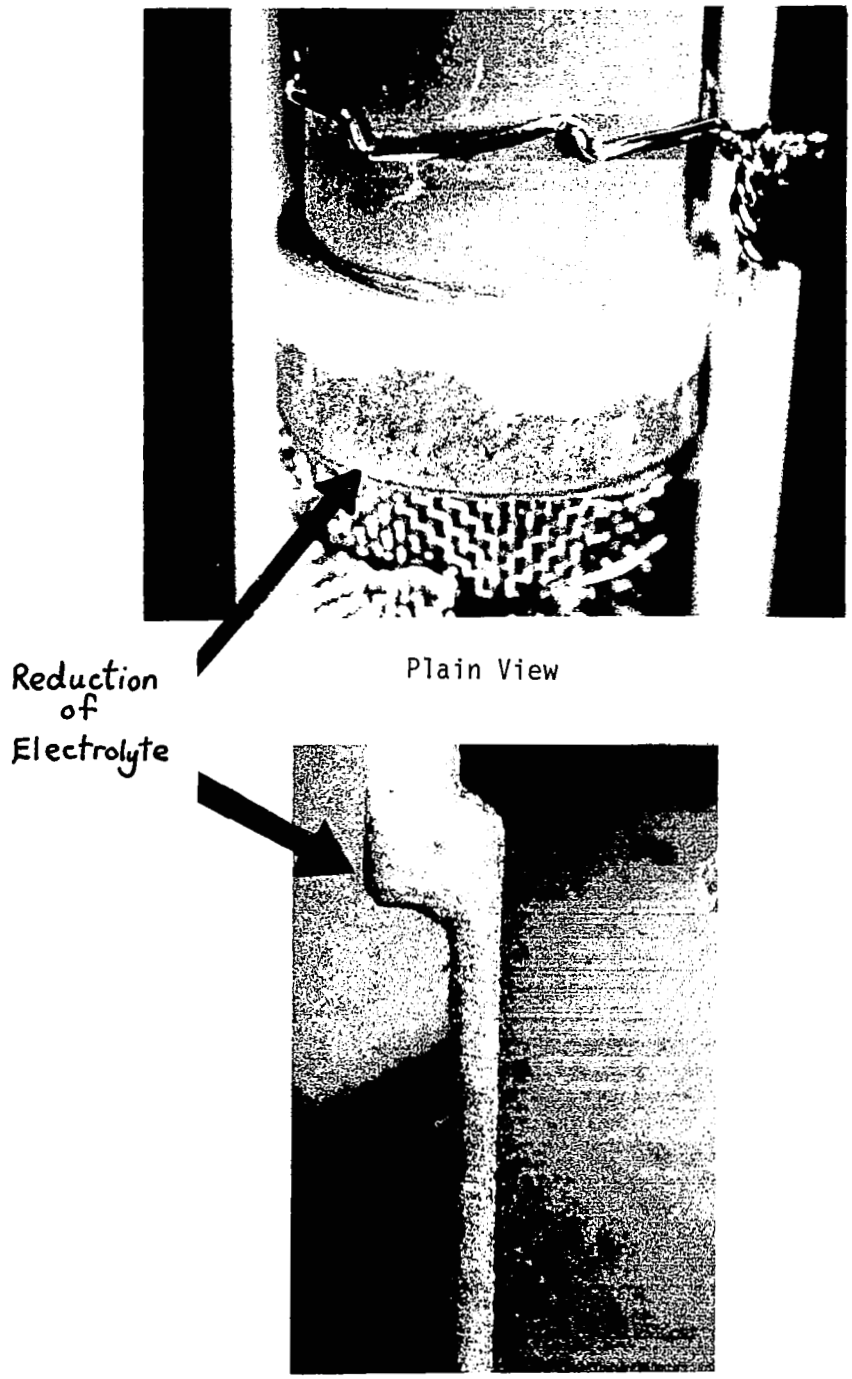

Fig. C8 - Reduction of electrolyte at the joint areas of OBS #26.

between the ZrO_2 at the outside of the bell (essentially at the cathode voltage, Vc) and the joint (V>Va) to rise above the decomposition voltage for ZrO_2. The reduction of the electrolyte on the outside of the joint, discussed previously, was thus a result of the partial discontinuity in the electrode caused by evaporation of platinum from the inside corner. Heavily coating the inside corner with dense platinum (as illustrated in Fig. C9) is suggested to insure electrical conductivity.

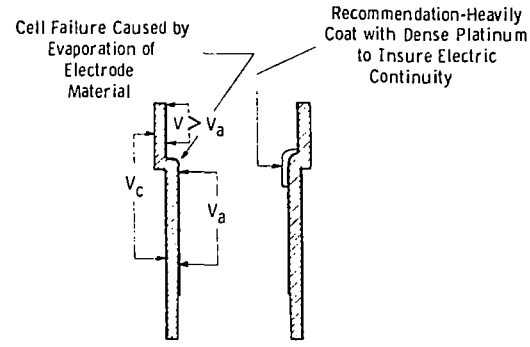

Fig. C9 -- Schematic Showing Evaporation of Electrode Material at Inside Connection of Bell and Spigot Cell and Recommendation for Improvement

The failure mode discussed above differs substantially from that observed for OBS #8, #9, and #10 during the previous contract work. In OBS #8, #9, and #10 deterioration occurred at the anode-joint interface because a large amount of gold remained at the interface from the gold wire which was placed there during the brazing operation. This gold caused sintering, increased local temperature, and, because of the oxidizing atmosphere, the evaporation of PtO_2. In the new fabrication technique, the gold wire is placed on the cathode which remains under reducing conditions throughout the test.

C.4.2 Operating at High Degrees of Decomposition

C.4.2.1 Recommended Changes

At high current densities and high degrees of decomposition (DD), electrolyte reduction was the principle cause of failure. It is not certain whether carbon deposition at the cathode-electrolyte interface preceded the electrolyte reduction in the case of DD greater than 0.8.

However, calculations, shown below, indicate that carbon deposition was favored thermodynamically at the interface.

Two approaches to operation at high DD's are recommended:

1. Use of electrode materials, such as nickel and cobalt, which give lower polarizations than platinum (Reference 17).
2. Use of low current densities (75-125 ma/cm^2) for those cells which operate at high DD.

In the above approaches, it is suggested that the cells at the end of the electrolysis unit, where high DD's are obtained, might be different from those at the beginning, either in cathode composition or operating current density.

C.4.2.2 Thermodynamic Feasibility of Carbon Deposition at the Cathode-Electrolyte Interface

The cross section of an electrolysis cell is illustrated by Fig. C10. In order to carry out the electrolysis process, the CO_2 must travel from the bulk gas to the electrode-electrolyte interface where it is decomposed into O_2 and CO. The transport of CO_2 from the bulk gas into the electrode-electrolyte interface is carried out by diffusion. The concentration at the interface is dependent upon the bulk concentration of CO_2, the overall mass transfer coefficient (a function of flow characteristics of the bulk gas and also the pore structure of the cathode), and the rate of oxygen transfer required to support the current drawn. If the electrolysis rate is higher than the mass transfer rate, CO_2 starvation will occur at the interface and result in carbon deposition, electrolyte reduction, or both.

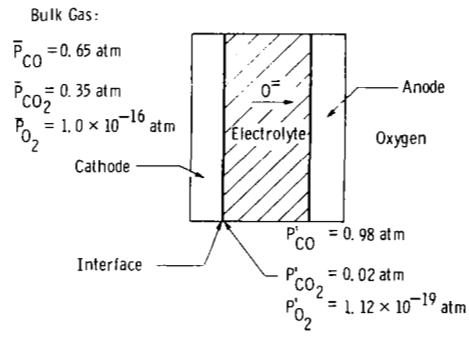

Fig. C10 -- Schematic Showing Difference in Gas Composition Between Bulk Gas and Cathode-Electrolyte Interface

Consider the two reactions which define the thermodynamic equilibrium of CO, CO_2, and O_2, at 1200°K (923°C):

$$CO_2 \overset{K_{p1}}{\rightleftharpoons} CO + 1/2\ O_2, \quad \Delta G_1 = 42,510 \text{ cal (Reference 18)} \qquad \text{(C-1)}$$

$$CO \overset{K_{p2}}{\rightleftharpoons} C + 1/2\ O_2, \quad \Delta G_2 = 52,150 \text{ cal} \qquad \text{(C-2)}$$

where

$$K_{p1} = \frac{P_{CO}\ P_{O_2}^{1/2}}{P_{CO_2}} = \exp\left(\frac{-\Delta G_1}{RT}\right) \qquad \text{(C-3)}$$

$$K_{p2} = \frac{P_{O_2}^{1/2}}{P_{CO}} = \exp\left(\frac{-\Delta G_2}{RT}\right) \qquad \text{(C-4)}$$

R = universal gas constant, 1.987 cal/(°K)(g mole); T = temperature, °K

Substituting ΔG_1 and ΔG_2 into (C-3) and (C-4)

$$K_{p1} = 1.85 \times 10^{-8} \qquad K_{p2} = 3.42 \times 10^{-10}$$

Dividing (C-3) by (C-4)

$$\frac{P_{CO}^2}{P_{CO_2}} = 54.6 \qquad \text{(C-5)}$$

The total pressure of the system is 1 atm; therefore

$$P'_{CO} + P'_{CO_2} + P'_{O_2} = 1 \qquad \text{(C-6)}$$

Since $P'_{CO_2} >> P'_{O_2}$, (C-6) can be simplified

$$P'_{CO} + P'_{CO_2} = 1 \qquad \text{(C-7)}$$

Let X represent P'_{CO}, then $1 - X = P'_{CO_2}$, and substituting into (C-5)

$$\frac{X^2}{1 - X} = 54.6$$

or

$$X^2 + 54.6X - 54.6 = 0 \qquad \text{(C-8)}$$

$$X = 0.98 \text{ atm}$$

Therefore carbon deposition can occur at the interface if $P'_{CO} \geq 0.98$ atm, and $P'_{CO_2} \leq 0.02$ atm. P'_{O_2} for these partial pressures of CO and CO_2 can be computed from C-4:

$$P'_{O_2} = (P'_{CO} \cdot K_{P_2})^2 = (0.98 \times 3.42 \times 10^{-10})^2 = 1.12 \times 10^{-19} \text{ atm}$$

The average partial pressure of O_2 in the bulk gas, $\bar{P}_{O_2}$, can be calculated by (C-3):

$$\bar{P}_{O_2} = \left(\frac{\bar{P}_{CO_2} K_{P_1}}{\bar{P}_{CO}}\right)^2 \qquad \text{(C-9)}$$

Where

$\bar{P}_{CO_2}$ = average partial pressure of CO_2 in the bulk gas

$\bar{P}_{CO}$ = average partial pressure of CO in the bulk gas

If $\bar{P}_{CO} = 0.65$ atm and $\bar{P}_{CO_2} = 0.35$ atm in the bulk gas

the average partial pressure of O_2,

$$\bar{P}_{O_2} = \left(\frac{0.35}{0.65} \times 1.85 \times 10^{-8}\right)^2 = 1 \times 10^{-16} \text{ atm}$$

The cathodic polarization then, which would cause carbon deposition can be evaluated by the Nernst Equation:

$$V_{pc} = \frac{RT}{4F} \ln \frac{\bar{P}_{O_2}}{P'_{O_2}{}_i} \qquad \text{(C-10)}$$

where V_{pc} = cathodic polarization

F = Faraday constant = 23,000 cal/volt

therefore

$$V_{pc} = \frac{1.987 \times 1200}{4 \times 23{,}000} \ln \frac{1 \times 10^{-16}}{1.12 \times 10^{-19}} = .175 \text{ volt}$$

The allowable cathodic polarization for other degrees of decomposition are listed in Table C-VI.

TABLE C-VI

Allowable Cathodic Polarization as a Function of Degree of Decomposition

Degree of Decomposition	E_T, volts	Allowable V_{pc}, volts
.65	0.950	.175
.70	0.960	.165
.75	0.975	.150
.80	0.990	.135

Thus, it is seen that carbon deposition at the electrode-electrolyte interface can occur when the sum of $V_{pc} + E \geq 1.12$ volts. Operating at a degree of decomposition of 0.80, carbon decomposition can be anticipated if V_{pc} exceeds 0.135 volts.

Evidence for carbon deposition playing a role in failure of cells operated at high degrees of decomposition is shown in the life test of OBS #20. This stack initially was tested at a degree of decomposition of 0.35. On the 10th day the degree of decomposition was increased to 0.85 by changing the composition of the feed gas. Accordingly, the voltage increased rapidly from 1.3 volts/cell to 1.9 volts/cell over a period of 8 days. All of the increase was due to polarization, rather than resistance. The current efficiency dropped from 90% on the first day to about 50% on the 19th day. Tests were conducted to determine the cause of rapid decline in performance. The stack was first operated in pure CO_2 and reverse pumped at very low current density (5 ma/cm^2) for six hours to oxidize the reduced electrolyte and any free carbon that may have deposited. The stack was then switched back to electrolysis of CO_2 containing 10% water at a current density of 200 ma/cm^2. The driving voltages remained high at 1.9 volts; however, the current efficiency was back up to 85%. Current interrupt pictures showed a high IR drop for each cell, indicating that a definite change in the resistivity had taken place during the reverse pumping operation.

One explanation for the observed results is that carbon deposited at the interface during the original high DD operation pushed the electrode away from the electrolyte. However, the voltage rise appeared as an increase in polarization rather than interface resistance because the deposited carbon provided an electronically conductive path. The reverse current pumping gasified the carbon, leaving a space between the cathode and electrolyte, which then caused the observed increase in electronic resistance.

The above does not provide conclusive evidence that carbon deposition is a prerequisite for electrolyte reduction in this system. In fact, analysis of the failure of OBS #22 indicated that electrolyte reduction occurred without an increase in polarization (and thus without carbon deposition). The essential conclusion is that if the interface

CO_2 partial pressure is maintained at a level sufficiently high to prevent carbon deposition, electrolyte reduction should be eliminated. Therefore, an operating criteria of maintaining the sum of E_T plus V_{pc} below 1.115 volts (at 923°C) is recommended.

C.5 Selected Operating Conditions for Breadboard System

The conditions chosen for operating the electrolysis unit of the breadboard system were as follows:

1. Current density $\leq$ 200 mA/cm^2
2. Degree of decomposition $\leq$ 70%
3. Temperature $\sim$ 900°C

Selection of a current density $\leq$ 200 mA/cm^2 was based on the steady performance and long life of OBS #19, #21, #23, #24, and #25. Electrolysis stacks which operated at 300 ma/cm^2 (OBS #26 and #27) had shown rapid decline in performance and early failure. DD $\leq$ 0.7 was selected to keep $E_T + V_{pc}$ values below 1.115 volts so that carbon decomposition at the cathode interface could be prevented. An operating temperature of approximately 900°C, the lowest temperature tested, was chosen for two reasons: (1) previous life tests indicated that life was increased by operating at low temperature and (2) it was thought that operation at this temperature would permit the palladium membranes to be integrated into the electrolysis unit. Based on test results cited in Section 5.5, even lower temperatures may be desirable in the future to improve palladium membrane life.

APPENDIX D

EFFECT OF COMPOSITION, FLOW RATE, AND DEPOSIT THICKNESS ON RATE AND PROPERTIES OF CARBON DEPOSITION

A differential reactor was built and used to study the influence of gas composition and flow rate on the rate of carbon deposition. This information was needed to aid in designing a reactor of appropriate size for the 1/4-man bread-board system.

Lack of time prevented including the effect of temperature in the study. Data on temperature dependence, however, had been obtained in the 100-day test of the previous contract (Reference 3, pp. 96-97). The results showed that the maximum conversion of CO to CO_2 and carbon occurs at about 540°C for the average flow conditions of the test. At higher temperatures conversion is limited by equilibrium which becomes more unfavorable as the temperature rises.

Using the results of the 100-day test, a reaction model based on gas phase diffusion control was developed. A theoretical calculation of the total resistance to diffusion, including the resistance of the carbon deposit, indicated, however, that diffusion alone could not be used to explain the experimental rate constants. A possibility of surface reaction resistance exists.

A major contribution of the previous work was the discovery that 3 to 5% hydrogen is needed in the feed gas to maintain constant catalyst activity. Without hydrogen, the activity of the catalyst declines steadily with time.

D.1 Apparatus

A schematic diagram of the differential reactor is shown in Fig. D1. The catalyst was a short cylinder of high purity iron that was sandwiched between sections of non-carbon-producing copper tubing.

A central thermocouple well was provided for temperature measurement. A movable scraping device (not shown in the diagram) was used to remove carbon from the catalyst surface so that runs could be continued from day to day without opening the reactor.

The catalyst cylinder was 0.625 in. in diameter and 0.25 in. long. Its surface area, when new, was 0.49 in^2. Both diameter and surface area decreased slowly as iron was consumed during use.

Gas mixtures for the tests were prepared by metering the individual gases and mixing before feeding to the reactor.

D.2 Test Procedure

Each experimental run consisted of a series of measurements conducted during an 8-hour period following overnight operation of the reactor at a low flow rate. A single gas composition was studied in each run and only the flow rate was varied.

Reproducible results could be obtained only after a dense, adherent carbon deposit had built up on the catalyst to a thickness of about 1/4 inch. Forming this deposit was the purpose of the overnight operation. With deposits thinner than 1/4 inch, the reaction rate varied with thickness.

Dense deposits were difficult to grow below 560°C. For this reason, all of the tests were conducted at 560 to 570°C.

The conversion rate of CO was determined by measuring the volume change due to the reaction, using calibrated wet test meters in the gas lines before and after the reactor. To provide a dry feed, the feed gas was passed through a Drierite bottle after metering. The water content of the feed could be varied from zero to 3% by bypassing part of the gas around the drying bottle. The water contents of the inlet and outlet streams were determined gravimetrically, using water absorption bulbs.

D.3 Results of Rate Measurements

The results of the rate experiments are presented in Fig. D2. The top four curves, which were run with a dry feed gas, show the effects of flow rate and CO to CO_2 ratio. The lower three curves show the influence of water in the feed and are to be compared with the fourth curve which represents the dry feed having the same CO to CO_2 ratio. Fig. D2 shows that the fractional conversion of CO decreases with increasing CO_2 and H_2O concentrations in the feed and with increasing flow rate. Conversion of CO was particularly sensitive to the concentration of water, 3% water being sufficient to reduce the reaction rate by half.

At the time that the differential reactor study was planned, the magnitude of the water effect was not realized and insufficient time was allowed for that part of the study. Furthermore, it was thought that the ratio of CO to CO_2 in the reactor feed would not be less than 1.5. In the 180-day test, however, the ratio ranged between 1.2 and 1.3. For these reasons, most of the differential reactor tests were run under conditions that were far removed from the conditions actually used in the bread-board. A number of theoretical and empirical models based on the differential reactor study and the previous 100-day test were formulated. However, none of these models were considered satisfactory, since they could not be extrapolated with confidence to the bread-board operating conditions.

D.4 Catalytic Behavior of Carbon Deposit

The primary benefit obtained from the differential reactor study was the discovery that the carbon deposit itself is catalytic and that the catalytic capacity of the carbon can be utilized by leaving a thick deposit on the wall of the reactor at all times. This procedure was found to reduce iron consumption in the differential reactor tests and also in the 180-day test.

The catalyst activity of the carbon deposit is apparently due to the presence of small fragments of iron. These are probably remnants

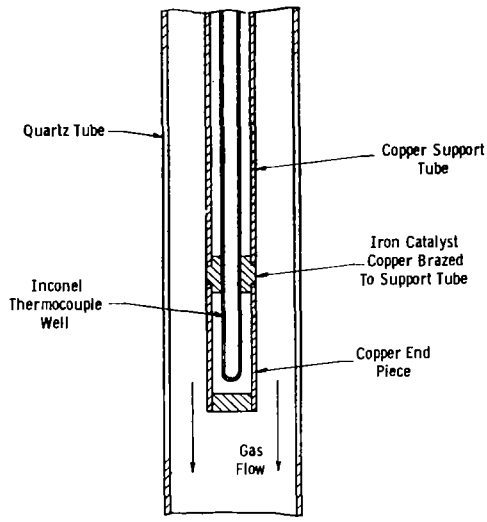

Fig. D1 -- Schematic Diagram of Differential Carbon Deposition Reactor

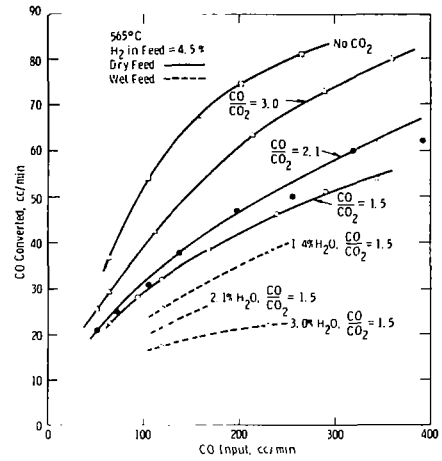

Fig. D2 -- Variation of CO Conversion with Input Rate and Gas Composition

of surface grains of iron that are dislodged from the bulk catalyst by carbon precipitation in the grain boundaries. Figure D3 shows iron fragments in carbon produced on a pure iron catalyst.

Since carbon is produced within the deposit itself, the ratio of iron to carbon is highest at the catalyst surface and decreases with distance away from the surface. This effect, which accounts for the reduction in iron consumption on leaving a thick deposit, is illustrated by results obtained in the differential reactor tests, which are presented in Table D-I.

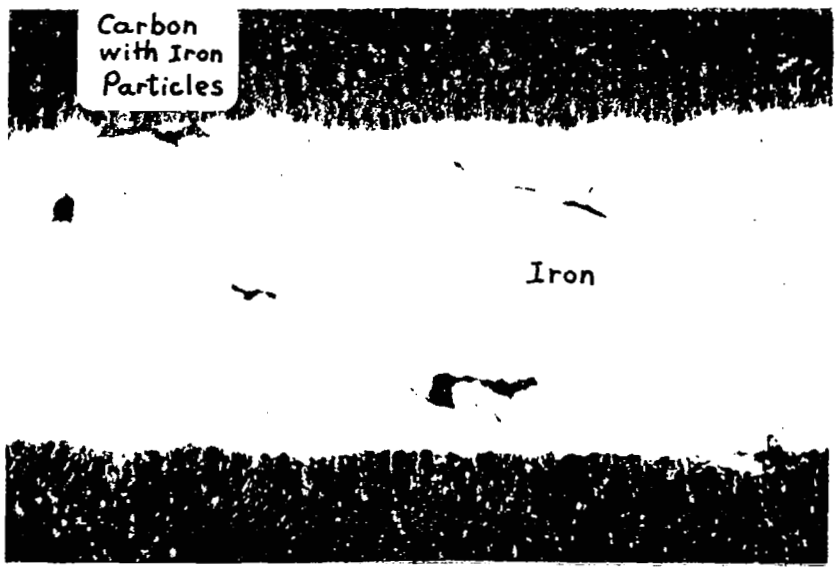

500X

Fig. D3 -- Section Through Pure Iron Catalyst After Carbon Deposition Showing Iron-Carbon Interface and Iron Particles in Carbon

TABLE D-I

Variation of Iron Content of Carbon Deposit with Distance from Catalyst Surface

Run No.	CO/CO_2 in Gas	Iron Content, % Distance from Catalyst Surface 1-4 mm	5-8 mm	9-12 mm
1	CO only	1.04	0.81	0.33
2	2.1	--	1.66	.85
3	2.1	--	1.55	.90
4	1.5	4.42	2.00	.70
5	3.0	1.04	0.67	.46
6	2.0	4.34	2.08	1.27

APPENDIX E

STUDY OF PERFORMANCE AND LIFE OF A PALLADIUM MEMBRANE OPERATING AT 850°C

E.1 Description of Life Test

A 71-day life test of a 2.5 in. long palladium membrane was conducted at 850°C prior to building the breadboard system. The test was designed to provide data in the following areas:

1. Membrane stability.
2. Consistency of performance during continuous operation.
3. Permeation rate constant.
4. Measurement and control of hydrogen separation.

A similar study was carried out under the previous contract (Reference 3, pp. 98-101) but the duration of the test was only 20 days. The palladium membrane tested previously stood up well under the conditions of operation, which included 2 days at 950°C although most of the test was run at 800°C. Carbon deposition on the membrane occurred at 700°C but not at 750°C or higher. The permeation rate constant for 800°C was 0.153 cc/(min)(cm)(mm Hg)$^{0.65}$.

The palladium membrane used in the present experiment was 0.125 in. o.d. by .005 in. wall by 2.5 in. long. One end was closed. The open end was gold-nickel brazed to a larger Inconel 600 support tube that connected the membrane to the vacuum system. The Inconel tube was copper plated to prevent carbon deposition. The palladium membrane was suspended vertically in the center of a clear quartz reactor which was heated by a 12-in. long 4-zone furnace, as shown in Fig. E1. A control panel was set up for metering and mixing the gases for the feed. The vacuum system was similar to that illustrated in Fig. 9, Sec. 4.3.2,except that a McCleod gauge was used in place of the absolute pressure gauge.

The rate of hydrogen separation by the membrane was determined by metering the reactor input and output with calibrated wet test meters. Since the gas feed consisted of a mixture of CO, CO_2, H_2, and H_2O, it was necessary to determine the water concentration in the input and output streams for each data point so that correction could be made for hydrogen that was generated or consumed by the water gas shift reaction:

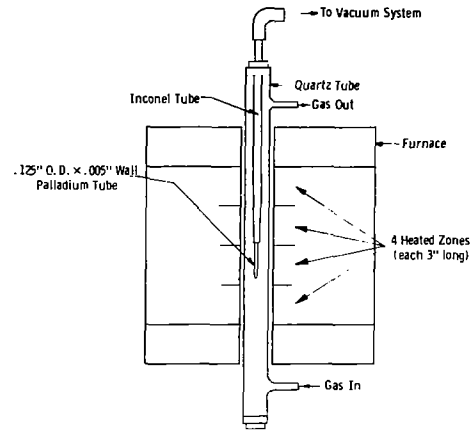

Fig. E1 -- Schematic Diagram of Hydrogen Separation Apparatus

$$CO + H_2O \rightleftarrows CO_2 + H_2 \qquad (E\text{-}1)$$

This reaction is catalyzed by the palladium membrane.

The life test was started on July 3, 1969 and was terminated on September 12, 1969. The palladium membrane was continuously evacuated and during most of the test the feed gas consisted of 64% CO, 32% CO_2, and 4% H_2. Up to 3% H_2O was introduced when measurements of the permeation rate were made. Rate measurements were made periodically to determine whether the rate constant changed with time.

The control study that was conducted consisted of correlating the two vacuum gauge readings with the rate of hydrogen removal.

E.2 Results

The results of the test are summarized as follows:

1. During the 71-day test period there was no significant change in the performance of the palladium membrane or in its physical appearance.

2. Measurements of the pressure in the vacuum line between the control valve and the vacuum pump showed that this pressure varies with the rate of hydrogen discharge in a reproducible manner; therefore, a vacuum gauge can be used to measure the hydrogen removal rate. In the range of hydrogen flow rates covered (7 to 30 cc/min) the relationship between pressure and flow rate was linear. This is true, of course, only when the pumping speed is constant.
3. The permeation rate of hydrogen was found to vary with the 0.65 power of hydrogen partial pressure in accordance with the following relation

$$Q = k\ell\ (p_1^{0.65} - p_2^{0.65}) \qquad \text{(E-2)}$$

where

Q = permeation rate, cc/min
ℓ = length of palladium membrane, cm
p_1 = average partial pressure of hydrogen in gas, mm Hg
p_2 = vacuum side pressure, mm Hg
k = rate constant, cc/(min)(cm)(mm Hg)$^{0.65}$

The value of the rate constant for 850°C was 0.166. It was unaffected by flow rate for rates between 250 and 650 cc/min or by the ratio of CO to CO_2 in the gas for ratios of 1.0 and 2.0. The experimental values of k are plotted versus the average partial pressure of hydrogen in Fig. E2.

The dependence of the permeation rate on the 0.65 power of the hydrogen partial pressure rather than on the 0.5 power probably means that surface processes, as well as diffusion in the metal lattice, are involved in the rate controlling mechanism. A 0.5 power relationship implies that diffusion is the only resistance to transfer (Reference 19).

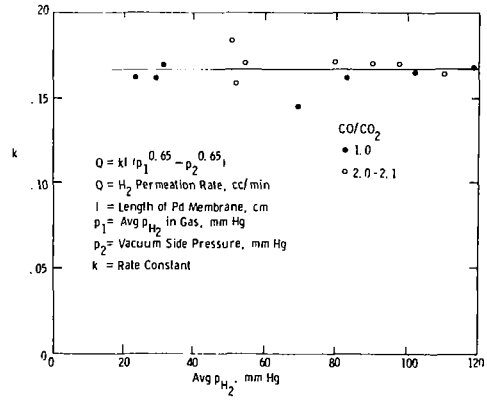

Fig. E2 -- Hydrogen Permeation Rate Constant Versus Hydrogen Partial Pressure in the Gas

APPENDIX F

PRELIMINARY TESTING OF BREADBOARD SYSTEM

F.1 Single Component Tests

Neither the electrolysis unit nor the carbon deposition reactor performs up to its design potential when first used and each requires a break-in period of operation. Single component runs were conducted for this purpose following assembly of the breadboard system. Initial characterization tests of the electrolysis stacks were also carried out.

The electrolysis stacks were broken in by electrolyzing a gas mixture composed of 89% CO_2, 10% CO, and 1% H_2, using a current density of 50 ma/cm^2. A reducing mixture was used to prevent oxidation of the copper lining of the gas feed tube. The flow rate was 900 cc/min, and the operating temperature was 900-915°C. After three days at these conditions, the stacks were characterized through V-I curves and current interrupt measurements.

Fifteen stacks were found to be fully operable. The initial performance characteristics of each is given in Table F-I. Of the stacks not fully operable, three were not completely insulated from the housing; one had been broken during assembly of the unit; and one had a measurable gas leak. All but the broken stack could be operated if needed, however.

The carbon deposition reactor was run as a single component for two weeks at an operating temperature of 540-550°C. During most of the period a low gas feed rate was used to conserve catalyst. Approximately two hours each day were devoted, however, to testing at high gas feed rates. The performance of the reactor improved with use and the catalyst was judged to be fully activated at the end of the two-week period.

TABLE F-I

INITIAL PERFORMANCE OF ELECTROLYSIS STACKS
IN BREADBOARD SYSTEM

Feed Gas 89% CO_2, 10% CO, 1% H_2; 900 cc/min
Current Density 166 ma/cm^2

Stack	V_T[a], Volts	E_T[b], Volts	R[c], Ohms	V_p[d], Volts	ε[e], %
1	1.63	0.86	0.27	0.25	96
2	1.52	0.85	0.24	0.25	96
3	1.57	0.87	0.30	0.27	95
4	1.62	0.85	0.24	0.28	96
5	1.80	0.87	0.33	0.33	96
7	1.69	0.85	0.45	0.34	95
8	1.63	0.85	0.39	0.33	95
10	1.58	0.87	0.37	0.24	95
11	1.72	0.84	0.33	0.27	90
12	1.65	0.85	0.28	0.32	88
13	1.79	0.87	0.41	0.29	94
17	1.76	0.86	0.44	0.35	96
18	1.58	0.85	0.37	0.40	94
19	1.82	0.88	0.29	0.24	96
20	1.77	0.88	0.35	0.31	96

a. V_T = average cell driving voltage including lead resistance

b. E_T = thermodynamic decomposition voltage

c. R = cell resistance excluding lead resistance

d. V_p = cell polarization

e. ε = current efficiency

F.2 Open Loop Tests

Integrated operation of the system in open loop mode began on June 6, 1970 and was continued for three weeks. The primary objectives were (1) to test the hydrogen removal system and (2) to select the recycle flow rate best suited for closed-loop operation. The criteria for the flow rate selection were:

1. The rate of carbon deposition should match the rate of CO_2 decomposition in the electrolysis unit.
2. A degree of decomposition (DD) less than 0.60.
3. The gas flow should provide good circulation in the electrolysis chamber to prevent a rise in polarization.

Short tests of 4 to 8 hours duration were run at feed gas rates of 900, 1200, 1500, and 1800 cc/min and at DD's ranging from 0.54 to 0.60. The oxygen generation rate was approximately 1/4-man (125 cc/min). The hydrogen separation system worked well although it was during these tests that the initial failures of palladium membranes occurred. In each test, the rate of carbon monoxide conversion was determined by measuring the change in gas volume due to the carbon deposition reaction. The results of the experiments are presented in Table F-II as Tests 1-5.

A perfect match between the rates of CO_2 decomposition and CO conversion was not achieved in any test. In all except Test 4, however, only minor adjustments of the degree of decomposition would have been needed to bring the two reactions into balance.

Conditions approximating those of Test 1 were selected for further study, primarily because the flow rate was the lowest at which the electrolysis unit did not show high polarization. The system was operated continuously for one week. After minor adjustment of the feed composition, performance stabilized at the conditions listed under Test 6 in Table F-II. The results met all of the preset requirements and it was concluded that these conditions would be suitable for closed loop operation.

TABLE F-II

SUMMARY OF OPEN-LOOP TESTS

	Test Number					
	1	2	3	4	5	6
Battery Feed, cc/min						
CO_2	796	636	668	549	957	753
CO	567	450	417	257	718	614
H_2	49	41	40	33	45	50
H_2O	84	65	65	69	93	84
Total	1496	1192	1190	908	1813	1501
H_2 Removed, cc/min	53	57	52	53	58	60
CDR[a] Feed, cc/min						
CO_2	609	441	469	355	784	552
CO	765	645	608	451	891	812
H_2	57	18	45	35	54	40
H_2O	23	31	18	13	26	22
Total	1454	1135	1138	855	1755	1425
CDR[a] Discharge, cc/min (dry)	1320	995	1016	775	1637	1311
O_2 produced, cc/min	128	121	125	125	120	135
H_2O converted	61	47	49	56	67	62
CO_2 converted	193	195	201	194	174	208
CO converted	203	230	192	134	184	204
Battery DD, %	57.5	59.5	57.6	57.0	53.9	60.0
Stacks Used [b]	6	8	7	8	7	7
Driving Voltage/Stack, volts	12.2	12.2	12.2	12.1	11.9	11.5
Current Density, ma/cm	145	110	125	110	125	133
Current Efficiency	92.5	90	90	90	90	90
Hours of Operation	8	6	6	3	3	168

[a] CDR = carbon deposition reactor

[b] All operable stacks used part of time

The polarizations shown in Table F-I average 0.30 volt at a current density of 166 ma/cm^2. This is significantly higher than anticipated on the basis of previous tests (see Table B-I). The major cause of the increase in polarization is believed to have been an uneven flow distribution within each of the electrolyzer compartments. Computations which estimate the gas velocity near the electrolysis stacks in comparison with that in the open center section of each compartment are shown below.

F.3 Estimation of Average Gas Velocity and Reynolds Number in the Vicinity of the Electrolysis Stacks

The average velocity of laminar gas flow through a circular duct is given by Poiseuille's equation:

$$\bar{V} = - \left(\frac{\Delta P}{\Delta Z}\right) \left(\frac{g_c}{\mu}\right) \left(\frac{D^2}{32}\right) \qquad \text{(F-1)}$$

where

$\left(\frac{\Delta P}{\Delta Z}\right)$ = pressure gradient along the tube

g_c = gravitational constant

μ = viscosity of the gas, poise

D = hydraulic diameter of the duct, cm

$\bar{V}$ = average velocity of the gas, cm/sec

When $\left(\frac{\Delta P}{\Delta Z}\right)$ is constant,

$$\frac{\bar{V}_1}{\bar{V}_2} = \frac{D_1^2}{D_2^2} \qquad \text{(F-2)}$$

A cross section of one compartment of the electrolysis unit is illustrated in Fig. F-1. Assume a frictionless wall dividing the gas flow into two channels, X and Y regions as indicated. The cross section areas, A_x and A_y, and the wetted surface perimeters, S_x and S_y, can be calculated from the compartment geometry:

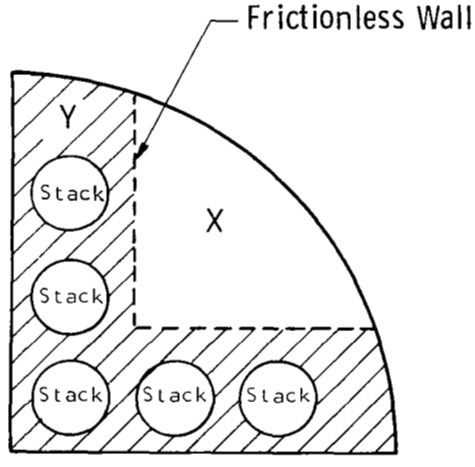

Fig. F1 - Cross section of electrolysis unit compartment

$A_x = 10 \text{ cm}^2$

$A_y = 14.54 \text{ cm}^2$

$S_x = 5.5 \text{ cm}$

$S_y = 36.8 \text{ cm}$

The equivalent hydraulic diameter = $\frac{4 \times \text{cross section area}}{\text{wetted perimeter}}$: (F-3)

$$D_x = 7.28 \text{ cm}$$

$$D_y = 1.69 \text{ cm}$$

Substituting D_x and D_y into equation (F-2) we have

$$\frac{\bar{V}_x}{\bar{V}_y} = \frac{D_x^2}{D_y^2} = \frac{7.28^2}{1.69^2} = 18.5$$

Therefore

$$\bar{V}_x = 18.5\ \bar{V}_y \qquad \text{(F-4)}$$

Since the sum of the flows through the X and Y channels must be equal to the total flow, then

$$A_x \cdot \bar{V}_x + \bar{A}_y \cdot \bar{V}_y = \text{Total flow rate} \qquad \text{(F-5)}$$

At 900°C the gas flow rate in the electrolysis unit = 117 cc/sec. Substituting the values of A_x, A_y, and the total flow rate into (F-5) and solving (F-4) and (F-5) simultaneously,we have

$$V_y = 0.585 \text{ cm/sec}$$

$$V_x = 10.83 \text{ cm/sec}$$

The viscosities and densities of the component gases at 900°C are:

Gas	Mole fraction	Viscosity (μ), poise	Density (ρ), g/cm^3
CO	0.50	4.56×10^{-4}	2.79×10^{-4}
CO_2	0.45	4.45×10^{-4}	4.41×10^{-4}
H_2	0.05	2.22×10^{-4}	2×10^{-5}

Therefore

$$\rho_{mix} = (0.5 \times 2.79 + 0.45 \times 4.41 + 0.05 \times 0.2) \times 10^{-4}$$

$$= 3.39 \times 10^{-4} \text{ gm/cm}^3$$

$$\mu_{mix} = (0.5 \times 4.56 + 0.45 \times 4.45 + 0.05 \times 2.22) \times 10^{-4}$$

$$= 4.49 \times 10^{-4} \text{ poise}$$

The Reynolds number, Re, is calculated by

$$Re = \frac{D\bar{V}\rho}{\mu} \qquad \text{(F-6)}$$

$$Re_x = \frac{7.28 \times 10.83 \times 3.4 \times 10^{-4}}{4.49 \times 10^{-4}} = 73.6$$

$$Re_y = \frac{0.585 \times 1.69 \times 3.4 \times 10^{-4}}{4.49 \times 10^{-4}} = 0.78$$

The results of the above calculations show that the velocity through the X-region was 19 times higher than through the Y-region which was adjacent to the electrolysis stacks. The low Reynolds number in the Y region indicated that high gas film diffusion resistance might have caused the high polarization of the electrolysis stacks.

F.4 Calculation of Theoretical Current Efficiency of Bell and Spigot Cell

The shunt resistance of the bell and spigot cell can be calculated as the equivalent resistance for two parallel paths (see Fig. F2):

$$R_s = \frac{R_{so} R_{si}}{R_{so} + R_{si}} \qquad \text{(F7)}$$

where

R_s = cell shunt resistance

R_{so} = outside shunt resistance

R_{si} = inside shunt resistance

R_{so} and R_i can be computed from the cell dimensions.

$$R_{so} = 28.05 \text{ ohms}$$

$$R_{si} = 62.30 \text{ ohms}$$

Then

$$R_s = \frac{(28.05)\ (62.30)}{28.05 + 62.30} = 19.33 \text{ ohms}$$

The ratio of shunt current to cell current can be expressed by

$$\frac{I_{shunt}}{I_{cell}} = \frac{V_T/R_s}{(V_T - E_T)/R_{cell}} \qquad \text{(F-8)}$$

where

V_T = 1.50 volts (total cell driving voltage)

E_T = 0.85 volts (decomposition voltage)

R_s = 19.33 ohms

R_{cell} = 0.29 ohms

Then

$$\frac{I_{shunt}}{I_{cell}} = \frac{1.50/19.33}{(1.50 - 0.85)/0.29} = \frac{0.078}{2.24} = 0.04$$

Thus, the theoretical current efficiency = $\frac{1 \times 100}{1 + 0.04} = 96.1\%$

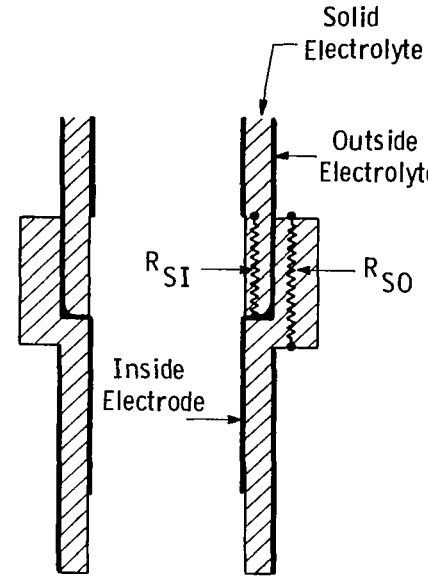

Fig. F2 - Shunt paths of bell and spigot electrolysis cells

F.5 Estimation of Loss of Current Efficiency Due to Ground Shunt

The electrical circuits of the electrolysis stacks were connected in parallel externally, except for the stack pairs 11 and 12, and 14 and 15, which were connected internally in series. During the life test, stack 12 was found to be shunted with respect to ground.

The electrical circuit of the operating stacks is illustrated in Fig. F3. The ground shunt resistance is given by

$$\frac{1}{R_{GS}} = \frac{1}{R_{11}^*} - \frac{1}{R_{11}'} \qquad \text{(F-9)}$$

where R_{11}^* is the equivalent resistance of stack 11 and the shunt was calculated by

$$\frac{V_{ab}}{I_{11}'} = \frac{12.7}{1.5} = 8.5 \text{ ohms}$$

$$R_{11}' = \frac{V_T'}{I_{11}} = \frac{E_T' + V_p + I_{11} R_{11}}{I_{11}} \qquad \text{(F-10)}$$

where

V_T' = total driving voltage of the stack

E_T' = decomposition voltage of the stack

R_{11} = sum of the resistances of the individual cells and electrical leads

Assume I_{11} carried by stack 11 is the same as the average of the other stacks, then

$$I_{11} = I_T \phi \qquad \text{(F-11)}$$

where

ϕ = average percentage of total current carried by stacks 1 through 5 (see Table VII, Section 5.3.1)

I_T = total current of electrolysis unit.

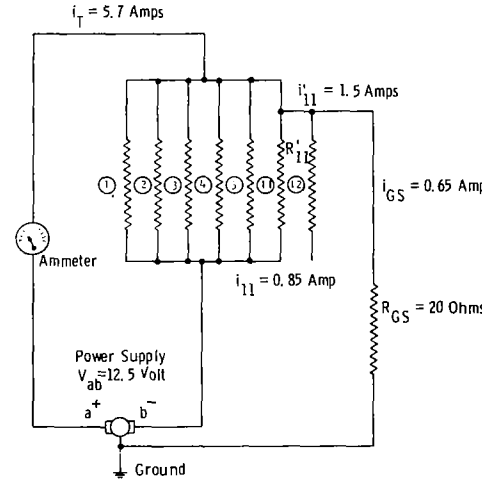

i_T = Total Electrolysis Current
i_{11} = Electrolysis Current Carried by 11th Stack
i'_{11} = Apparent Current of 11th Stack Measured by Clip-On Ammeter
R'_{11} = Equivalent Resistance for 11th Stack
R_{GS} = Ground Shunt Resistance
i_{GS} = Ground Shunt Current
① = Number of Electrolysis Stack

Fig. F3 - Apparent location of ground shunt in electrical circuit of the operating stacks

Substituting (F-11) into (F-10), we have

$$R_{11}' = \frac{V_T'}{I_T \phi}$$

For V_T' = 12.7 volts (on the 70th day)

I_T = 5.7 amps

ϕ = 0.147

$$R_{11}' = \frac{12.7}{5.7 \times 0.147} = 15.1 \text{ ohms}$$

Substituting R_{11}' and R^*_{11} into (F-9)

$$\frac{1}{R_{GS}} = \frac{1}{8.5} - \frac{1}{15.1} = 0.118 - 0.066 = 0.05$$

Therefore R_{GS} = 20 ohms

The percentage loss of current due to ground shunt was equal to

$$\frac{I_{11}' - I_{11}}{I_T} = \left(\frac{1.5 - 0.84}{5.7}\right) \times 100 = 11.5\%$$

APPENDIX G

OPERATING INSTRUCTIONS

G.1 Startup Procedure

It is assumed that the electrolysis unit and the carbon deposition reactor have been broken-in by operating each as a single component as described in Appendix F.

G.1.1 System Purge

1. Start with all valves closed.
2. Open valve 1 (see Fig. G1) to CO_2 cylinder and adjust pressure regulator before valve 4 to 2.0 psig.
3. Purge pressure fail-safe apparatus by partially opening valve 2, allowing gas to bubble through water columns of the two fail-safe bulbs.
4. Open following valves: 3, 7, 8, 9, 10, 11, 12, 13A, 13B, 15A, 15B, 16A, 16B, 17, 18, 19, and R.
5. Open valve T and adjust valve 2 to give slow stream of CO_2 through valve T, as indicated by bubble bottle. (This stream provides CO_2 to system if system pressure goes negative by more than 2 in. of water.
6. Open solenoid valve 20 (with Lab-Stat controller) and valve 5 and purge bypass line around valve 4.
7. Close valve 20 and valve 5 and open valve 4 to purge main part of system, discharging gas through valve R. Control CO_2 flow with valve 4 at 200-300 cc/min.

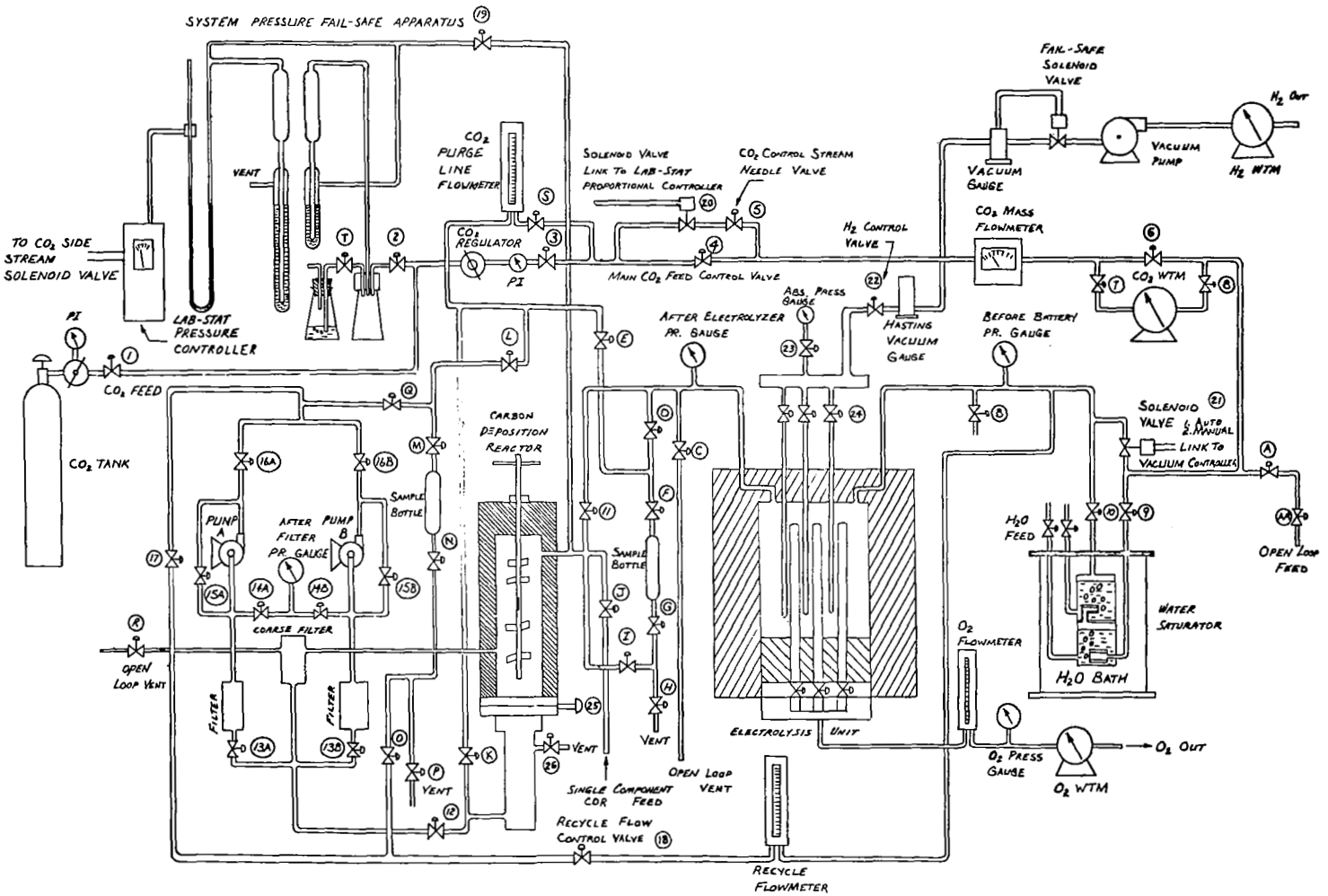

Fig. G1—Schematic flow diagram of breadboard system

8. Operate both recycle pumps to eliminate air from recycle line. Valves 15A and 15B in bypasses around recycle pumps must be partially closed to force gas through recycle loop.

9. Purge system for 1 hour. Then turn off recycle pumps; close valves 4, R, 9, and 10; and open solenoid valve 21.

G.1.2 Heat Components to Operating Temperature

1. Heat carbon deposition reactor to operating temperature (540 to 560°C). Pressure fail-safe apparatus will automatically maintain system pressure at safe level.

2. Start one recycle pump and circulate gas through electrolysis unit at 200-300 cc/min. Close valves 13 and 16 of backup recycle pump. (Gas from carbon deposition reactor contains CO which will prevent oxidation of copper cladding in electrolysis unit.)

3. Open all oxygen manifold valves to electrolysis stacks.

4. Heat electrolysis unit to operating temperature (900-915°C) at rate of 5 to 10°C per min.

G.1.3 Start Electrolysis

1. Open valves 9 and 10 and close solenoid valve 21 so that CO_2 feed will pass through water saturator.

2. Open valve 23 and six vacuum manifold valves 24 and start vacuum pump.

3. Increase recycle flow rate to 1750-1800 cc/min with valve 18.

4. Slowly open hydrogen control valve 22 to pump down vacuum manifold and palladium membranes and set valve 22 at 7 turns open.

5. Select eight stacks to be operated and connect to power supply. Close oxygen manifold valves of the other twelve

stacks. (After operation of the system has become stable, the number of operating stacks can be reduced to six.)

6. Start electrolysis current. Adjust to 1/4-man rate, which is about 5.6 amps.

7. Immediately increase CO_2 feed rate with valve 4 and adjust so that system pressure remains constant at about 4 in. of water, as read on "After Electrolyzer Pressure Gauge".

8. Set water saturator thermostat to 75°C.

9. Adjust vacuum manifold pressure to 10 mm Hg, using control valve 22.

10. When system has stablizied, the CO_2 feed rate should be 98 to 100 cc/min.

G.1.4 Start CO_2 Feed Controller

1. Set sensor of Lab-Stat controller at 4 in. of water and switch on controller.

2. Lower CO_2 feed rate with valve 4 to 80 cc/min.

3. Immediately open needle valve 5 to give total feed rate of 120 cc/min.

4. Readjust sensor, if necessary, to control at 4 in. of water pressure.

G.1.5 Hydrogen Separation

Hydrogen control valve 22 is used to control hydrogen concentration in recycle stream. The concentration of hydrogen is not critical but the optimum range is 4 to 5%. Analyze recycle stream for hydrogen and adjust control valve accordingly. To lower the hydrogen concentration, reduce manifold pressure by opening valve 22. To increase hydrogen concentration, partially close valve 22.

G.2 Shutdown Procedure

1. Turn off electrolysis current.
2. Turn off Lab-Stat CO_2 feed controller
3. Close CO_2 feed control valve 4.
4. Open solenoid valve 21 and close valves 9 and 10 to bypass water saturator.
5. Turn off water saturator temperature controller.
6. Open all oxygen manifold valves.
7. With recycle pump running, decrease power input to electrolysis unit furnace. Regulate cooling rate to 200 to 250°C per hour. As furnace cools, CO_2 will automatically feed into system from pressure fail-safe apparatus.
8. When electrolysis unit has cooled to 300°C, turn off power to carbon deposition reactor heater.
9. When both furnaces are cold, open valve R and purge system with CO_2.
10. Turn off recycle pump and vacuum pump.

G.3 Carbon Scraping Procedure

1. Remove thermocouple from scraper shaft.
2. Check carbon deposition reactor gate valve position. Valve must be open (pushed in).
3. Check valve 12 in carbon jar discharge line. Valve must be open.
4. Check valve K in CO_2 purge line. Valve must be closed.
5. Loosen brass nut of O-ring gland aroung scraper shaft.
6. Turn off Lab-Stat controller, CO_2 control valve (valve 4), and electrolysis current.

7. Stop recycle pump.

8. Rotate scraper (counterclockwise) slowly one complete turn. Continue counterclockwise rotation and push scraper downward as far as handle will allow.

9. Lift scraper back to original position.

10. Hand tighten brass nut of O-ring gland.

11. Start recycle pump.

12. Start electrolysis current and immediately open CO_2 control valve to a reading of 80 cc/min on CO_2 mass flowmeter.

13. Turn on Lab-Stat controller.

14. Replace thermocouple in scraper shaft.

15. Leak test O-ring gland with liquid leak detector.

G.4 Procedure for Emptying Carbon Jar

1. Close gate valve 25 (pulled out position).

2. Close needle valve 12.

3. Unscrew O-ring glands at bottom and top of jar. Remove jar.

4. Empty jar into weighed container.

5. Clean rim of jar and reconnect to O-ring glands.

6. Open valves 26 and K and purge jar with CO_2 for 5 min at purge flowmeter setting of 10.0. Control flow with valve 5.

7. Close valves K and 26 and open valve 12.

8. Open gate valve 25 (pushed in position).

9. Weigh carbon and record.

G.5 Switch Recycle Pumps

To switch from pump A to pump B:

1. Open valve 15B in bypass loop of pump B one to two turns.
2. Start pump B.
3. Open valves 13B and 16B.
4. Stop pump A.
5. Close valves 13A and 16A.
6. Adjust valve 15B to give a reading of 12.0 to 14.0 on recycle flowmeter.
7. Adjust recycle control valve on instrument panel to give reading of 10.0 on flowmeter (1780 cc/min).
8. Open valve 14B to after-filter pressure gauge and close valve 14A.

G.6 Clean Filters

The porous stainless steel filters in inlet lines of the pumps can be cleaned without interrupting oxygen production because only one pump is used at a time. The procedure is as follows:

1. Check valves 13, 14, and 16 associated with the filter to be cleaned. Valves must be closed.
2. Remove filter cartridge by unscrewing O-ring gland at each end.
3. Back flush filter with carbon dioxide at pressure of 20-30 lb.
4. Connect cartridge back into system.
5. Check orientation of cartridge. Arrow on side must point down.

G.7 Clean Coarse Filter and Discharge Line of Carbon Deposition Reactor

1. Turn off Lab-Stat controller, CO_2 control valve 4, and electrolysis current.
2. Stop recycle pump.
3. Close valve 13 (A or B) to isolate filter and recycle pump.
4. Unscrew two clean-out plugs at bottom and at side of filter.

5. Tap filter to discharge loose carbon.

6. Insert push-rod through side clean-out opening into gas discharge line and push loose carbon back into reactor.

7. Replace clean-out plugs.

8. Open valve 13 and start recycle pump.

9. Start electrolysis current and immediately open CO_2 control valve 4 to give a reading of 80 cc/min on mass flowmeter.

10. Turn on Lab-Stat controller.

11. Check recycle flow rate and adjust if necessary.

12. Leak check clean-out plugs.

APPENDIX H

DATA LOG OF 180 DAY LIFE TEST OF BREADBOARD SYSTEM

Day			1	2	3	4	5	6	7	8	9	10	11	12	13	14	15	16	17	18	19	20
Flow	CO_2 Feed	cc/min	97.0	97.4	98.1	96.9	96.2	97.6	95.6	96.1	94.8	95.0	94.5	94.8	95.4	95.4	97.4	94.8	97.6	97.7	100.6	99.6
	H_2O Feed	cc/min	56.1	56.7	56.1	57.8	60.7	58.1	62.7	57.7	56.9	58.2	59.2	58.4	59.2	58.7	54.8	50.6	51.4	52.6	54.2	53.9
	Recycle	cc/min	1300	1340	1440	1410	1410	1400	1350	1360	1350	1360	1330	1354	1330	1360	1350	1360	1360	1380	1360	1360
Pressure	Before Battery	in. H_2O	4.66	9.36	4.18	2.98	4.42	3.06	4.79	7.35	7.87	7.78	7.72	7.73	7.58	7.70	7.72	7.15	7.75	7.94	7.03	7.42
	After Battery	in. H_2O	1.18	0.69	0.26	0.1	0.76	0.0	1.46	3.70	4.00	4.22	4.24	4.04	4.04	4.05	4.11	3.49	4.02	4.0	3.31	3.22
	After Filter	in. H_2O	0.21	−0.56	−1.2	−2.65	−1.21	−2.24	−0.29	2.00	2.20	2.56	1.86	0.93	1.00	1.17	1.43	1.20	1.70	2.1	1.10	0.88
	Oxygen	in. H_2O	1.13	1.13	1.13	1.12	1.12	1.12	1.12	1.12	1.12	1.13	1.13	1.13	3.0	2.90	2.40	2.37	2.27	2.25	2.95	2.82
Electrolysis	No. of Stacks in Operation		8	8	6	6	6	7	7	7	7	7	7	7	7	7	7	7	7	7	7	7
	Current	Amps	5.32	5.33	5.24	5.29	5.27	5.29	5.27	5.22	5.19	5.19	5.2	5.27	5.25	5.28	5.30	5.37	5.37	5.39	5.42	5.43
	Voltage	Volts	11.5	12.2	12.8	12.3	12.1	12.1	12.1	12.1	12.2	12.4	12.4	12.5	12.3	12.6	12.2	12.7	12.5	12.7	12.7	12.8
	Temperature	°C	910	910	910	910	910	910	910	910	910	910	910	910	910	910	910	910	910	910	910	910
	Oxygen Production:																					
	Wet Test Meter Reading	cc/min	130.6	130.6	131.0	133.1	133.9	133.9	133.9	133.2	132.3	133.8	131.9	132.8	135.4	136.6	136.4	138.1	138.1	138.3	136.1	137.3
	Total Gas Flow	cc/min	126.7	126.7	127.1	129.2	129.8	129.9	129.9	129.3	129.2	128.3	129.8	128.0	128.9	131.3	132.5	132.4	133.9	134.1	132.0	133.2
	CO_2 Impurity	cc/min	–	–	–	3.3	–	–	–	–	–	–	–	–	–	6.1	–	–	–	–	4.4	–
	H_2O Impurity	cc/min	–	–	–	0.1	–	–	–	–	–	–	–	–	–	0.2	–	–	–	–	0.2	–
	Pure Oxygen Flow	cc/min	125.7	125.7	126.1	125.8	126.5	126.6	126.6	125.9	125.8	125.0	126.4	124.7	125.5	125.0	126.1	126.0	127.5	127.7	127.4	128.5
	Oxygen Purity	%	.992	–	–	.974	–	–	–	–	–	–	–	–	–	.952	–	–	–	–	.965	–
	Current Efficiency	%	87.6	87.5	89.0	85.9	86.7	86.5	86.7	87.4	87.6	87.0	87.8	85.6	86.3	83.8	84.1	83.5	83.8	83.7	84.2	84.7
	Power per Man	Watts	242	258	265	258	251	252	251	250	251	256	254	263	256	265	255	270	262	267	269	269
	Effective DD		0.64	0.64	0.63	0.64	0.64	0.64	0.64	0.63	0.63	0.63	0.63	0.63	0.64	0.63	0.63	0.63	0.63	0.63	0.63	0.63
Hydrogen Removal	Hydrogen Output	cc/min	53.1	53.7	53.9	54.7	57.5	55.0	54.9	48.8	49.1	47.5	51.2	50.3	52.3	49.9	46.7	47.0	49.5	47.8	48.6	48.4
	Manifold Pressure	mmHg	13.7	13.6	13.5	14.0	14.6	13.4	12.6	10.2	11.2	12.8	13.4	13.2	13.6	13.1	12.8	12.7	13.2	13.0	13.1	13.1
	Hydrogen Purity	%	–	–	–	–	99.7	–	–	–	–	–	–	–	–	99.7	–	–	–	–	–	–
Carbon Deposition Reactor	Temperature	°C	545	545	545	545	545	545	545	545	545	545	545	545	545	545	545	545	545	545	545	545
	Carbon Collected	g/Day	36.1	34.1	39.2	56.8	76.8	62.0	53.5	58.7	54.5	53.3	61.6	56.8	72.0	61.6	59.7	70.1	79.2	49.7	45.2	82.3
	5-Day Average	g/Day	–	–	–	–	48.6	–	–	–	–	56.4	–	–	–	–	62.4	–	–	–	–	65.4
	Iron Content	%	–	–	1.70	–	1.28	1.33	1.44	1.47	–	0.93	–	0.75	–	–	0.77	–	–	0.70	–	–

APPENDIX H - CONTINUED

DATA LOG OF 180 DAY LIFE TEST OF BREADBOARD SYSTEM

Day			21	22	23	24	25	26	27	28	29	30	31	32	33	34	35	36	37	38	39	40
Flow	CO_2 Feed	cc/min	98.6	98.7	100.3	99.8	100.4	100.2	100.6	98.7	101.9	102.6	101.5	98.5	99.0	99.7	101.9	102.3	102.3	100.1	101.4	100.9
	H_2O Feed	cc/min	55.4	55.4	57.6	56.1	56.4	57.6	57.8	56.7	58.5	60.2	62.2	58.0	60.1	61.1	63.8	63.2	62.9	61.8	62.1	59.5
	Recycle	cc/min	1350	1370	1340	1580	1410	1520	1765	1760	1780	1780	1800	1300	1795	1780	1780	1780	1780	1780	1780	1780
Pressure	Before Battery	in. H_2O	6.60	6.60	6.67	7.01	7.05	7.36	8.11	7.76	7.80	7.80	7.83	7.71	7.80	7.83	7.79	7.87	7.81	7.77	7.92	7.94
	After Battery	in. H_2O	2.90	2.90	3.05	3.07	3.15	3.19	3.24	3.64	3.01	2.94	2.93	2.91	2.98	3.00	2.96	3.07	3.00	3.00	3.08	3.10
	After Filter	in. H_2O	0.86	0.75	0.75	1.00	0.80	0.30	−0.16	−0.70	0.43	0.20	0.20	−0.48	−0.64	−0.60	0.85	0.60	0.16	−0.10	0.10	0.10
	Oxygen	in. H_2O	2.75	2.80	2.85	3.18	3.28	3.22	3.21	3.24	3.25	3.14	3.00	2.93	3.23	3.62	3.70	4.25	4.18	4.02	3.94	4.51
Electrolysis	No. of Stacks in Operation		7	7	7	7	7	7	7	7	7	6	6	7	6	6	6	6	6	6	6	6
	Current	Amps	5.53	5.66	5.65	5.68	5.65	5.62	5.62	5.52	5.47	5.57	5.58	5.60	5.60	5.67	5.67	5.66	5.68	5.67	5.64	5.66
	Voltage	Volts	12.8	12.8	12.9	12.9	12.8	12.8	12.3	12.4	12.7	12.9	12.0	12.2	12.8	12.8	12.9	12.8	12.6	12.9	12.8	12.6
	Temperature	°C	910	910	910	910	910	910	910	910	910	910	910	910	910	910	910	910	910	910	910	910
	Oxygen Production:																					
	Wet Test Meter Reading	cc/min	126.6	126.9	128.0	128.2	127.9	128.7	130.4	126.5	133.6	132.3	129.9	130.5	130.0	133.4	132.6	132.3	133.0	131.5	133.3	132.3
	Total Gas Flow	cc/min	–	–	–	–	128.6	129.4	131.1	127.2	134.3	133.0	130.6	131.4	130.7	134.1	133.3	133.0	133.7	132.2	134.0	133.1
	CO_2 Impurity	cc/min	4.58	4.59	4.63	4.64	3.54	3.2	3.26	3.16	3.34	3.31	3.25	3.55	4.84	4.96	3.91	3.74	3.76	3.72	3.77	3.73
	H_2O Impurity	cc/min	–	–	–	–	0.75	0.7	0.71	0.69	0.73	0.72	0.71	0.87	0.72	0.74	0.71	0.72	0.72	0.71	0.72	0.77
	Pure Oxygen Flow	cc/min	122.0	122.3	123.4	123.6	124.4	125.4	127.1	123.3	130.3	129.0	126.7	125.0	125.2	128.4	128.7	128.6	129.2	127.8	129.5	128.6
	Oxygen Purity	%	–	–	–	–	96.7	97.0	–	97.0	–	–	–	95.1	95.8	–	96.5	96.6	–	–	–	96.6
	Current Efficiency	%	80.7	79.1	79.9	79.6	80.5	81.7	82.7	81.7	81.7	84.7	83.0	81.6	81.8	82.9	83.0	83.1	83.2	82.4	84.0	83.1
	Power per Man	Watts	289	295	294	295	290	286	271	277	266	277	263	272	285	281	283	280	276	285	278	276
	Effective DD		–	–	–	–	–	0.634	–	–	0.618	–	–	–	–	–	0.625	–	–	–	–	0.619
Hydrogen Removal	Hydrogen Output	cc/min	48.1	46.3	47.2	47.6	48.5	48.1	48.1	50.0	47.2	45.4	52.8	54.4	52.8	54.0	53.5	54.4	54.4	55.3	53.8	54.2
	Manifold Pressure	mmHg	13.0	12.7	12.8	12.9	13.0	12.3	10.6	10.8	9.5	8.0	9.5	9.3	8.3	8.3	8.3	8.4	8.5	8.5	8.4	8.6
	Hydrogen Purity	%	–	–	–	–	–	–	–	–	–	–	–	–	–	–	–	98.5	–	–	–	–
Carbon Deposition Reactor	Temperature	°C	558	558	561	559	559	555	555	554	553	559	550	557	561	555	560	557	556	558	558	561
	Carbon Collected	g/Day	82.3	81.3	68.1	62.0	60.0	69.3	68.6	63.1	59.7	67.0	67.0	66.0	66.0	73.5	73.5	67.6	67.6	76.9	76.9	70.1
	5-Day Average	g/Day	–	–	–	–	72.7	–	–	–	–	65.6	–	–	–	–	69.2	–	–	–	–	71.8
	Iron Content	%	0.64	–	–	–	0.89	–	–	1.08	–	–	0.80	–	–	–	0.72	–	–	–	0.67	–

APPENDIX H - CONTINUED

DATA LOG OF 180 DAY LIFE TEST OF BREADBOARD SYSTEM

	Day		41	42	43	44	45	46	47	48	49	50	51	52	53	54	55	56	57	58	59	60
Flow	CO_2 Feed	cc/min	101.1	102.2	101.7	103.3	103.1	103.1	103.8	103.8	101.7	104.1	103.2	102.2	101.9	101.5	103.5	102.7	103.7	103.6	104.0	102.9
	H_2O Feed	cc/min	55.5	55.5	54.4	54.8	54.7	57.6	52.8	50.2	51.0	57.3	47.9	65.1	47.5	56.7	51.8	62.1	61.0	–	54.0	54.0
	Recycle	cc/min	1780	1780	1780	1780	1800	1780	1780	1780	1780	1780	1780	1795	1780	1780	1795	1800	1780	1780	1720	1661
Pressure	Before Battery	in. H_2O	7.89	7.86	7.89	7.85	7.86	7.89	7.86	7.87	7.87	7.84	7.85	7.83	7.72	7.83	7.87	7.93	7.80	7.86	7.70	7.50
	After Battery	in. H_2O	3.00	3.03	3.05	3.00	2.99	3.02	3.05	3.04	2.98	2.99	3.02	2.98	2.94	2.99	3.03	3.04	2.99	3.00	3.00	3.00
	After Filter	in. H_2O	0.20	−0.05	−0.20	−0.27	−0.15	−0.25	0.91	0.80	1.00	0.92	0.27	1.13	0.70	0.50	0.92	0.74	1.50	1.44	1.38	0.80
	Oxygen	in. H_2O	4.45	4.54	4.43	4.68	4.55	4.42	3.53	4.03	4.39	4.46	4.72	4.45	4.47	4.78	4.70	4.76	4.14	4.53	4.35	4.25
Electrolysis	No. of Stacks in Operation		6	6	6	6	6	6	6	6	6	6	6	6	6	6	6	6	6	6	6	6
	Current	Amps	5.65	5.67	5.69	5.69	5.69	5.69	5.69	5.69	5.69	5.69	5.68	5.69	5.69	5.67	5.70	5.70	5.70	5.70	5.70	5.70
	Voltage	Volts	12.7	12.8	12.8	12.8	12.8	12.8	12.5	12.5	12.5	12.8	12.5	12.9	12.8	12.9	12.9	12.8	12.7	12.7	12.8	12.9
	Temperature	°C	910	910	910	910	910	910	910	910	910	910	910	910	910	910	910	910	910	910	910	910
	Oxygen Production:																					
	Wet Test Meter Reading	cc/min	133.2	134.5	133.0	134.6	134.5	134.3	134.2	134.2	134.2	134.0	135.0	134.4	134.7	131.8	132.6	133.2	134.1	135.6	131.0	132.0
	Total Gas Flow	cc/min	134.0	134.4	133.8	135.5	135.4	135.3	135.2	135.2	135.1	135.3	135.9	135.3	135.6	132.7	133.5	134.2	135.2	136.4	131.8	132.8
	CO_2 Impurity	cc/min	3.69	3.73	3.64	3.69	3.69	3.99	3.99	5.03	3.88	6.81	3.69	3.67	3.68	3.56	3.62	4.36	4.47	3.92	3.79	3.81
	H_2O Impurity	cc/min	0.76	0.87	0.84	0.85	0.85	0.93	0.93	1.04	0.93	1.29	0.92	0.92	0.93	0.89	0.88	1.02	1.11	0.85	0.82	0.82
	Pure Oxygen Flow	cc/min	129.5	130.8	129.4	130.9	130.8	130.3	130.3	129.2	130.3	127.2	131.3	130.7	131.0	128.2	129.0	128.8	129.6	131.7	127.2	128.2
	Oxygen Purity	%	96.7	96.6	96.6	–	–	96.4	96.4	95.5	96.4	94.0	96.6	–	–	96 6	96.6	96.0	95.9	96.5	–	–
	Current Efficiency	%	83.9	84.4	83.2	84.2	84.1	83.8	83.8	83.0	83.8	81.8	84.4	84.1	84.2	82.7	82.8	82.7	83.2	84.5	81.6	82.3
	Power per Man	Watts	276	276	280	277	277	278	272	272	278	276	271	279	281	284	284	280	274	283	283	288
	Effective DD		–		–	–	–	0.600	–	0.595	–	–	–	–	–	–	0.595	–	–	–	–	–
Hydrogen Removal	Hydrogen Output	cc/min	54.4	53.9	54.4	53.9	56.2	54.0	54.5	54.8	54.2	54.6	53.0	53.3	53.8	53.5	54.4	57.3	54.3	55.6	52.6	53.5
	Manifold Pressure	mmHg	10.0	10.1	10.1	10.1	10.2	10.1	10.3	10.3	10.2	10.3	10.0	10.1	10.1	10.2	10.3	10.3	10.4	–	–	–
	Hydrogen Purity	%	–	–	–	–	–	–	–	–	98.2	–	–	–	–	97.8	–	–	98.9	98.6	–	–
Carbon Deposition Reactor	Temperature	°C	561	566	570	567	567	567	569	569	567	569	567	566	565	565	566	569	567	568	570	569
	Carbon Collected	g/Day	70.1	67.5	67.5	72.6	72.6	67.0	67.0	69.5	69.5	74.3	74.3	78.0	78.0	77.2	77.2	73.3	73.3	70.7	70.7	73.3
	5-Day Average	g/Day	–	–	–	–	70.0	–	–	–	–	69.5	–	–	–	–	76.9	–	–	–	–	72.3
	Iron Content	%	0.80	–	–	–	–	–	–	–	1.62	–	1.60	–	–	–	1.65	–	2.24	–	–	–

APPENDIX H - CONTINUED

DATA LOG OF 180 DAY LIFE TEST OF BREADBOARD SYSTEM

Day			61	62	63	64	65	66	67	68	69	70	71	72	73	74	75	76	77	78	79	80
Flow	CO_2 Feed	cc/min	101.8	101.3	100.8	102.6	103.0	105.0	105.9	106.9	104.0	106.5	106.3	106.8	108.1	110.3	114.3	110.6	105.9	101.3	101.7	104.1
	H_2O Feed	cc/min	67.3	61.8	58.2	50.0	59.6	53.8	58.9	52.8	50.9	50.7	64.2	43.4	44.5	44.5	60.9	45.7	55.6	52.5	61.2	42.3
	Recycle	cc/min	1791	1780	1780	1780	1780	1780	1678	1780	1730	1780	1780	1695	1738	1683	1766	1780	1780	1797	1916	1780
Pressure	Before Battery	in. H_2O	7.86	7.95	7.89	7.88	7.95	7.84	7.63	7.90	7.85	7.86	7.87	7.84	7.68	7.73	7.76	7.87	7.87	8.16	8.09	7.97
	After Battery	in. H_2O	2.99	3.07	3.01	2.99	3.07	3.01	3.00	3.02	3.01	3.04	3.05	3.02	3.00	3.00	2.96	2.96	3.00	3.10	2.98	2.98
	After Filter	in. H_2O	0.88	1.43	1.05	1.22	1.41	1.44	0.15	1.49	1.63	1.73	1.8	1.34	1.30	0.97	0.76	1.39	1.66	1.84	1.73	1.69
	Oxygen	in. H_2O	4.84	5.04	5.01	4.89	4.80	4.72	4.55	4.49	4.46	4.54	4.49	4.50	4.43	4.32	4.26	4.53	4.54	4.44	4.45	4.38
Electrolysis	No. of Stacks in Operation		6	6	6	6	6	6	6	6	6	6	6	6	6	6	6	6	6	10	10→8	6
	Current	Amps	5.71	5.70	5.70	5.70	5.70	5.70	5.70	5.70	5.70	5.70	5.70	5.70	5.70	5.70	5.71	5.69	5.69	5.72	5.74	5.70
	Voltage	Volts	12.8	12.9	12.5	12.5	12.8	13.0	12.9	12.6	12.6	12.6	12.7	12.4	12.7	12.9	12.9	12.9	11.0	12.0	12.5	12.5
	Temperature	°C	910	910	910	910	910	910	910	910	910	910	910	910	910	910	910	910	910	910	910	910
	Oxygen Production:																					
	Wet Test Meter Reading	cc/min	131.1	133.4	132.2	132.3	131.5	132.7	131.8	132.5	131.9	133.4	134.0	129.8	137.0	133.8	134.2	130.4	133.7	124.7	127.5	131.1
	Total Gas Flow	cc/min	131.9	134.3	133.1	133.2	132.5	133.7	132.8	133.6	133.0	134.5	135.1	130.9	138.2	135.0	135.4	131.4	134.7	125.6	128.5	132.2
	CO_2 Impurity	cc/min	3.79	3.48	3.45	3.44	3.87	3.90	3.87	4.35	4.33	4.00	4.01	3.75	3.96	3.87	3.86	3.79	3.89	3.63	3.71	3.83
	H_2O Impurity	cc/min	0.82	0.89	0.88	0.88	1.02	1.03	1.02	1.12	1.12	1.10	1.11	1.13	1.19	1.16	1.15	0.97	1.00	0.93	0.95	1.07
	Pure Oxygen Flow	cc/min	127.3	129.9	128.7	128.9	127.6	128.8	127.9	128.2	127.6	129.4	130.0	126.0	133.0	129.9	130.3	126.6	129.8	121.1	123.8	127.3
	Oxygen Purity	%	–	96.7	96.7	–	96.3	–	–	95.9	–	96.2	–	96.3	–	–	–	–	96.4	–	–	96.3
	Current Efficiency	%	81.6	83.4	82.6	82.7	81.9	82.7	82.1	82.3	81.9	83.1	83.4	80.9	85.4	83.4	83.5	81.4	83.5	77.4	78.9	81.7
	Power per Man	Watts	280	285	275	285	278	289	286	283	276	275	286	265	278	282	289	282	259	277	279	277
	Effective DD		–	0.586	–	–	–	–	–	–	0.574	–	–	–	–	–	–	0.589	–	–	–	–
Hydrogen Removal	Hydrogen Output	cc/min	53.3	57.3	56.4	56.9	56.6	56.9	56.2	56.3	55.1	56.9	56.1	57.2	59.0	58.7	61.4	63.5	55.7	52.2	53.4	56.9
	Manifold Pressure	mmHg	–	–	–	–	8.1	8.1	8.1	8.2	8.2	8.2	8.2	8.5	9.5	10.5	11.5	11.7	5.8	5.5	5.6	5.9
	Hydrogen Purity	%	–	–	–	98.5	98.4	–	–	98.2	–	–	96.5	–	–	–	83.2	–	98.9	–	–	98.8
Carbon Deposition Reactor	Temperature	°C	565	568	565	563	567	567	561	563	563	562	563	561	561	561	565	561	563	559	559	563
	Carbon Collected	g/Day	73.3	79.2	79.2	67.1	67.1	72.2	72.2	75.1	75.1	66.3	66.3	71.1	71.1	78.7	78.7	71.6	71.6	–	64.0	64.0
	5-Day Average	g/Day	–	–	–	–	73.2	–	–	–	–	72.2	–	–	–	–	73.2	–	–	–	–	–
	Iron Content	%	2.23	–	–	–	2.58	–	–	–	3.22	–	–	–	3.25	–	–	–	–	–	–	3.94

APPENDIX H - CONTINUED

DATA LOG OF 180 DAY LIFE TEST OF BREADBOARD SYSTEM

	Day		81	82	83	84	85	86	87	88	89	90	91	92	93	94	95	96	97	98	99	100
Flow	CO_2 Feed	cc/min	103.2	103.7	104.1	105.7	104.2	101.8	105.6	105.1	105.0	104.2	104.1	104.1	103.1	102.2	101.7	101.2	105.3	101.3	107.1	107.4
	H_2O Feed	cc/min	61.0	55.1	41.4	49.8	57.9	45.2	52.3	54.4	55.9	50.2	53.4	41.9	54.9	47.7	–	58.9	60.7	47.5	54.9	50.7
	Recycle	cc/min	1780	1780	1780	1780	1780	1780	1780	1780	1780	1780	1780	1780	1746	1780	1787	1780	1780	1780	1780	1780
Pressure	Before Battery	in. H_2O	8.01	7.97	7.95	8.03	8.01	7.98	8.02	8.03	8.05	8.01	8.03	8.03	7.91	7.98	8.05	8.01	8.10	8.04	8.05	8.03
	After Battery	in. H_2O	3.00	2.99	3.00	3.01	3.01	2.93	2.99	3.02	3.02	3.00	3.00	3.00	3.00	3.00	3.01	3.00	3.02	3.00	3.05	3.05
	After Filter	in. H_2O	1.76	1.64	1.74	1.82	1.7	1.47	1.29	1.67	1.65	1.59	1.67	1.69	1.70	1.71	1.61	1.50	1.56	1.46	1.58	1.65
	Oxygen	in. H_2O	4.45	4.50	4.44	4.53	4.50	4.45	4.50	4.42	4.50	4.29	4.25	4.25	4.25	4.25	4.50	4.46	4.54	4.50	4.54	4.53
Electrolysis	No. of Stacks in Operation		6	6	6	6	6	6	6	6	6	6	6	6	6	6	6	6	6	6	6	6
	Current	Amps	5.70	5.70	5.70	5.71	5.70	5.70	5.70	5.70	5.70	5.70	5.70	5.70	5.70	5.70	5.70	5.70	5.70	5.70	5.70	5.70
	Voltage	Volts	12.5	12.8	12.8	12.8	12.9	12.9	12.6	12.7	12.7	12.7	12.8	12.8	12.7	12.7	12.6	12.9	12.8	12.3	12.2	12.4
	Temperature	°C	910	910	910	910	910	910	910	910	910	910	910	910	910	910	910	910	910	910	910	910
	Oxygen Production:																					
	Wet Test Meter Reading	cc/min	131.8	132.4	132.4	139.7	131.8	130.1	130.5	131.3	131.2	130.4	130.8	129.9	129.7	130.1	130.7	130.8	130.5	129.3	129.6	130.1
	Total Gas Flow	cc/min	132.9	133.5	133.5	140.9	132.9	131.2	131.6	132.4	132.3	131.8	132.1	131.2	131.0	131.7	131.9	132.0	131.7	130.5	130.6	131.3
	CO_2 Impurity	cc/min	3.85	4.33	4.33	4.57	4.31	4.25	4.35	4.37	4.37	4.59	4.55	4.52	4.51	4.39	4.14	4.15	4.14	4.10	4.35	4.76
	H_2O Impurity	cc/min	1.08	1.09	1.09	1.16	1.09	1.08	1.11	1.11	1.11	1.38	1.35	1.34	1.34	1.63	1.23	1.25	1.23	1.21	1.03	1.25
	Pure Oxygen Flow	cc/min	128.0	128.1	128.1	135.1	127.5	125.8	126.2	126.9	126.8	125.8	126.2	125.4	125.2	125.2	126.6	126.7	126.4	125.2	125.2	125.3
	Oxygen Purity	%	–	95.9	–	–	–	–	95.9	–	–	95.5	95.5	–	–	95.0	95.9	–	–	–	95.9	95.4
	Current Efficiency	%	82.1	82.2	82.2	86.6	81.8	80.8	81.0	81.5	81.4	80.7	81.0	80.5	80.3	80.4	81.2	81.3	81.1	80.4	80.4	80.4
	Power per Man	Watts	277	284	269	287	291	290	282	284	287	286	290	290	288	285	282	290	290	279	276	277
	Effective DD		–	–	–	–	–	–	0.585	–	–	–	–	–	–	–	–	–	–	0.587	–	–
Hydrogen Removal	Hydrogen Output	cc/min	58.0	58.9	57.3	57.0	53.8	56.4	54.3	58.7	58.8	57.7	53.4	55.3	54.4	57.1	56.8	56.4	57.2	56.3	56.5	55.3
	Hydrogen Partial Pressure	mm Hg	6.0	5.8	5.7	5.6	5.6	5.6	5.6	5.8	5.8	5.7	5.7	5.6	5.6	5.6	5.7	5.8	5.8	5.7	5.7	5.7
	Hydrogen Purity	%	–	–	–	–	–	–	–	–	98.8	–	–	–	–	–	–	–	–	–	–	–
Carbon Deposition Reactor	Temperature	°C	563	564	566	564	560	561	563	566	565	563	562	558	560	565	563	562	559	560	562	563
	Carbon Collected	g/Day	72.8	72.8	64.3	64.3	97.6	64.8	64.8	67.8	67.8	72.6	72.6	59.1	59.1	75.2	75.2	62.4	62.4	64.1	64.1	77.7
	5-Day Average	g/Day	–	–	67.6	–	–	–	–	71.9	–	–	–	–	66.2	–	–	–	–	67.9	–	–
	Iron Content	%	–	3.37	–	3.19	–	–	3.56	–	–	–	3.28	–	–	–	2.99	–	–	–	–	–

APPENDIX H - CONTINUED

DATA LOG OF 180 DAY LIFE TEST OF BREADBOARD SYSTEM

Day			101	102	103	104	105	106	107	108	109	110	111	112	113	114	115	116	117	118	119	120
Flow	CO_2 Feed	cc/min	107.8	104.8	104.6	105.3	105.2	109.0	106.4	104.1	105.5	105.0	104.5	105.2	104.1	105.8	106.4	106.1	107.4	105.8	105.0	105.8
	H_2O Feed	cc/min	51.5	55.6	50.4	52.3	62.7	48.7	31.1	50.0	58.8	47.5	57.8	47.9	47.9	59.1	56.6	55.6	64.8	48.2	60.0	67.9
	Recycle	cc/min	1780	1780	1780	1780	1780	1780	1750	1780	1780	1780	1780	1780	1780	1780	1780	1780	1780	1780	1780	1780
Pressure	Before Battery	in. H_2O	8.02	8.06	8.04	8.06	8.02	8.01	8.03	8.05	8.05	8.03	8.06	8.05	8.01	8.07	8.04	8.08	8.11	8.17	8.13	8.13
	After Battery	in. H_2O	3.00	3.01	3.03	3.01	3.03	3.00	3.03	3.0	3.0	3.01	3.02	3.00	2.98	3.00	3.00	3.02	3.00	3.00	3.00	3.00
	After Filter	in. H_2O	1.67	1.61	1.61	1.60	1.66	1.70	1.77	1.7	1.68	1.70	1.67	1.70	1.56	1.63	1.62	1.70	1.70	1.70	1.68	1.70
	Oxygen	in. H_2O	4.50	4.48	4.53	4.50	4.53	4.50	4.50	4.50	4.50	4.50	4.50	4.50	4.42	4.50	4.50	4.57	4.50	4.47	4.50	4.34
Electrolysis	No. of Stacks in Operation		6	6	6	6	6	6	6	6	6	6	6	6	6	6	6	6	6	6	6	6
	Current	Amps	5.70	5.70	5.70	5.70	5.70	5.70	5.70	5.70	5.70	5.70	5.70	5.70	5.70	5.70	5.70	5.70	5.70	5.70	5.70	5.70
	Voltage	Volts	12.5	12.6	12.6	12.7	12.7	12.6	12.7	12.6	12.7	12.7	12.5	12.6	12.6	12.6	12.6	12.6	12.7	12.7	12.7	12.8
	Temperature	°C	910	910	910	900	900	900	900	900	900	900	900	900	900	900	900	900	900	900	900	900
	Oxygen Production:																					
	Wet Test Meter Reading	cc/min	131.4	130.5	130.6	131.4	130.6	132.8	131.4	130.9	129.2	130.3	130.0	129.7	130.5	130.4	131.3	130.8	132.2	132.3	131.9	131.7
	Total Gas Flow	cc/min	132.6	131.7	132.1	133.5	132.8	135.0	133.5	133.0	131.3	132.4	132.0	131.7	132.6	132.5	133.4	132.9	134.4	134.4	134.0	133.8
	CO_2 Impurity	cc/min	4.35	4.32	4.56	4.71	4.68	4.76	4.89	5.05	4.97	4.85	4.84	4.83	4.86	4.86	4.89	4.87	4.93	4.93	4.91	4.91
	H_2O Impurity	cc/min	1.22	1.21	1.48	1.24	1.24	1.26	1.67	2.08	2.06	2.09	2.09	2.09	2.10	2.10	2.11	2.10	2.12	2.12	2.12	2.12
	Pure Oxygen Flow	cc/min	127.1	126.2	126.0	127.5	126.8	128.9	126.9	125.8	124.2	125.4	125.1	124.7	125.6	125.5	126.4	125.9	127.3	127.3	126.9	126.7
	Oxygen Purity	%	95.8	–	95.4	95.5	–	–	–	–	94.6	–	–	–	–	94.9	–	–	–	94.5	–	–
	Current Efficiency	%	81.5	81.0	80.9	81.8	81.3	82.7	81.4	80.7	79.7	80.4	80.3	80.0	80.6	80.6	81.1	80.8	81.7	81.7	81.4	81.3
	Power per Man	Watts	281	284	281	284	280	282	287	284	290	287	284	287	287	285	285	283	286	283	283	286
	Effective DD		–	–	–	.592	–	–	–	–	–	.584	–	–	–	–	–	–	–	.590	–	–
Hydrogen Removal	Hydrogen Output	cc/min	56.3	56.6	56.3	54.75	54.75	55.25	55.25	54.75	54.70	53.70	52.05	52.7	54.27	53.30	53.08	55.56	55.43	55.22	55.24	53.57
	Manifold Pressure	mmHg	5.7	5.7	5.7	5.70	5.70	5.85	5.82	5.80	5.70	5.71	5.71	5.78	5.84	5.82	5.79	6.00	5.96	5.80	5.40	5.50
	Hydrogen Purity	%	–	98.0	–															96.9		
Carbon Deposition Reactor	Temperature	°C	556	561	564	563	564	563	562	562	563	562	564	552	559	563	563	562	561	568	567	555
	Carbon Collected	g/Day	77.7	62.8	62.8	60.0	60.0	77.1	77.1	69.6	69.6	68.2	68.2	76.8	76.8	85.8	85.8	65.2	65.2	69.4	69.4	68.2
	5-Day Average	g/Day	–	–	69.0	–	–	–	–	68.76	–	–	–	–	71.92	–	–	–	–	74.3	–	–
	Iron Content	%	–	–	–			2.25				2.67				4.27				5.32		

APPENDIX H - CONTINUED

DATA LOG OF 180 DAY LIFE TEST OF BREADBOARD SYSTEM

Day		Units	121	122	123	124	125	126	127	128	129	130
Flow	CO_2 Feed	cc/min	106.4	108.1	104.4	106.2	105.1	107.1	105.7	105.6	103.8	109.9
	H_2O Feed	cc/min	44.5	48.9	56.9	73.4	49.64	52.8	54.0	66.16	64.3	50.3
	Recycle	cc/min	1780	1780	1780	1780	1780	1780	1780	1780	1780	1780
Pressure	Before Battery	in. H_2O	8.13	8.21	8.17	8.16	8.13	8.08	8.05	8.14	8.16	8.20
	After Battery	in. H_2O	3.03	3.03	3.00	3.06	3.02	3.00	3.00	2.99	3.03	3.01
	After Filter	in. H_2O	1.65	1.69	1.62	1.70	1.71	1.8	1.76	1.72	1.76	1.77
	Oxygen	in. H_2O	4.53	4.48	4.58	4.57	4.31	4.50	4.50	4.48	4.53	4.51
Electrolysis	No. of Stacks in Operation		6	6	6	6	6	6	6	6	6	6
	Current	Amps	5.70	5.70	5.70	5.70	5.70	5.70	5.70	5.70	5.80	5.80
	Voltage	Volts	12.7	12.7	12.6	12.7	12.6	12.7	12.8	12.8	12.9	12.9
	Temperature	°C	900	900	900	900	900	900	900	900	900	900
	Oxygen Production:											
	Wet Test Meter Reading	cc/min	131.3	131.0	132.9	132.9	133.2	130.8	131.1	129.3	129.7	131.1
	Total Gas Flow	cc/min	133.4	133.2	135.1	135.1	135.1	133.0	133.2	[illegible]	131.8	133.2
	CO_2 Impurity	cc/min	4.90	4.88	4.95	4.95	4.95	4.88	[illegible]	[illegible]	5.32	[illegible]
	H_2O Impurity	cc/min	2.11	2.11	2.14	2.14	2.14	2.10	2.11	[illegible]	2.09	2.37
	Pure Oxygen Flow	cc/min	126.4	126.2	127.9	127.9	127.9	126.0	126.1	[illegible]	124.9	[illegible]
	Oxygen Purity	%	95.0	—	—	—	—	—	—	96.7	—	96.2
	Current Efficiency	%	81.1	80.9	82.1	82.1	82.1	[illegible]	[illegible]	79.9	[illegible]	79.2
	Power per Man	Watts	*285	286	280	282	[illegible]	[illegible]	[illegible]	[illegible]	[illegible]	[illegible]
	Effective DD		—	—	—	—	.593	—	—	—	.603	
Hydrogen Removal	Hydrogen Output	cc/min	54.92	57.14	54.06	55.97	53.7	52.70	[illegible]	[illegible]	56.04	[illegible]
	Manifold Pressure	mmHg	5.60	5.70	5.50	5.60	5.54	5.5	5.48	5.54	5.66	[illegible]
	Hydrogen Purity	%								96.7		[illegible]
Carbon Deposition Reactor	Temperature	°C	567	568	566	567	565	[illegible]	[illegible]	[illegible]	[illegible]	[illegible]
	Carbon Collected	g/Day	68.2	71.5	71.5	69.1	69.1	[illegible]	[illegible]	74.9	[illegible]	[illegible]
	5-Day Average	g/Day	—	—	69.8	—	—	—		[illegible]	—	
	Iron Content	%		6.05				5.69				

Day		Units	131	132	133	134	135	136	137	138	139	140
Flow	CO_2 Feed	cc/min	116.7	[illegible]	115.4	115.3	116.4	117.2	118.6	126.7	133.8	143.1
	H_2O Feed	cc/min	54.3	58.1	47.4	[illegible]	71.1	63.4	41.2	79.6	24.6	25.3
	Recycle	cc/min	1780	1780	1780	1780	1780	1780	1780	1780	1780	1780
Pressure	Before Battery	in. H_2O	8.19	8.22	8.23	8.23	8.28	8.30	8.30	8.30	8.15	8.31
	After Battery	in. H_2O	3.01	3.00	3.00	3.00	3.00	3.00	3.00	3.00	3.00	3.00
	After Filter	in. H_2O	1.80	1.86	1.81	1.78	1.85	1.79	1.80	1.69	1.60	1.80
	Oxygen	in. H_2O	4.50	4.49	4.47	4.50	4.50	4.49	4.50	4.48	4.40	4.57
Electrolysis	No. of Stacks in Operation		6	6	6	6	6	6	6	6	6	6
	Current	Amps	5.80	5.80	5.80	5.77	5.80	5.80	5.80	5.80	5.80	5.80
	Voltage	Volts	12.8	[illegible]	12.8	12.8	12.8	12.8	12.8	12.9	12.9	12.9
	Temperature	°C	900	900	900	900	900	900	900	900	900	900
	Oxygen Production:											
	Wet Test Meter Reading	cc/min	132.5	133.3	[illegible]	[illegible]	[illegible]	131.8	131.5	133.0	132.1	129.9
	Total Gas Flow	cc/min	134.6	[illegible]	[illegible]	[illegible]	135.2	134.2	133.9	135.4	134.5	132.3
	CO_2 Impurity	cc/min	[illegible]	[illegible]	[illegible]	[illegible]	[illegible]	5.43	5.42	5.48	5.44	5.35
	H_2O Impurity	cc/min	[illegible]	[illegible]	[illegible]	[illegible]	[illegible]	2.39	2.38	2.41	2.39	2.35
	Pure Oxygen Flow	cc/min	126.2	[illegible]	[illegible]	[illegible]	127.4	126.4	126.1	127.5	126.7	124.5
	Oxygen Purity	%	—			[illegible]	—	—	—	—	—	—
	Current Efficiency	%	[illegible]	[illegible]	[illegible]	[illegible]	[illegible]	79.7	79.5	80.4	79.9	78.6
	Power per Man	Watts	[illegible]	[illegible]	[illegible]	[illegible]	[illegible]	[illegible]	293	292	294	299
	Effective DD			[illegible]		—	—	—	—	—	—	—
Hydrogen Removal	Hydrogen Output	cc/min	[illegible]	[illegible]	[illegible]	[illegible]	[illegible]	46.44	67.70	64.24	70.10	59.00
	Manifold Pressure	mmHg	5.70	[illegible]	[illegible]	[illegible]	5.97	5.36	4.57	5.35	6.15	10.29
	Hydrogen Purity	%	[illegible]					88.1				43.3
Carbon Deposition Reactor	Temperature	°C	[illegible]	[illegible]	[illegible]	[illegible]	[illegible]	576	576	566	558	570
	Carbon Collected	g/Day	[illegible]	[illegible]	[illegible]	[illegible]	[illegible]	74.7	74.7	59.3	59.3	73.6
	5-Day Average	g/Day			[illegible]		—	—	—	68.1	—	—
	Iron Content	%		[illegible]				—	6.03	—	—	—

APPENDIX H - CONTINUED

DATA LOG OF 180 DAY LIFE TEST OF BREADBOARD SYSTEM

	Day		141	142	143	144	145	146	147	148	149	150	151	152	153	154	155	156	157	158	159	160
Flow	CO_2 Feed	cc/min	151.7	124.3	122.8	122.6	123.4	120.5	120.9	118.7	126.1	116.7	123.3	124.6	129.0	124.9	122.2	127.3	126.2	128.1	126.4	126.4
	H_2O Feed	cc/min	23.4	23.1	28.8	21.4	20.5	27.6	28.5	18.8	19.7	27.4	35.8	—	21.1	24.9	27.7	31.3	15.2	35.7	31.2	30.3
	Recycle	cc/min	1780	1780	1780	1780	1780	1780	1780	1780	1780	1780	1780	1780	1780	1780	1780	1780	1780	1780	1780	1780
Pressure	Before Battery	in. H_2O	8.32	8.48	8.52	8.37	8.28	8.35	8.34	8.40	8.39	8.41	8.42	8.42	9.29	9.14	8.95	9.83	9.92	9.92	10.04	10.03
	After Battery	in. H_2O	3.01	3.08	3.12	3.03	3.00	3.00	3.03	3.03	3.14	3.02	3.05	3.00	3.35	3.20	3.00	3.84	4.01	4.04	4.09	4.00
	After Filter	in. H_2O	1.80	1.80	1.87	1.90	1.25	1.85	1.50	1.80	1.80	1.65	1.70	1.70	0.45	0.60	0.35	1.30	1.30	1.35	1.30	1.30
	Oxygen	in. H_2O	4.55	4.58	4.50	4.50	4.51	4.60	4.63	4.56	4.50	4.51	4.49	4.50	4.45	4.50	4.50	4.48	4.46	4.48	4.50	4.50
Electrolysis	No. of Stacks in Operation		6	6	6	6	6	6	6	6	6	6	6	6	6	6	6	6	6	6	6	6
	Current	Amps	5.80	5.80	5.80	5.80	5.80	5.80	5.81	5.80	5.80	5.80	5.80	5.80	5.80	5.81	5.80	5.80	5.80	5.80	5.81	5.81
	Voltage	Volts	12.4	12.4	12.4	12.5	12.8	12.8	12.8	12.8	12.8	12.8	12.8	12.8	12.2	12.5	12.9	12.8	12.9	12.8	12.9	12.9
	Temperature	°C	900	900	900	900	900	900	900	900	900	900	900	900	900	900	900	900	900	900	900	900
	Oxygen Production:																					
	Wet Test Meter Reading	cc/min	130.4	130.4	132.5	131.1	132.8	127.5	128.1	125.1	126.0	131.5	131.4	130.6	134.0	129.5	126.9	130.5	128.3	132.6	129.9	131.4
	Total Gas Flow	cc/min	132.6	132.6	133.9	132.4	134.0	128.7	129.3	126.3	127.2	132.7	133.1	132.3	135.7	131.2	128.6	132.2	130.0	134.3	131.7	133.2
	CO_2 Impurity	cc/min	6.75	6.75	5.67	5.61	5.72	5.50	5.52	5.39	5.43	5.67	6.81	6.77	6.94	6.71	6.57	6.76	6.65	6.87	5.95	6.02
	H_2O Impurity	cc/min	2.17	2.17	1.35	1.34	1.25	1.20	1.20	1.17	1.18	1.23	1.70	1.69	1.74	1.68	1.65	1.69	1.66	1.72	1.78	1.80
	Pure Oxygen Flow	cc/min	123.6	123.6	126.8	125.5	127.1	122.0	122.6	119.7	120.6	125.8	124.6	123.8	127.1	122.8	120.3	123.7	121.7	125.7	124.0	125.4
	Oxygen Purity	%	93.3	—	94.8	—	94.8	—	—	—	—	—	93.6	—	—	—	—	—	—	—	94.1	—
	Current Efficiency	%	78.0	78.0	80.0	79.2	80.2	77.0	77.2	75.5	76.1	79.4	78.6	78.1	80.1	77.3	75.9	78.1	76.7	79.3	78.1	79.0
	Power per Man	Watts	290	290	282	288	291	303	302	309	307	294	297	299	277	294	310	299	306	294	301	298
	Effective DD		—	0.57	0.56	—	—	—	—	—	0.61	—	—	0.59	—	—	—	—	—	—	0.59	—
Hydrogen Removal	Hydrogen Output	cc/min	67.22	27.68	26.61	26.24	27.17	—	25.73	24.80	24.87	30.82	28.50	29.39	31.54	29.99	27.91	29.97	28.39	32.29	32.04	33.03
	Manifold Pressure	mmHg	17.86	9.46	4.54	4.55	4.48	4.54	4.50	4.50	4.50	4.85	4.93	4.89	6.29	5.18	5.03	5.09	5.10	5.40	5.36	5.18
	Hydrogen Purity	%						96.9						97.9								96.9
Carbon Deposition Reactor	Temperature	°C	570	580	576	572	574	574	562	567	574	574	574	574	567	575	576	574	574	573	574	573
	Carbon Collected	g/Day	73.5	68.3	68.4	56.7	56.7	59.4	59.4	61.7	61.6	99.8	75.2	75.3	73.0	73.0	72.9	72.9	68.7	68.8	64.5	64.4
	5-Day Average	g/Day	—	—	68.6	—	—	—	—	58.8	—	—	—	—	77.0	—	—	—	—	71.3	—	—
	Iron Content	%	5.35	—	4.89	—	3.71	—	1.91	—	—	—	—	1.47	—	—	—	2.26	—	—	—	2.06

DATA LOG OF 180 DAY LIFE TEST OF BREADBOARD SYSTEM

Day			161	162	163	164	165	166	167	168	169	170	171	172	173	174	175	176	177	178	179	180
Flow	CO_2 Feed	cc/min	126.3	127.4	123.2	122.6	123.0	123.4	123.8	120.7	120.9	120.4	120.0	120.1	122.2	127.3	123.2	121.7	123.7	124.4	124.2	119.9
	H_2O Feed	cc/min	22.6	32.5	35.2	32.7	35.9	21.5	32.3	32.3	26.4	30.4	27.5	31.5	29.1	29.1	33.1	24.4	35.7	23.6	33.2	27.2
	Recycle	cc/min	1780	1780	1780	1780	1780	1780	1780	1780	1780	1780	1780	1780	1780	1695	1661	1780	1780	1780	1780	1780
Pressure	Before Battery	in. H_2O	10.03	10.00	10.06	10.09	10.00	9.97	10.10	10.10	10.19	10.19	10.12	10.12	10.12	9.88	9.88	10.12	10.11	10.12	10.12	10.12
	After Battery	in. H_2O	4.00	4.00	4.04	4.09	4.00	3.96	4.00	4.00	4.00	4.21	4.00	4.00	4.00	3.85	4.00	4.00	4.00	4.00	4.00	4.00
	After Filter	in. H_2O	1.08	1.21	1.03	1.00	1.00	0.92	1.09	1.00	0.85	0.85	0.85	0.85	0.80	1.20	1.48	1.40	1.08	1.00	1.00	1.00
	Oxygen	in. H_2O	4.50	4.49	4.60	4.61	4.50	4.50	4.54	4.50	4.50	4.51	4.50	4.53	4.48	4.35	3.69	4.56	4.52	4.52	4.50	4.50
Electrolysis	No. of Stacks in Operation		6	6	6	6	6	6	6	6	6	6	6	6/7	6/7	6/7	6/7	6/7	6/7	6/7	6/7	6/7
	Current	Amps	5.81	5.81	5.81	5.86	5.83	5.82	5.80	5.81	5.79	5.81	5.83	5.85/4.50	5.83/5.40	5.80/6.50	5.80/6.50	5.80/6.54	5.80/6.55	5.80/6.00	5.79/6.00	5.80/6.00
	Voltage	Volts	12.9	12.9	13.0	12.9	12.9	12.9	12.9	12.8	12.8	12.8	12.7	12.6/12.8	12.8/12.1	12.9/11.0	12.8/12.3	12.8/12.2	12.9/12.9	12.9/12.4	12.9/12.5	12.8/12.0
	Temperature	°C	900	900	900	900	900	900	900	900	900	900	900	900	900	900	900	900	900	900	900	900
	Oxygen Production:																					
	Wet Test Meter Reading	cc/min	130.0	129.3	130.7	130.4	131.1	130.8	131.4	129.1	128.7	130.1	131.2	131.2	133.7	137.7	133.8	132.2	135.1	134.9	134.2	129.8
	Total Gas Flow	cc/min	131.8	131.1	132.5	131.9	132.6	132.3	132.9	130.6	130.2	131.6	132.7	132.7	135.2	139.3	135.3	133.7	136.8	136.6	135.9	131.4
	CO_2 Impurity	cc/min	5.95	5.92	5.99	5.79	5.82	5.81	5.83	5.73	5.71	5.78	5.64	5.64	5.75	5.92	5.75	5.69	5.85	5.84	5.81	5.62
	H_2O Impurity	cc/min	1.78	1.77	1.79	1.52	1.53	1.52	1.53	1.50	1.50	1.51	1.51	1.51	1.54	1.59	1.54	1.52	1.68	1.68	1.67	1.62
	Pure Oxygen Flow	cc/min	124.1	123.4	124.7	124.6	125.3	125.0	125.6	123.4	123.0	124.3	125.6	125.6	128.0	131.8	128.1	126.5	129.3	129.1	128.4	124.2
	Oxygen Purity	%	—	—	—	94.5	—	—	—	—	—	—	94.6	—	—	—	—	—	94.5	—	—	—
	Current Efficiency	%	78.1	77.7	78.5	77.8	78.6	78.6	79.2	77.7	77.7	78.3	78.8	75.7	76.6	78.4	76.2	75.0	76.6	76.2	75.8	77.0
	Power per Man	Watts	301	302	302	302	299	299	297	300	300	298	293	310	305	297	304	313	304	309	310	305
	Effective DD		—	—	—	0.55								0.56							0.58	
Hydrogen Removal	Hydrogen Output	cc/min	30.96	30.13	31.97	30.22	31.07	31.07	30.48	30.64	30.12	29.36	30.36	29.67	29.88	29.88	28.06	30.31	30.71	29.84	28.92	29.82
	Manifold Pressure	mmHg	5.23	5.08	5.38	5.14	5.10	5.06	4.94	5.11	5.25	5.04	5.09	5.13	5.39	5.25	5.25	5.42	5.60	5.60	5.54	5.21
	Hydrogen Purity	%				—	—	—	—	—	—	95.7	—	—	—	—	—	—	—	95.8	95.2	—
Carbon Deposition Reactor	Temperature	°C	568	570	575	575	571	566	571	574	580	580	579	576	578	576	574	576	571	574	570	563
	Carbon Collected	g/Day	74.6	74.6	69.3	70.5	70.4	78.3	78.3	64.4	64.5	63.6	63.6	73.5	73.5	73.5	73.5	73.5	73.5	73.5	73.2	73.3
	5-Day Average	g/Day	—	—	69.5	—	—	—	—	72.4	—	—	—	—	67.7	—	—	—	—	73.5	—	—
	Iron Content	%	—	—	—				1.62				2.18				1.91			1.85		

* 6/7 Six stacks in operation over night (5p.m to 8.a.m.) 15 hours.
Seven stacks in operation over day (8a.m. to 5p.m.) 9 hours.

APPENDIX I

METHODS OF CHEMICAL ANALYSIS

I.1 Oxygen Product

Water and CO_2 were determined by absorption and weighing, using Stetser-Norton bulbs filled with anhydrous magnesium perchlorate for absorbing water and Indicarb (Fisher Scientific Company) for absorbing CO_2. The absorption bulbs were flushed with dry nitrogen and weighed, and then were connected to the oxygen discharge line ahead of the wet test meter with the water bulb first. Oxygen was passed through the bulbs for exactly one or two revolutions of the wet test meter. After allowing the bulbs to cool, they were flushed with nitrogen and weighed.

Carbon monoxide in the oxygen was determined by infrared spectrographic analysis, using a special absorption cell having a 10-meter path length. The cell was evacuated and then filled with oxygen from the breadboard system to a pressure of 1 atm. The scanning speed was 80 wave numbers/min and the resolution was 2 wave numbers. The infrared spectrum of an oxygen sample is shown in Fig. I1.

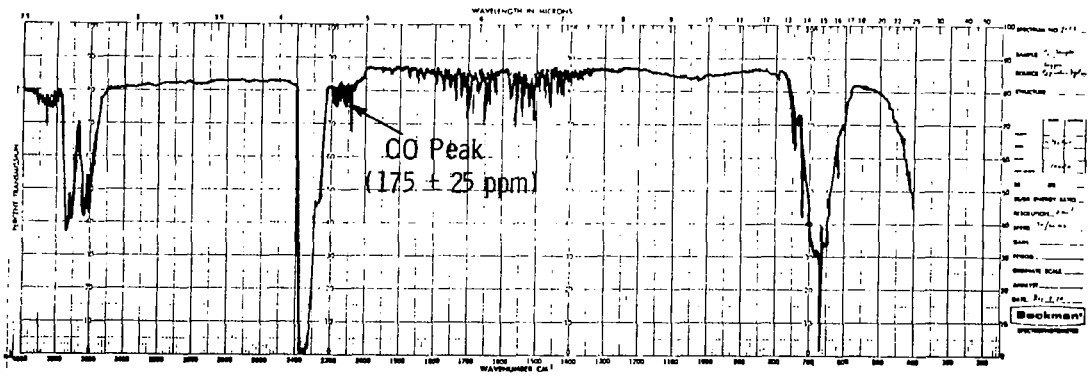

Fig. I1 - Infrared spectrum for carbon monoxide analysis of oxygen sample

I.2 Hydrogen Product

Water and CO_2 were determined by the same procedure described in Section I.1. The absorption bulbs were placed in the discharge line between the vacuum pump and the wet test meter. CO was determined by mass spectrometer.

I.3 Carbon Product

Carbon and hydrogen analyses were performed by Galbraith Laboratories, Knoxville, Tennessee.

Iron analyses were done gravimetrically by weighing 1.5 to 2.0 grams of the carbon sample into a weighed platinum crucible, burning off the carbon in air at a low temperature, and igniting at 1000°C under oxidizing conditions. The residue was weighed as Fe_2O_3 (Reference 20). The error due to impurities in the steel catalyst is less than 1%. Before sampling the carbon product, the entire batch was passed through a 20-mesh screen and well mixed.

I.4 Gas Sample Collection for Mass Spectrometric Analysis

All of the gas streams were analyzed periodically by mass spectrometer. The samples were collected in glass or stainless steel bottles that were placed directly in the gas lines for 1 to 2 hours. The recycle loop was provided with bypass branches before and after the carbon deposition reactor for this purpose. The sample bottles were purged with CO_2 before putting "on stream".

APPENDIX J

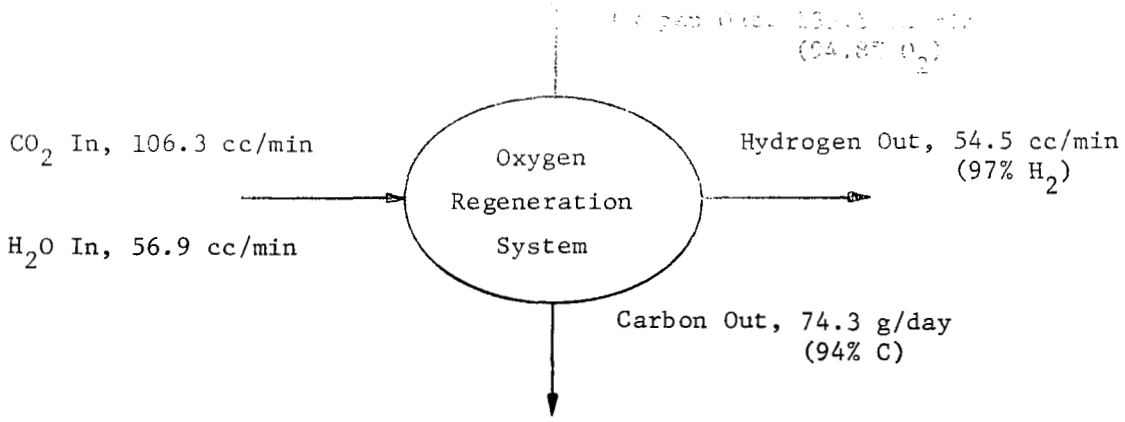
CO_2 In, 106.3 cc/min
H_2O In, 56.9 cc/min
Oxygen Regeneration System
Hydrogen Out, 54.5 cc/min (97% H_2)
Carbon Out, 74.3 g/day (94% C)

CARBON

Out (1) as carbon black = 74.3 x 0.94 = 69.8 g/day

Out (2) as CO_2 = 5.3 x 1440 x 12/25,300 = 3.6 g/day

Total Out = 73.4 g/day

Total In = 106.3 x 1440 x 12/25,300 = 72.6 g/day

Difference = +0.8 g/day

$$\text{Deviation} = \frac{+0.8 \times 2}{73.4 + 72.6} \times 100 = +1.1\%$$

OXYGEN

Out (1) as O_2 = 126.5 cc/min

Out (2) as CO_2 = 5.3 cc/min

Out (3) as H_2O = 1.1 cc/min

Total Out = 132.9 cc/min

In (1) as H_2O = 1/2 (56.9) = 28.5 cc/min

In (2) as CO_2 = 106.3 cc/min

Total In = 28.5 + 106.3 = 134.8 cc/min

Difference = -1.9 cc/min

$$\text{Deviation} = \frac{-1.9 \times 2}{134.8 + 132.9} \times 100 = -1.4\%$$

HYDROGEN

Out (1) through Pd tubes = 54.5 x 0.97 = 52.8 cc/min

Out (2) in carbon = $\frac{.005 \times 74.2 \times 25,300}{1440 \times 2}$ = 3.3 cc/min

Out (3) as H_2O = 2.2 cc/min

Total Out = 58.3 cc/min

Total In = 56.9 cc/min

Difference = +1.4 cc/min

$$\text{Deviation} = \frac{+1.4 \times 2}{58.3 + 56.9} \times 100 = +2.4\%$$

APPENDIX K

HEAT BALANCE FOR CARBON DEPOSITION REACTOR

A heat balance for the carbon deposition reactor of the breadboard system was calculated, using data obtained on the 88th day of the life test. The objective was to identify the major sources of heat loss and to check the thermal conductivity data for the insulation and metal parts so that heat losses for larger systems can be estimated with confidence.

The following data were recorded:

1. Electrical power input to reactor heaters
2. Gas flow rate and composition
3. Surface temperature of reactor at 150 locations
4. Temperature inside reactor throughout the heated zone.

To measure the surface temperature, eight 1/8-in. diameter holes were drilled vertically into the insulation from the top immediately behind the outer aluminum shell of the reactor (see Section 4, Fig. 10). Thermocouples were inserted in these holes and the temperature was measured at 1-in. intervals from the bottom to the top of the reactor. Measurements were also made of the top surface temperature by contacting the surface with a bare, shielded thermocouple. Temperatures inside the reactor were determined by probing the hollow scraper shaft with a thermocouple.

The thermal conductivity values used in calculating the heat losses through the insulation and metal parts of the reactor were:

	Mean Temperature Range, °F	Thermal Conductivity, Btu-ft/hr-ft^2-°F
Fiberflax block insulation	400 to 600	.05
Inconel 600	400 to 800	10.1 to 11.1
Aluminum bronze	57[illegible] to 100	[illegible]

The thermal conductivity [illegible] was obtained by the manufacturer. The [illegible] were obtained from the literature [illegible] leading the need of [illegible] taken from Touchin (Reference [illegible]) and Kaiser (Reference [illegible]).

The heat balance is presented in Table K-I. The good balance of the balance lends confidence to the accuracy of the data used. Table K-I shows that about half of the heat loss was by conduction through the metal parts of the reactor and that the contribution of the aluminum bronze parts was especially large, despite their small size. It was concluded that the cross section of metal parts that extend through the insulation should be minimized and that the use of aluminum bronze for the gas lines should be avoided, if possible.

TABLE K-I
HEAT BALANCE FOR CARBON DEPOSITION REACTOR
ON 88TH DAY OF LIFE TEST

Heat Input	Btu/hr
From electrical energy	451
Heat of carbon deposition reaction	39
Sensible heat of feed gas	18
Total	508
Heat Output	
Through insulation	277
Through Inconel base tube	24
Through Inconel scraper assembly	49
Through aluminum bronze gas inlet and outlet tubes	99
Sensible heat of exhaust gas	32
Total	481
Difference	-27 (-5.5%)

APPENDIX L

DATA SHEETS AND SCHEMATIC DIAGRAMS FOR CO_2 CONCENTRATION AND O_2 GENERATION SYSTEMS FOR A 9-MAN 500-DAY MISSION AFTER HAMILTON STANDARD (Reference 1)

SUBSYSTEM: CO_2 Removal and Concentration

CONCEPT: Steam Desorbed Resin

FLIGHT AVAILABILITY: 1976
(1970 go-ahead)

RELIABILITY: 0.999433 MTBF: 17 000 hr

Spares/Redundant (R) Units:

1 - Ion Exchange Resin Bed	3 - Timer
2 - Fan	2 - Solenoid Valve, Shutoff
4 - Diverter Valve, Solenoid	2 - Compressor
1 - Steam Generator	2 - Water Regulator
10 - Condenser/Separator	1 - Check Valve

CREW TIME (Hr/Mission):	Scheduled	Unscheduled
	16.0	1.5

EQUIVALENT WEIGHT (lb):	Design 1 (Solar Cell)	Design 2 (Solar Cell/Isotopes)	Design 3 (Brayton)
Basic Unit	269	231	200
Expendables	0	0	0
Spares/Redundant Units	231	231	231
Electrical Power	453	81	81
Thermal Power	0	62	0
Radiator Load	195	195	195
Total Equivalent Weight	1148	800	707
POWER (Watts):			
Electrical	1008	180	180
Thermal	0	828	828

VOLUME (ft^3):	Installed	Spares/Expendables	Total
	18	6	24

Fig. L1 - Steam desorbed resin concept

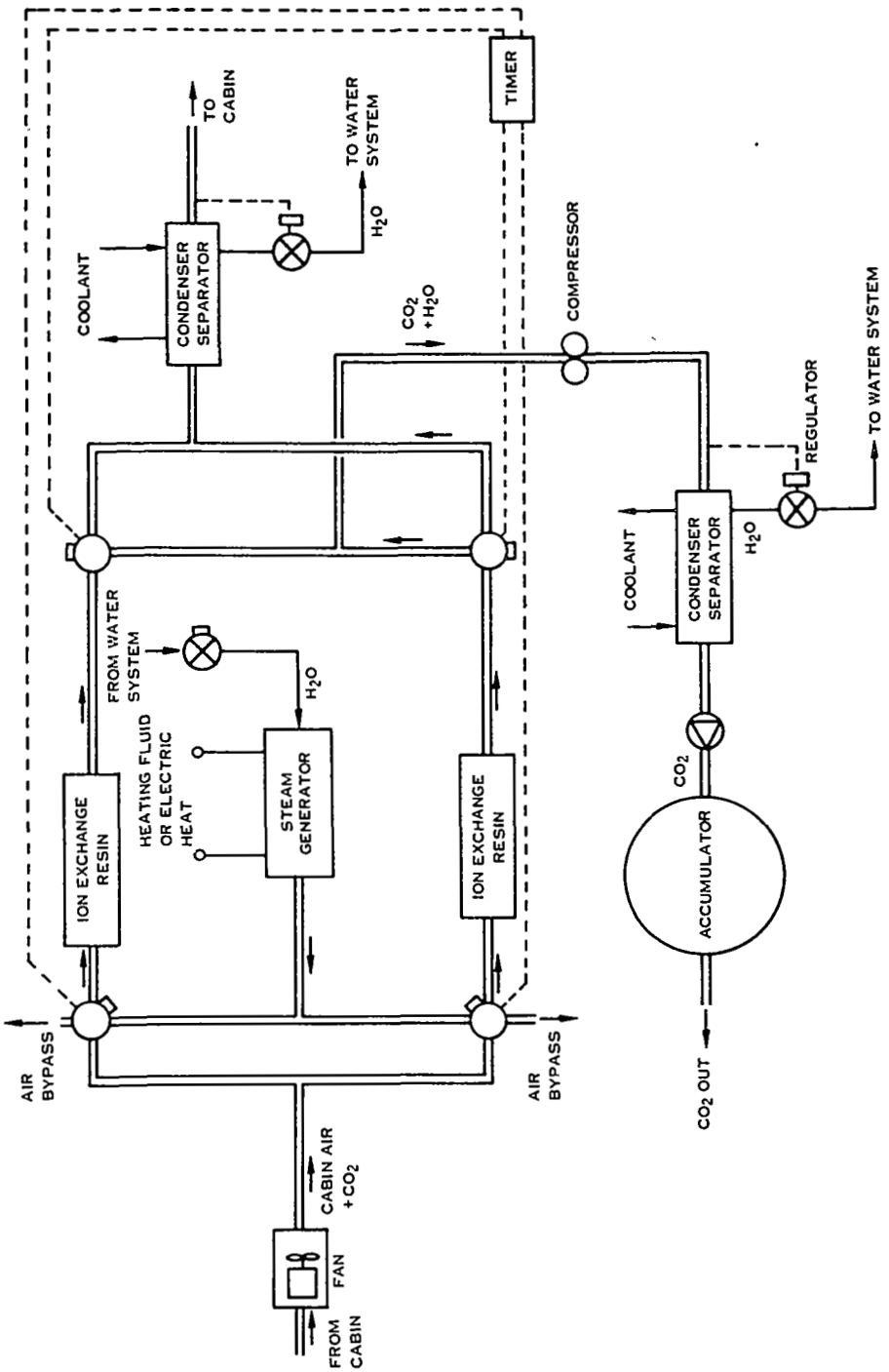

Fig. L1 - (Concluded)

SUBSYSTEM: CO_2 Removal and Concentration

CONCEPT: Molecular Sieve

FLIGHT AVAILABILITY: 1973
(1970 go-ahead)

RELIABILITY: 0.999578 MTBF: 10 500 hr

Spares/Redundant (R) Units:

- 2 - Molecular Sieve Canister
- 2 - Silica Gel Canister
- 2 - Fan
- 1 - Heat Exchanger
- 3 - Timer
- 5 - Canister Diverter Valve
- 3 - Actuator
- 1 - Check Valve
- 2 - Compressor
- 2 - Solenoid Valve, 3-way, Coolant
- 1 - Heater (Designs 2 and 3)
- 2 - Heater Controller
- 2 - Solenoid Valve, 3-way
- 1 - Manual Diverter Valve

CREW TIME (Hr/Mission):	Scheduled	Unscheduled
	0	2.3

EQUIVALENT WEIGHT (lb):	Design 1 (Solar Cell)	Design 2 (Solar Cell/Isotopes)	Design 3 (Brayton)
Basic Unit	379	393	385
Expendables	0	0	0
Spares/Redundant Units	324	331	331
Electrical Power	376	237	237
Thermal Power	0	15	0
Radiator Load	114	114	114
Total Equivalent Weight	1193	1090	1067
POWER (Watts):			
Electrical	837	528	528
Thermal	0	309	309

VOLUME (ft^3):	Installed	Spares/Expendables	Total
	28	9	37

Fig. L2 - Molecular sieve concept

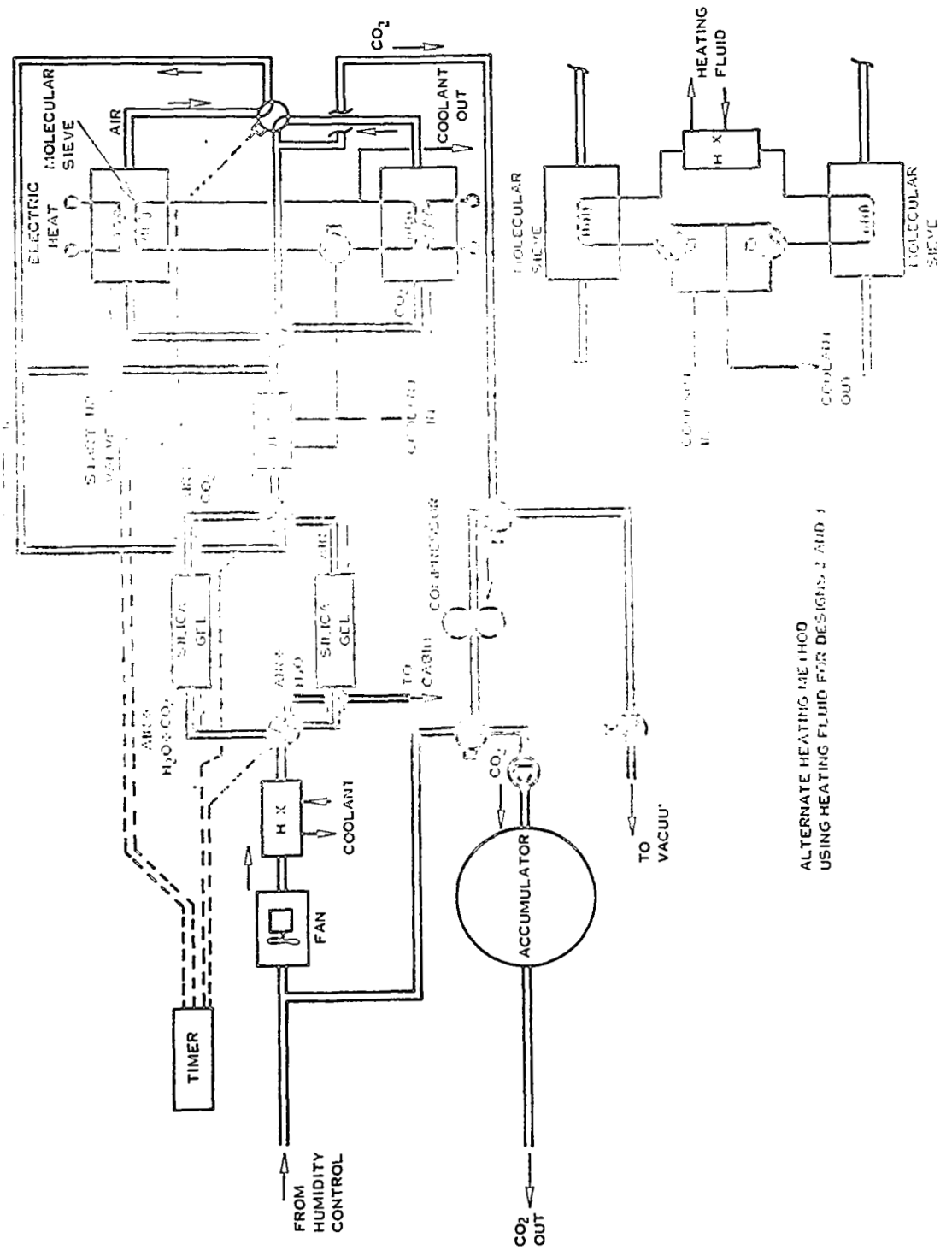

Fig. L2 - (Concluded)

SUBSYSTEM: CO_2 Removal and Concentration

CONCEPT: Hydrogen Depolarized Cell

FLIGHT AVAILABILITY: 1978
(1970 go-ahead)

RELIABILITY: 0.999623 MTBF: 4600 hr

Spares/Redundant (R) Units:

- 1 - CO_2 Concentrator
- 3 - Fan
- 2 - Power Converter
- 2 - Compressor
- 9 - Condenser/Separator
- 2 - Water Regulator
- 1 - Check Valve
- 1 - Diverter Valve
- 1 - Temp Conditioner
- 1 - H_2 Regulator
- 1 - O_2 Regulator
- 1 - Water Pump
- 1 - Control

CREW TIME (Hr/Mission):	Scheduled	Unscheduled
	8.0	7.8

EQUIVALENT WEIGHT (lb):	Design 1 (Solar Cell)	Design 2 (Solar Cell/Isotopes)	Design 3 (Brayton)
Basic Unit	255	255	255
Expendables	0	0	0
Spares/Redundant Units	193	193	193
Electrical Power	357	357	357
Thermal Power	0	0	0
Radiator Load	68	68	68
Total Equivalent Weight	873	873	873
POWER (Watts):			
Electrical	619	619	619
Thermal	0	0	0

VOLUME (ft^3):	Installed	Spares/Expendables	Total
	51	6	57

Fig. L3 - Hydrogen depolarized cell concept

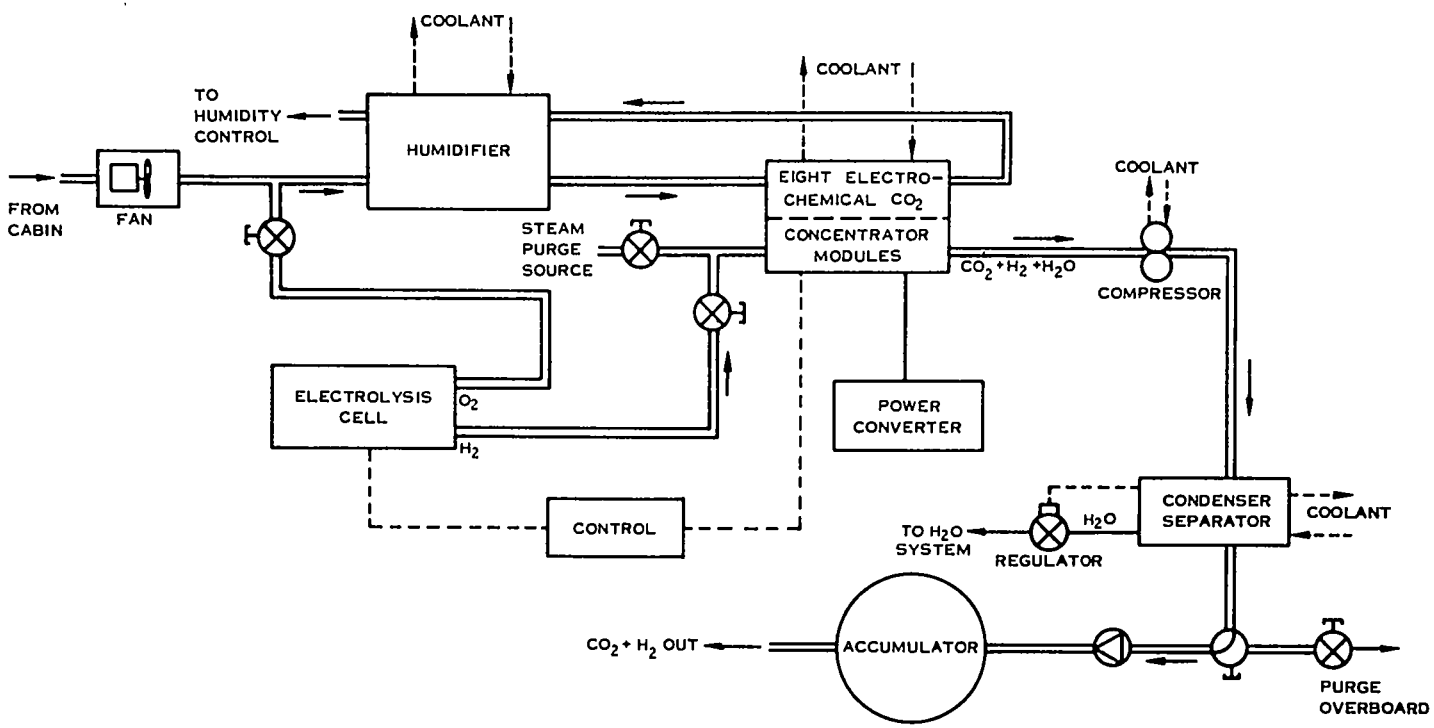

Fig. L3 - (Concluded)

SUBSYSTEM: CO_2 Removal and Concentration

CONCEPT: Carbonation Cell

FLIGHT AVAILABILITY: 1979
(1970 go-ahead)

RELIABILITY: 0.999621 MTBF: 3900 hr

Spares/Redundant (R) Units:

1 - Basic
1 - Acidic Cell
1 - Electrochemical Scrubber
2- Fan
1-Water Vapor Exchanger
2-Check Valve
4-Regulator (2 each type)
2-Power Supply
6-Condenser-Separator
2-Compressor

CREW TIME (Hr/Mission):	Scheduled	Unscheduled
	8.0	7.7

EQUIVALENT WEIGHT (lb):	Design 1 (Solar Cell)	Design 2 (Solar Cell/Isotopes)	Design 3 (Brayton)
Basic Unit	341	341	341
Expendables	0	0	0
Spares/Redundant Units	312	312	312
Electrical Power	825	825	825
Thermal Power	0	0	0
Radiator Load	250	250	250
Total Equivalent Weight	1728	1728	1728
POWER (Watts):			
Electrical	1832	1832	1832
Thermal	0	0	0

VOLUME (ft^3):	Installed	Spares/Expendables	Total
	19	7	26

Fig. L4 - Carbonation cell concept

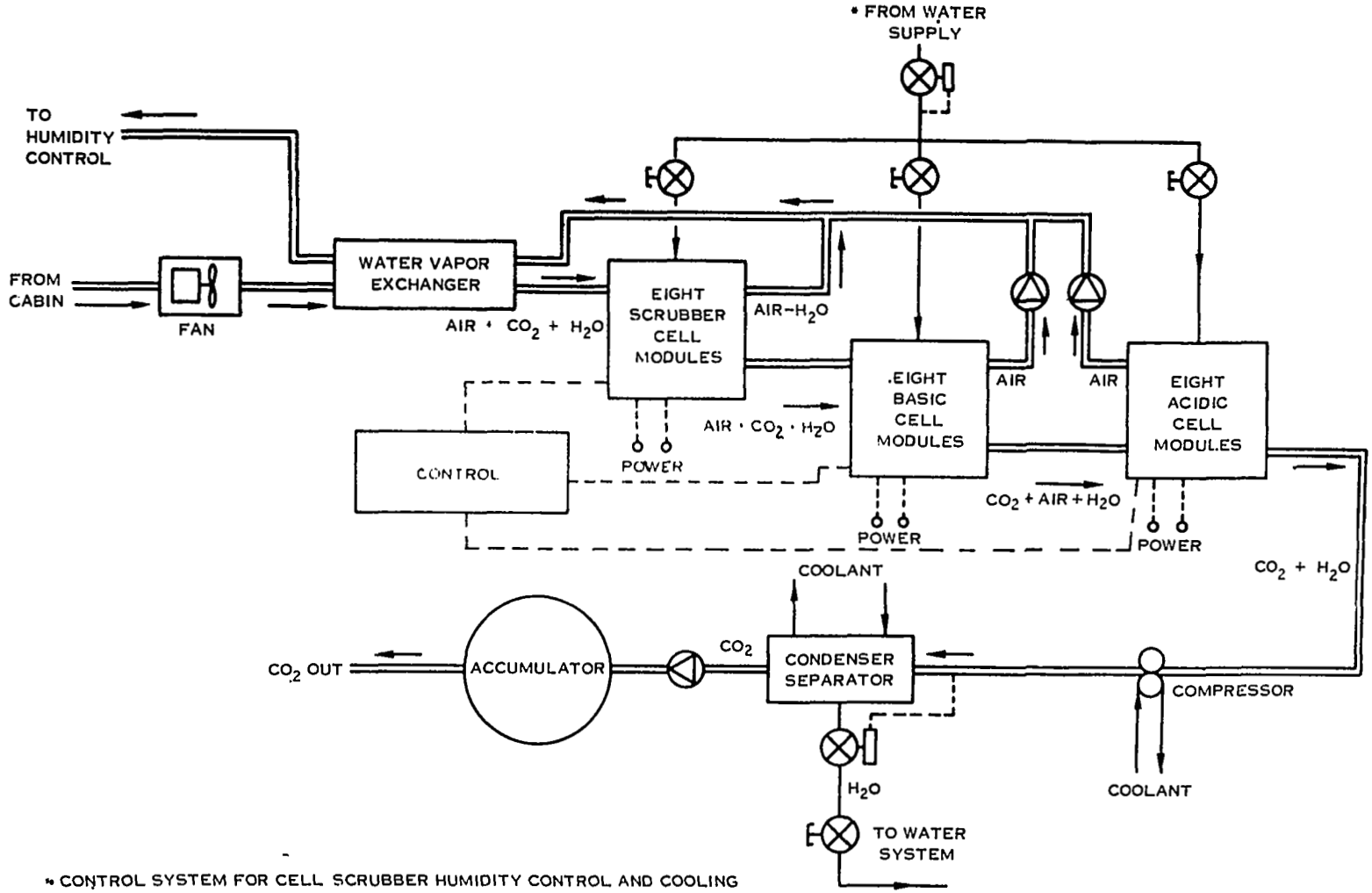

* CONTROL SYSTEM FOR CELL SCRUBBER HUMIDITY CONTROL AND COOLING

Fig. L4 - (Concluded)

SUBSYSTEM: O_2 Generation/CO_2 Control

CONCEPT: Solid Electrolyte/Steam Desorbed Resin Concentrator

FLIGHT AVAILABILITY: 1979
(1970 go-ahead)

RELIABILITY: 0.999106 (includes CO_2 concentrator) MTBF: 3480 hr

Spares/Redundant (R) Units:

5-R-Standby Solid Electrolyte	2 - Master Control	1 - Hydrogen Separator
	2 - CO_2 Inlet Regulator	1 - Heat Exchanger
	2 - Check Valve	3 - 4-way Valve
Expendables:	1 - Humidifier	1 - Catalyst Cartridge
50 catalyst cartridges	2 - Solenoid Valve	1 - Catalyst Reactor
	2 - Heater Control	2 - Compressor

NOTE: Spares list does not include CO_2 Concentrator. See individual data sheets.

CREW TIME (Hr/Mission):	Scheduled	Unscheduled
	126.8	8.4

EQUIVALENT WEIGHT (lb):	Design 1 (Solar Cell)	Design 2 (Solar Cell/Isotopes)	Design 3 (Brayton)
Basic Unit	525	487	456
Expendables	640	640	640
Spares/Redundant Units	373	373	373
Electrical Power	1351	979	979
Thermal Power	0	62	0
Radiator Load	331	331	331
Total Equivalent Weight	3220	2872	2779
POWER (Watts):			
Electrical	3004	2872	2779
Thermal	0	828	828

VOLUME (ft^3):	Installed	Spares/Expendables	Total
	99	150	249

Fig. L5 - Solid electrolyte concept

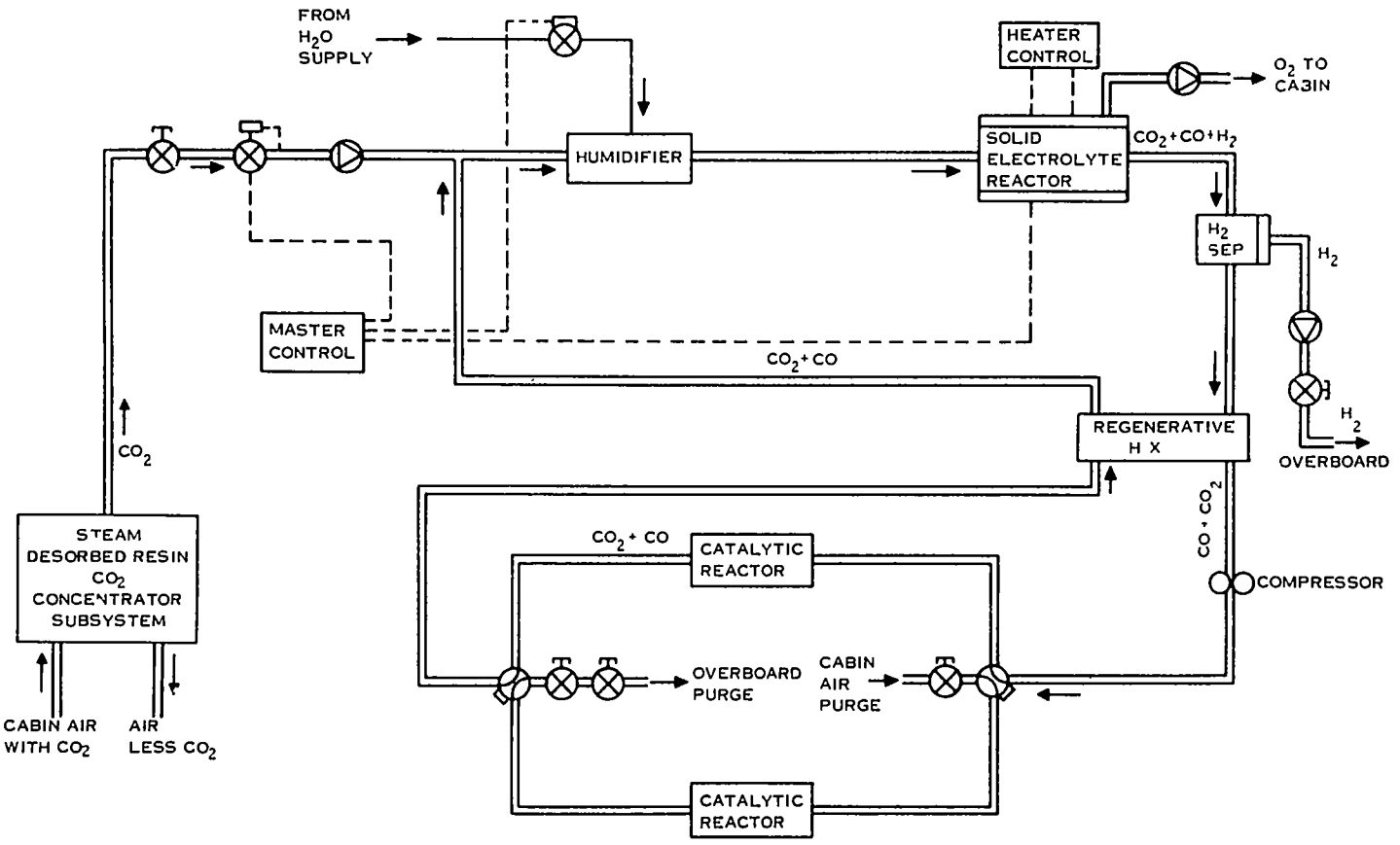

Fig. L5 - (Concluded)

REFERENCES

1. Hamilton Standard Division of United Aircraft Corporation: Trade-Off Study and Conceptual Designs of Regenerative Advanced Life Support Systems (AILSS). NASA-CR1458 (Jan. 1970).
2. Elikan, L., D. H. Archer, R. L. Zahradnik: Aerospace Life Support, L. Elikan, Editor, American Inst. of Chem. Eng., New York (1966), pp. 30-37.
3. Elikan, L. and J. P. Morris: Solid Electrolyte System for Oxygen Regeneration. NASA CR-1359 (June 1969).
4. Chandler, H. W. and W. Oser: AMRL-TDR-62-16 (1962).
5. Chandler, H. W.: AMRL-TDR-64-62 (May 1964).
6. Chandler, N. W. and F. Z. Pollara: Aerospace Life Support. L. Elikan, Editor, American Inst. of Chem. Eng., New York (1966) pp. 38-42.
7. Weissbart, J. and W. H. Smart: NASA CR-680 (February 1967).
8. Weissbart, J. and W. H. Smart: A Two-Cell 8-Ampere CO_2-H_2O Solid Electrolyte Electrolyzer for Oxygen Production. Presented at Fall Meeting, The Electrochem. Soc., Atlantic City, New Jersey (October 1970).
9. Smart, W. and J. Weissbart: A 127-Ampere CO_2-H_2O Solid Oxide Electrolyzer-Reactor System for Production of Oxygen. Presented at Fall Meeting, The Electrochem. Soc., Atlantic City, New Jersey (October 1970).
10. Waldschmidt, E., Metall, 8 (1954) pp. 749-58.
11. Tepper, F. et al: Development of a Regenerable Carbon Dioxide Removal System. NASA Contractor Report No. 66571 (January 1968).
12. Martin, R. B. and H. F. Brose: An Amine Polymer CO_2 Concentrator for the 90-Day LRC/MDAC Manned Chamber Test. Presented at Space Technology and Heat Transfer Conference, Am. Soc. of Mechanical Eng., Los Angeles (June 1970).

13. Kiraly, R. J., A. D. Babinsky and J. D. Powell: Aircrew Oxygen System Development Flight Breadboard System Flight and Environmental Tests. NASA CR-73393 (April 1970).

14. Macklin, M.: Electrochemical Concentration of Carbon Dioxide. Presented at Symposium on New Developments in Aerospace Life Support - Part II, Am. Inst. Chemical Eng., Houston (February 1965).

15. Sverdrup, E. F. et al: Testing of Electrodes for High-Temperature Solid Electrolyte Fuel Cells. Hydrocarbon Fuel Cell Technology. Academic Press, New York (1965) pp. 311-333.

16. Popma, D. C. and V. G. Collins: Space Vehicle Water Reclamation Systems - A Status Report. Aerospace Life Support. L. Elikan, Editor, American Inst. of Chem. Eng., New York (1966) pp. 1-9.

17. Sverdrup, E. ,. et al: Final Report Project Fuel Cell, OCR Research and Development Report No. 57, Government Printing Office Cat. No. I63.10:57 (1970) pp. 258-264.

18. Coughlin, James P.: Contributions to the Data on Theoretical Metallurgy, XII. Heats, and Free Energies of Formation of Inorganic Oxides. Bur. Mines Bull. 542 (1954).

19. Hunter, J. P.:. Ultrapure Hydrogen by Diffusion Through Palladium Alloys. Presented at Symposium on the Production of Hydrogen, Am. Chem. Soc., New York (1963).

20. Hillebrand, W. F., G. E. F. Lundell, H. A. Bright, and J. I. Hoffman: Applied Inorganic Analysis, 2nd Ed. John Wiley & Sons, New York (1953) p. 390.

21. Engineering Properties of Inconel Alloy 600. Huntington Alloy Products Division, The International Nickel Company, Technical Bull. T-7 (1964) p. 5.

22. Properties and Selection of Metals. Metals Handbook, Vol. 1, 8th Ed., Americal Society for Metals, Metals Park, Ohio (1961) p. 1033.

23. Kelley, K. K.: Contributions to the Data on Theoretical Metallurgy, XIII. High-Temperature Heat-Content, Heat Capacity, and Entropy Data for the Elements and Inorganic Compounds. Bur. Mines Bull. 584 (1960).